TRANSPORTATION RESEARCH RECORD

532

Frost, Moisture, and Erosion

9 reports prepared for the 54th Annual Meeting of the Transportation Research Board

TRB

TRANSPORTATION RESEARCH BOARD

NATIONAL RESEARCH COUNCIL

Washington, D. C., 1975

Transportation Research Record 532
Price $4.60
Edited for TRB by Joan B. Silberman

Subject areas
23 highway drainage
24 roadside development
61 exploration-classification (soils)
62 foundations (soils)
64 soil science

These papers report research work of the authors that was done at institutions named by the authors. The papers were offered to the Transportation Research Board of the National Research Council for publication and are published here in the interest of the dissemination of information from research, one of the major functions of the Transportation Research Board.

Before publication, each paper was reviewed by members of the TRB committee named as its sponsor and accepted as objective, useful, and suitable for publication by the National Research Council. The members of the review committee were chosen for recognized scholarly competence and with due consideration for the balance of disciplines appropriate to the subject concerned.

Responsibility for the publication of these reports rests with the sponsoring committee. However, the opinions and conclusions expressed in the reports are those of the individual authors and not necessarily those of the sponsoring committee, the Transportation Research Board, or the National Research Council.

Each report is reviewed and processed according to the procedures established and monitored by the Report Review Committee of the National Academy of Sciences. Distribution of the report is approved by the President of the Academy upon satisfactory completion of the review process.

LIBRARY OF CONGRESS CATALOGING IN PUBLICATION DATA

National Research Council. Transportation Research Board.
Frost, moisture, and erosion.

(Transportation research record; 532)
1. Roads–Foundations–Addresses, essays, lectures. 2. Soil freezing–Addresses, essays, lectures. 3. Soil moisture–Addresses, essays, lectures. 4. Soil erosion–Addresses, essays, lectures. I. Title. II. Series.
TE7.H5 no. 532 [TE210] 380.5'08s [625.7'01'5516]
ISBN 0-309-02380-7 75-17571

CONTENTS

FOREWORD

The effects of climate and water on roadway design, construction, and performance have always been of the highest importance. Without temperature changes, structural portions of a roadway would be rather easy to design for anticipated loads as they would be if moisture changes were also not present. Therefore, the information in this RECORD will be of interest to soils and design engineers who are concerned with the performance of the roadway structure under variations of climate, temperature, and moisture.

The combined effects of moisture and temperature resulting in frost action are generally considered to be a problem in the northern states, but much evidence has come to light to indicate that some southern states also have their problems. The problems may in fact be amplified by the higher number of freeze-thaw cycles that are encountered. Carpenter, Lytton, and Epps discuss some of the problems in west Texas by showing that a reorientation of particles and structure occurs, which brings about residual tensile stress in the asphalt concrete pavement surface. Pagen and Khosla add theoretical support by pointing out a major reduction in load-carrying capacity as indicated by freeze-thaw cycles in relation to a high degree of saturation.

Vaswani's study shows a sharp rise in subgrade moisture during construction and immediately thereafter. The rate of increase decreases and levels off at about 10 years after construction. Dunn and Razouki interpret in situ permeability tests in anisotropic deposits, and Tayabji and Barenberg evaluate open-graded bituminous aggregate bases with regard to permeability. They outline some of the methods that must be used to ensure satisfactory performance and point out the particular care that must be taken to prevent migration of subgrade fines into the permeable base layer.

The measurement of soil moisture by remote methods is being aided by the development of new measuring devices. Selig, Wobschall, Mansukhani, and Motiwala and Matzkanin and Gardner present two new methods with much promise for refining the state of the art in soil moisture determinations.

Rosen and Marks present the results of a study of the filtration characteristics of one nonwoven fabric filter.

In an effort to further the control of soil erosion by the identification of soils subject to erosion, Petry and Haliburton present the results of their study of a new physical test method for identification of dispersive clay soil behavior.

All of the papers in this RECORD make contributions toward a solution to the problems of roadway soil moisture and temperature variation. A single solution is not applicable nationwide nor, in most cases, statewide, but engineering judgment based on the continuing development of the state of knowledge will produce the most economic and satisfactory solutions.

PAVEMENT CRACKING IN WEST TEXAS DUE TO FREEZE-THAW CYCLING

Samuel H. Carpenter, Robert L. Lytton, and Jon A. Epps,
Civil Engineering Department, Texas A&M University

Freeze-thaw contraction of the base course material used in west Texas is considered an important element in pavement deterioration. Samples from two compactive efforts were frozen in a biaxial closed system. Suction and temperature within the samples were monitored and volume changes after each freeze-thaw period were recorded. Coefficients of thermal activity were calculated from the dimension measurements. These coefficients showed a relationship with the as-compacted total soil moisture suction, which was similar for all materials. Finite element studies of the thermal strains that develop in a typical pavement showed that the thermally induced tensile stresses in the base course are far in excess of typical tensile strengths for initially intact pavements. The surface course did not develop excessive stress levels. Freeze-thaw cycling produced plastic deformations in all samples, and the permanent expansion or contraction was related to the as-compacted total soil moisture suction. These permanent deformations from freeze-thaw cycling imparted a residual tensile stress to the asphalt concrete. During a freeze, the suction in the sample showed a marked increase, often 10 to 20 times the initial value. The suction then dropped below the initial value during the thaw cycle. This drop was consistent regardless of the thermal activity or plastic deformation. This indicated a reorganization of the moisture in the sample, which may be related to strength losses caused by freeze-thaw cycling. The data in this study give new insight into the mechanism of freeze-thaw in pavement deterioration.

•GROWING concern for environmentally controlled cracking of pavements has been stimulated by the relatively large amounts of mileage on roads experiencing cracking that cannot be directly attributed to traffic. Ample evidence of this transverse cracking can be found in the northern United States, Canada, and even in the arid portions of the western United States.

Common forms of environmental influence on pavements are temperature extremes and cycles; moisture movement under a pavement, which is caused by the climate; and radiation. These influences interact to produce massive pavement cracking failures even in the best designed pavements.

This paper examines the freeze-thaw activity of the base course as an important mechanism in pavement cracking.

BACKGROUND

Many studies have investigated the cracking of pavement under extremely low temperatures (4, 7, 19, 22). They have mainly considered the properties of the asphalt concrete surface in predicting cracking during the life of a pavement. This theory cannot explain the large amount of transverse cracking found in the western United States and, in particular, west Texas if, as McLeod claims (13), low-temperature crack-

Publication of this paper sponsored by Committee on Frost Action.

ing is commonly found only in areas with a design freeze index above 250. This excludes nearly all of Texas, which currently has extensive transverse cracking problems. Figure 1 shows typical cracking patterns for two widely separated areas in west Texas.

Thermal fatigue or temperature cycling has been studied (19) and used in computer codes to account for the difference between predicted and actual cracking due to low temperatures. The results obtained from these computer codes have still not proved wholly satisfactory, and they give only limited insight into the mechanisms causing this deterioration.

One area missing from the study is an analysis of the foundation material of the pavement system. Much work has been done in the area of frost-heave damage (9, 11). This damage mode requires a near-saturated soil and access to capillary water, neither of which applies to pavement in west Texas.

By using a heat-transfer program developed at the University of Illinois (5), one can obtain reliable temperature distributions in a pavement system that show that the freezing front will seldom penetrate below a typical asphalt concrete surface and base course during a severe winter in west Texas. Thus, if thermal activity were to be studied as a possible area to account for the discrepancies mentioned, the base course would be a logical area to examine.

The base course material is typically an untreated, indurated limestone: caliche. This material, when compacted for use in a roadbed, is an unsaturated soil material with a relatively small percentage of plastic fines. It is usually placed over a subgrade material that is composed of a much higher percentage of plastic fines, often of a more active nature.

The field behavior of the unsaturated soil material depends on its unsaturated, moisture stress state (1). Determination of the separate components of this state requires special equipment, which is not suitable for in situ testing. However, the total moisture energy or suction may be determined conveniently in the field and in the laboratory. The soil moisture suction is a measure of the free energy of the moisture in a soil compared to the free energy of a pool of pure water at the same datum. Thus, as a soil becomes drier and moisture is removed, work must be expended to accomplish this, and energy is in effect taken away. The pure water is commonly given a free energy of zero so that as moisture content decreases the free energy or suction increases in the negative direction. Thus, all suction values are negative quantities.

This energy quantity may be determined by measuring the relative humodity of the soil mass, which is a measure of the relative vapor pressures in the soil (18). The common units are atmospheres, bars (kPa), or psi (kPa). Several methods exist for measuring the soil moisture suction such as tensiometers, gypsum blocks, resistivity blocks, pressure plates, and thermocouple devices. These devices have extremely fine thermocouples to measure dew-point depression temperatures, and they are called psychrometers because they are similar to traditional wet bulb-dry bulb sling-psychrometers. The performance and accuracy of these psychrometers for soils work are discussed in a number of papers (1, 3, 14, 15, 16). Psychrometers are typically suited for laboratory and field work that require a range from 0 to > -142,000 psi (-979 MPa), and they have a nominal accuracy of 5 percent of the reading, including temperature corrections. In the low range of measurements, temperature control during a measurement is extremely important in the psychrometric technique. The newly developed dew-point technique, which has internal temperature compensation and provides a continuous output, overcomes many of the previous complaints about the psychrometric technique.

The use of soil moisture suction is complicated because total soil moisture suction has two forms:

1. Osmotic suction, which is due to salts in the fluid portion of the three-phase soil system, and
2. Matric suction, which is due to the matrix phase, in which the soil particles themselves form various-sized capillaries.

These two components together give the total soil moisture suction (1). To date, most studies have reported suction values in terms of matric suction.

During a freeze, however, the change in suction is due to a decrease in the amount of free water as a result of ice formation (20). This causes both components of suction to increase in magnitude by increasing the ion concentration and decreasing the capillary size. Both of these mechanisms can contribute to a volume change because of changes in the radius of hydration of the ions and forced particle reorientation. Thus, the total suction can be measured without any loss in understanding the mechanisms that will occur in freeze-thaw cycling.

Suction has been used in previous studies to describe the behavior of subgrade material under varied situations. Richards et al. (17) demonstrated the effects of compaction on the initial suction values and the effect of the initial suction on the overall load-carrying ability of the pavement structure. The suction developed in a freezing soil is nearly identical to that obtained for the soil water characteristic (SWC) curve (10). SWC is a plot of suction versus moisture content during wetting and drying of the soil. Figure 2 shows the data for a Na-montmorillonite clay. This relationship shows that the freeze-thaw mechanisms are similar to the wetting-drying cycle and that they may provide a valid analogue to study the freezing phenomenon in soils.

Bergan and Monismith (2) have shown that subgrade material loses load-carrying ability between fall and spring for roads in Canada. Resilient modulus testing clearly showed that freeze-thaw cycles are responsible for the loss. Furthermore, a relationship was shown to exist between suction loss in the soil and the effects of freeze-thaw.

As a soil undergoes freezing, the moisture in the finer voids will not freeze (12). Differing amounts of moisture freeze as the temperature is decreased. The amount of moisture remaining unfrozen at any temperature has been related to original suction levels (20, 21) and to the amount and type of clay fraction, surface area, and original moisture content (6).

Thus, soil suction provides a means for obtaining a description of the energy state in a sample, which would not be shown unless more detailed information such as pore structure, clay mineralogy, and the unsaturated pore pressure parameters were known. Psychrometers provide a means of obtaining in situ information of this energy state of the moisture on a continuous basis regardless of the mechanisms acting. For these reasons, the value of total soil moisture suction was chosen to relate measured material variables to the observed actions of freezing and thawing.

PROCEDURE

Six base course materials from west Texas were collected for this study. The material was chosen to represent typical base courses being used in west Texas where cracking is a major problem. The material was sieved to pass $\frac{3}{8}$-in. (0.953-cm) material. The size that is larger than the $\frac{1}{4}$-in. (0.635-cm) material, which is called for in the compaction specifications, was chosen because the authors felt that by using only the finer portion of the base material they would not adequately represent the behavior of the in situ material.

Mechanical analyses were performed on each material. These are given in Table 1. The distribution curves of the grain size were nearly identical for all the materials, and a nominal 10 percent passed the No. 200 sieve. The data show that all materials are similar, but there is some variation in the plasticity index.

Two moisture density curves were constructed for each material. Modified AASHO compaction produced one curve, and the Harvard miniature compaction with a spring-loaded compactor calibrated to produce 95 percent of modified AASHO compaction produced the other. Psychrometers were placed in preformed cavities in the 4.6-in. - tall (11.6-cm), 4.0-in.-diameter (10.2-cm) modified AASHO samples. The samples were lightly wrapped in tinfoil and heavily coated with wax. Suction determinations were made until an equilibrium value was attained. The psychrometers were sealed with the smaller Harvard samples, $1\frac{5}{16}$ in. (3.33 cm) wide and $2\frac{1}{2}$ in. (6.35 cm) high, so that suction values could be obtained.

Figure 1. Typical cracking observed in west Texas.

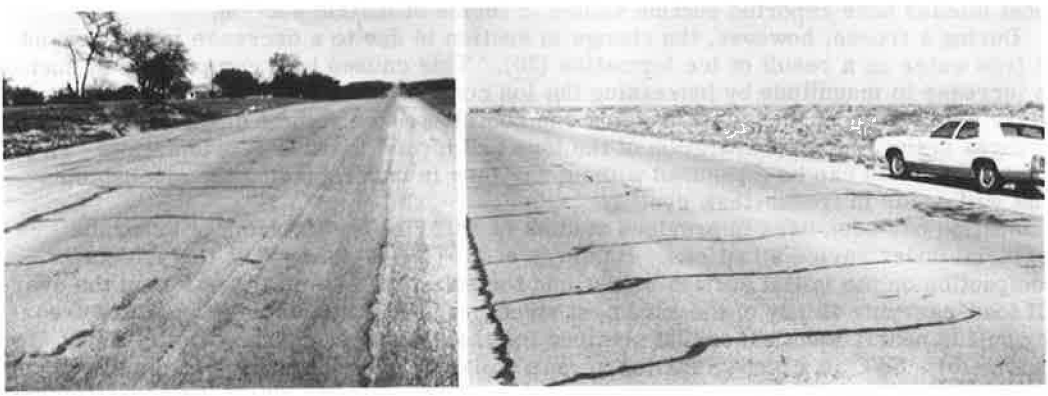

Figure 2. Relationship between water content and suction for freezing and drying, thawing and wetting (10).

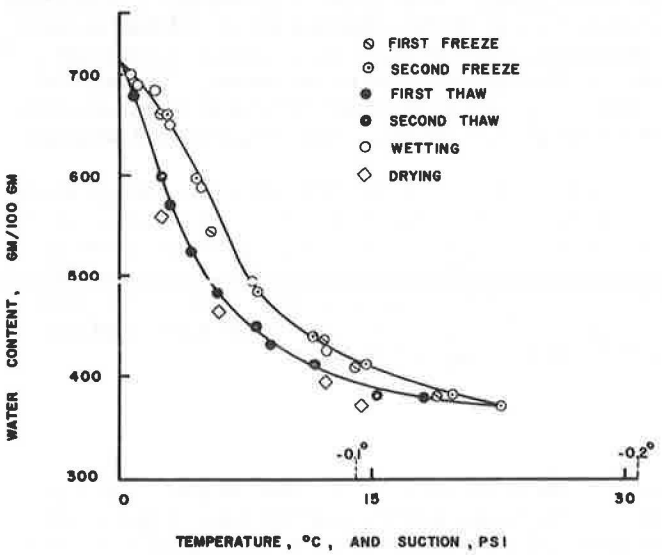

Table 1. Properties of tested base course material.

Material Number	Specific Gravity	Fines Passing No. 200 Sieve (percent)	Liquid Limit (percent)	Plastic Limit (percent)	Clay (percent <2μ)	Maximum Freeze Coefficient[a]
4	2.65	11	30	21	9.0	-2.7
5	2.68	9	32	21	7.7	-2.5
6B	2.67	10	27	20	6.2	-1.3
6JD	2.69	10	22	18	4.3	-4.0
6FS	2.66	9	16.7	16.5	1.6	-0.5
7SA	2.68	10	22	12	6.5	-1.85

Note: 1 in. = 2.54 cm. 1 C = (1 F - 32)/1.8.

[a] $\frac{in./in.}{°C} \times 10^{-4}$.

The psychrometers furnished an as-compacted suction value for each sample. These values allowed contours to be plotted on the moisture density curves. Figure 3 shows a typical curve. These data substantiate previous investigations (17), which showed that suction was affected only slightly by compaction effort for a given moisture content. The psychrometers were removed from the Harvard miniature samples but were left within the modified AASHO samples to monitor suction changes during subsequent freeze-thaw testing.

Several methods of freeze-thaw testing are currently used. The open system allows the sample free access to the moisture. The closed system maintains a constant moisture content in the sample. Uniaxial freezing results from the advance of a freezing front along the axis of the sample. Biaxial freezing results from a uniform drop in temperature around the entire sample. The nature of west Texas dictated closed-system testing to control the moisture. Biaxial freezing was chosen because uniaxial freezing has major importance primarily in frost-heave problems and because previous studies have not shown ice segregation or lensing to be a major problem in unsaturated samples of similar materials tested in the closed-system mode of freezing (8).

For freezing, the samples were placed in a constant temperature room at 20 F (-6.7 C). Previous studies show that if volume change is to occur, 10 percent of the total change will occur between ambient and 32 F (0 C). The remaining 90 percent will occur between 32 F (0 C) and 20 F (-6.7 C). Only random minor changes will occur below 20 F (-6.7 C) (8). For this reason, it was felt that to cool the samples to 20 F (-6.7 C) in existing operational environmental rooms would be sufficient. There is not one uniform method for the freeze-thaw testing of soil materials. The freeze parameters will vary in different areas of the country. Studies similar to those done by Dempsey (5) in predicting pavement temperatures during a year should be conducted to define the freeze-thaw parameters in the area in which the material will be used.

The height and diameter of each sample were recorded with a dial gauge and micrometer to 0.0001 in. (0.0003 cm). The temperature was monitored by using thermocouples embedded with the psychrometers in the modified AASHO samples. The samples were frozen for a different period of time depending on their size. The modified AASHO samples were frozen completely in 24 hours, and the Harvard miniature samples were frozen after 12 hours. The thaw periods were of a similar length.

EXPERIMENTAL DATA

Results of the freeze-thaw cycling tests produced three major sets of data:

1. Thermal strain due to a freeze,
2. The permanent deformation remaining after a freeze-thaw cycle, and
3. Suction values during and after a freeze-thaw cycle.

The thermal strains were converted to a coefficient of thermal activity, which was calculated in two parts. The total thermal deformation was divided into two parts: (a) Ten percent of it was assumed to occur from ambient temperature down to 32 F (0 C), and (b) the remaining 90 percent was assumed to occur from freezing to 20 F (-6.7 C). The coefficient of thermal activity was calculated by dividing the thermal strain, change in height divided by original height, by the corresponding change in temperature. This gave two coefficients: The first applies to situations in which the temperature remained above freezing (the thermal coefficient), and the second applies to situations when the temperature fell below freezing (the freezing coefficient). When plotted directly on the moisture density curves, the freezing coefficient produces contours similar to those obtained by Hamilton (8). Typical curves are shown in Figure 4. These data showed that contraction prevailed in all materials tested. When these freezing coefficients are plotted against $\log_{10}$ of the as-compacted suction, a unique relationship is observed, which is shown in Figure 5. Generally, as suction increases, the freeze coefficient becomes more contractive.

The plastic, or residual, strains produced in a sample are similar to data obtained

Figure 3. Compaction curve and soil moisture suction values for base material.

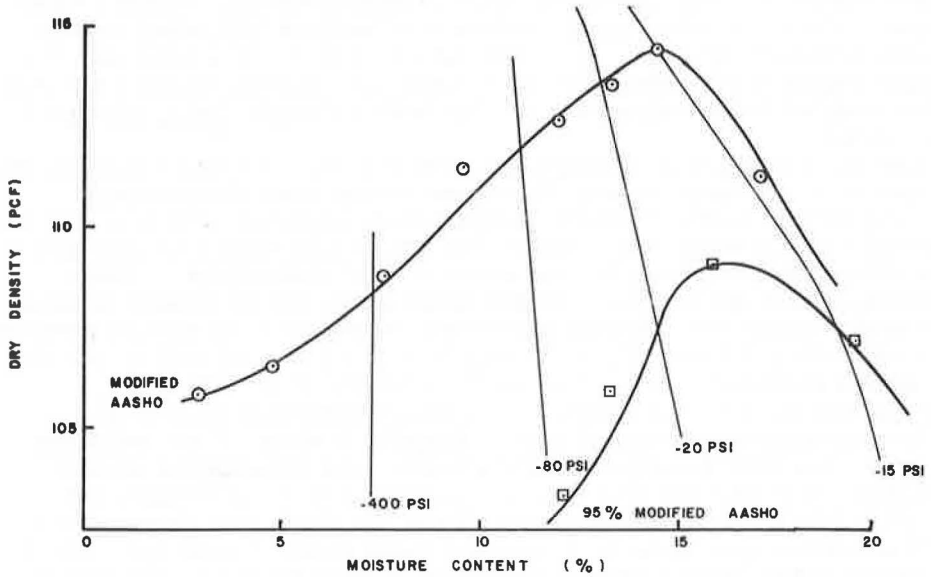

Figure 4. Moisture density curves and freeze coefficients for base material.

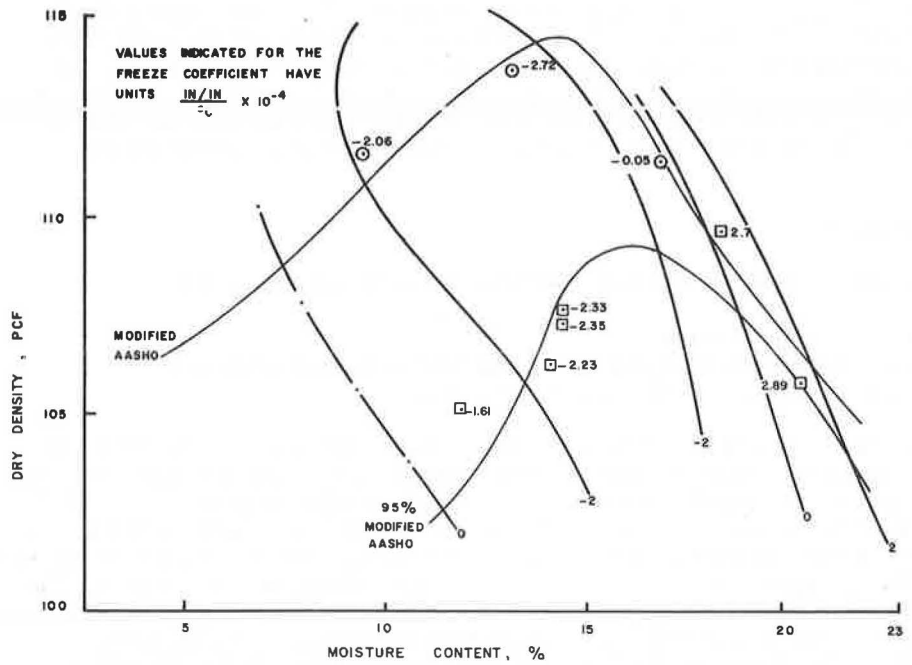

Figure 5. Freeze coefficient plotted against $\log_{10}$ of suction and varied compactive efforts for base material.

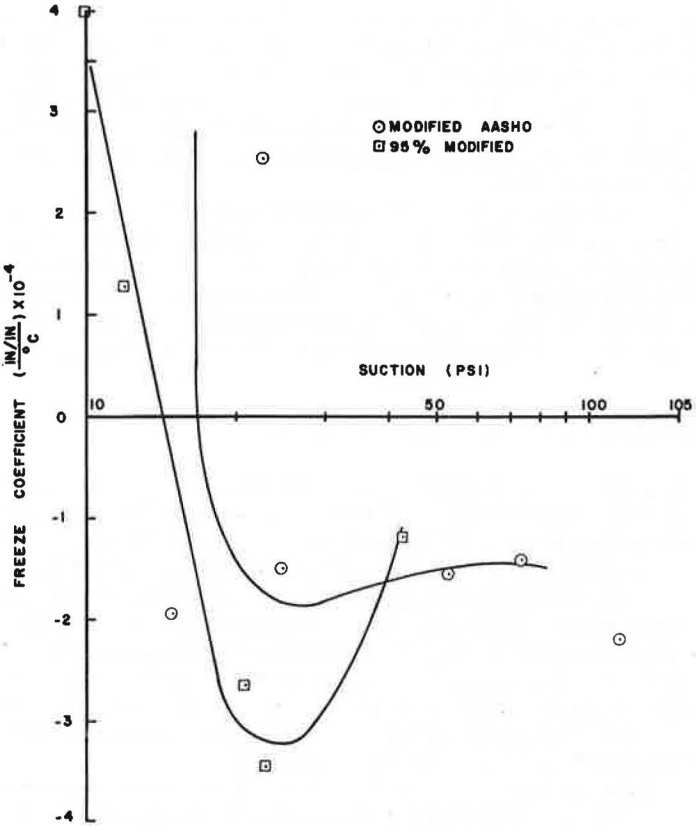

Figure 6. Residual strain plotted against $\log_{10}$ of number of freeze-thaw cycles.

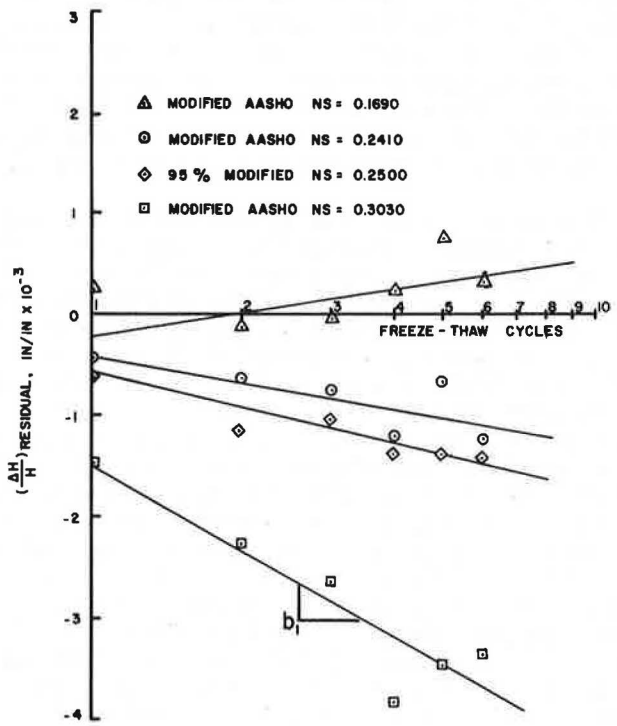

in triaxial repetitive load tests. The residual strain plotted against log $_{10}$ of the number of freeze-thaw cycles is a linear relationship; this is shown in Figure 6. The slope of each line, obtained by standard linear regression techniques, is plotted against $\log_{10}$ of the suction in Figure 7. This relationship shows the influence of suction on residual strains to be the opposite of that for the freeze coefficient; i.e., as suction increases, the residual contraction decreases and even produces expansion for high values of suction.

The suction behaved as expected during freezing. Measured values jumped well up above -700 to -800 psi (-4830 to -5520 kPa) during a freeze, indicating that there is, effectively, less free water available. During the thaw portion of the cycle, the suction fell below the original value. This drop was consistent for all samples independent of whether the thermal activity was expansion or contraction. Suction values for two samples undergoing freeze-thaw are shown in Figure 8.

INTERPRETATION AND ANALYSIS

Data indicate that thermal activity of a soil can be related to the total soil moisture suction of the sample. This term indicates that suction variations, although very small, are highly influential in the thermal activity (or freeze behavior) and in the plastic or residual behavior of a soil undergoing freeze-thaw cycling, although in opposite directions.

Thermal activity data show a rather narrow range in which soils exhibit a change from expansive to contractive behavior during freezing. This range may vary considerably from material to material depending on the initial suction, which will be unique to each material. This can be seen when the freeze coefficient is compared with moisture content alone (Fig. 4). This demonstrates the need for identifying the clay mineralogy in the base course material because it is highly influential in determining the suction level that develops.

Thermal behavior of a base course is influenced somewhat by the compactive effort. The point at which the thermal activity changes from expansion to contraction is consistently shifted to the wet side of the optimum moisture content as compactive effort increases. This means that increased compaction effort would produce a material more likely to exhibit freeze contraction over a larger range of water contents because most material is compacted near, or dry of, optimum moisture (Figs. 4 and 5).

Suction has an opposite influence on the residual deformation. As suction increases, the sample becomes drier, and the residual deformation will change from contraction to expansion (Fig. 6). Compaction effort changes the residual deformation characteristics; therefore, increased compaction reduces residual shrinkage for the same suction value.

The heat transfer program mentioned earlier was used to calculate several temperature distributions from west Texas weather data. These calculations show that the freezing front nearly always penetrates the base course but never penetrates to the subgrade during any winter. Typical profiles were used in an elastic, finite element computer code to predict induced tensile stresses due to thermal strains.

The finite element code was modified slightly to more closely model the situation as it occurs in the field. The initial and final temperature distributions in Figure 9 were used. The coefficients of thermal activity above and below freezing were stored with typical values of Young's modulus above and below freezing. Figure 10 shows these values and the mesh configuration for an initially uncracked pavement.

Figure 11 shows the maximum induced tensile stresses in the asphalt and base course plotted against the freezing coefficient of the base course. It clearly shows that the range of values determined for the samples in this study will produce excessive tensile stresses, which can easily crack the base course of an initially uncracked pavement. The asphalt concrete surface develops tensile stresses, which are nearly the same as typical asphalt concrete tensile strength values. Therefore, the asphalt concrete will be less likely to crack than the base course material.

As the temperature rises above freezing, the thermal stresses will be relieved; however, the base course undergoes permanent residual deformation as a result of the

Figure 7. Residual strain versus freeze-thaw cycles plotted against suction.

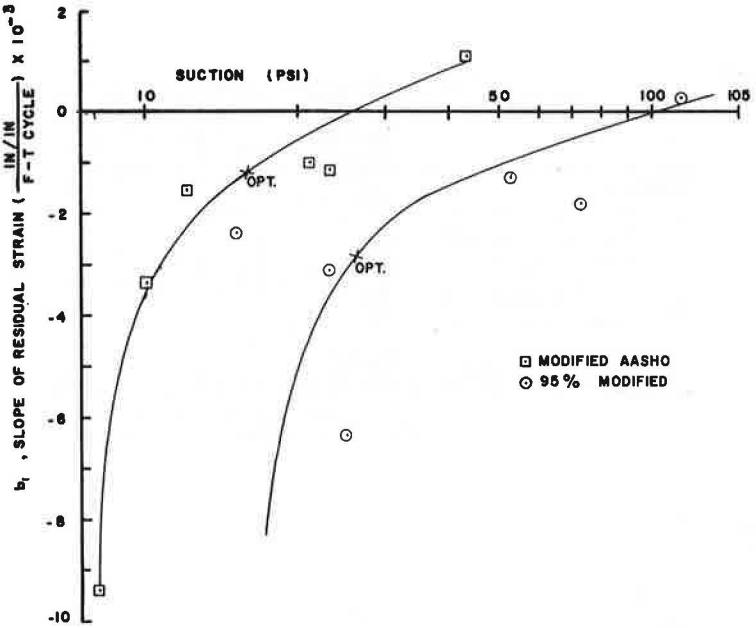

Figure 8. Suction values during thaw cycle and frozen values for two samples.

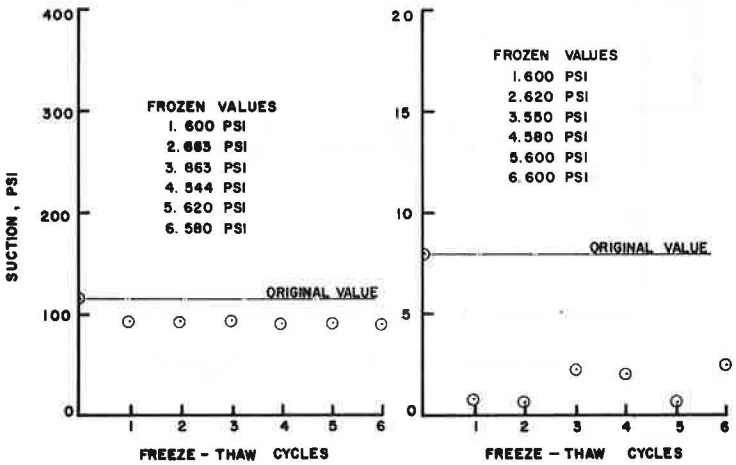

Figure 9. Temperature distributions used in finite element analysis.

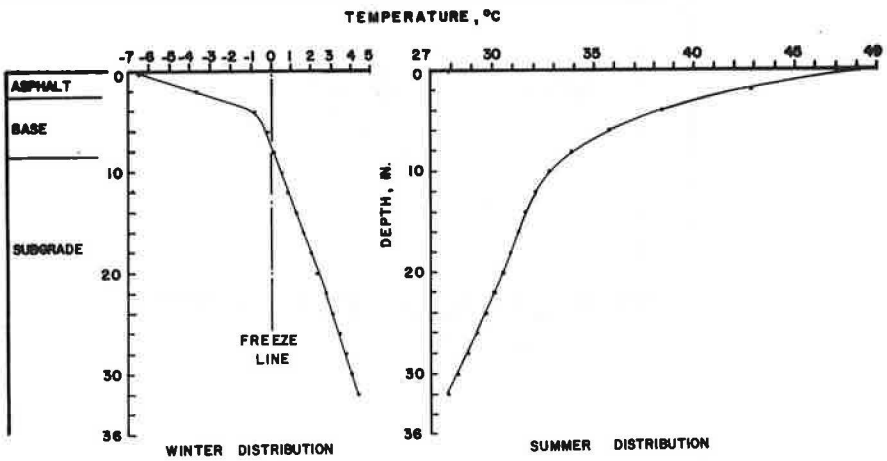

Figure 10. Cross section of pavement and typical values used in finite element analysis.

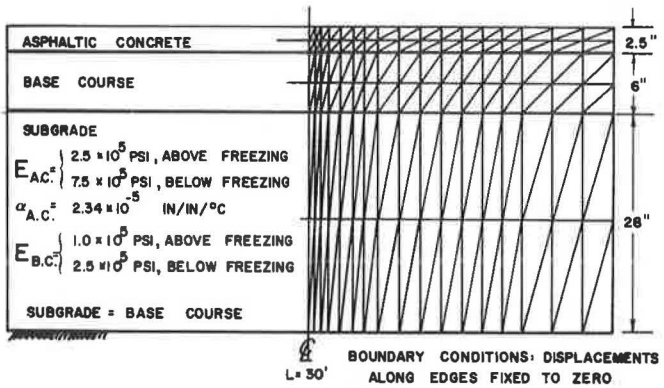

Figure 11. Thermal tensile stresses in asphalt and base course plotted against freeze coefficient of base course.

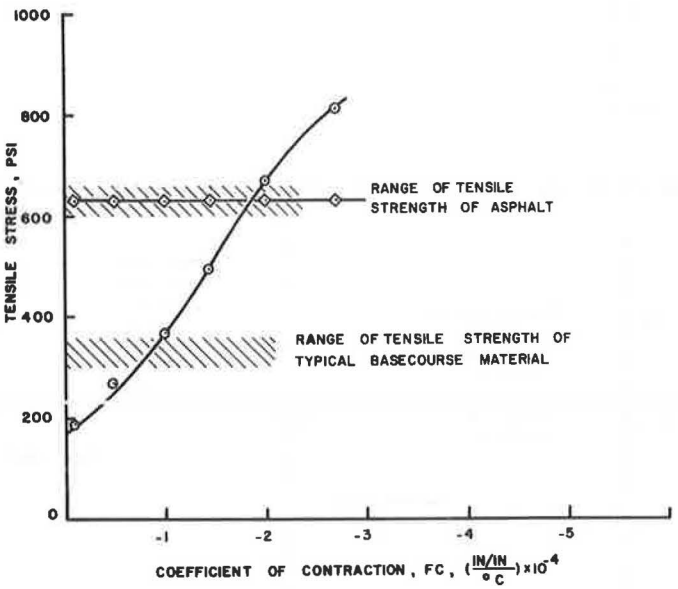

Figure 12. Residual stresses in asphalt concrete due to volume change for four freeze-thaw cycles.

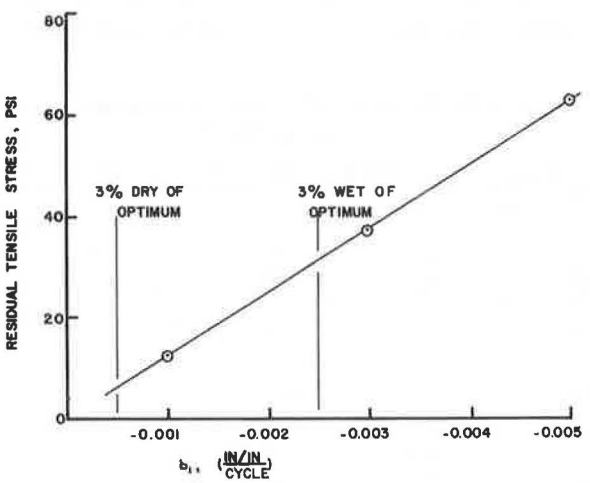

freeze-thaw cycle. As there may be several freeze-thaw cycles, which extend into the base curing during any winter, the total change in volume could be appreciable. This action may induce residual tensile stresses in the asphalt concrete.

Typical values of residual volume change were converted to strains, assuming isotropy. These strains were then used in the previously mentioned finite element code to predict stresses. Figure 12 shows induced tensile stresses in the asphalt concrete plotted against the residual constants for various samples compacted near optimum moisture. These values of b_1 represent samples covering a range of 3 percent dry of optimum to 3 percent wet of optimum. This shows that after a winter there will be some residual stress left in the pavement structure. These stress levels, while not high enough to crack the asphalt concrete, will serve to reduce the life of the pavement. This result assumes the base course and the asphalt concrete remain bonded together.

CONCLUSIONS AND RECOMMENDATIONS

This study deals with the environmental deterioration of pavements in west Texas due to freeze-thaw. Previous models have not considered base course material as an important cause of transverse cracking due to temperature cycles or extremes. The mechanisms involved in pavement cracking in west Texas are better explained by the thermal activity of the base course material than by the properties of asphalt concrete surfaces. Data presented in this study clearly show that the base course is active when undergoing freeze-thaw cycling. Any analysis of pavement cracking due to low temperature or thermal fatigue should include a characterization of the base course.

The base course material is much more thermally active, than the asphaltic concrete. The calculated freezing coefficients possessed a unique relationship with the total soil moisture suction. The freezing coefficients for the base course material produced the tensile stresses produced by the coefficients in the base were greater than tensile strengths, but stresses in the asphalt concrete were of the same order of magnitude as typical tensile strengths. Thus, during a freeze, the base course would be likely to crack before the asphalt.

Soil moisture suction was selected to describe the behavior of the material during freeze-thaw cycling because it required no extensive experiments to determine the quantities that are reflected in the influence of grain size, pore size, particle structure, clay mineralogy of a sample, and the energy state. It was also found that the level of compaction effort produced a difference in thermal behavior: Increased compaction may increase freeze contraction while it reduces the residual contraction. Thus, an increase of compactive effort will reduce the likelihood of damage due to freeze-thaw cycling but will increase the likelihood of tensile cracking due to a single hard freeze.

A more theoretically correct analysis would include the viscoelastic behavior of the asphalt concrete and base course. Inclusion of this behavior would show stress relief in the pavement caused by the time between temperature extremes. This stress relief would be far greater in the asphalt concrete than in the base course and, therefore, would not seriously affect the conclusions regarding the freeze behavior of the pavement during freeze-thaw. However, the residual stress levels in the asphalt would be overpredicted by the analysis used in this study.

Studies concerning additives that reduce the thermal activity of frost-susceptible materials should be applied to the base course to limit thermal activity and thereby to reduce the chance of cracking in the base course, which would readily reflect through the asphalt concrete surface.

This analysis has concerned itself mainly with the effect of freeze-thaw on the formation of transverse cracks. Although the formation of longitudinal cracks is not addressed directly, it is explainable by the data presented. As the base course shrinks during a freeze to cause transverse cracking, it will also contract inward from the shoulders, and tensile stresses will develop in the base course as a result of the restraint offered by the asphalt concrete surface. These tensile stresses will produce

longitudinal cracking if they exceed the tensile strength, which could then reflect through the asphalt concrete to the surface. Thus, longitudinal cracking may be related to an environmental factor in much the same way as transverse cracking is.

ACKNOWLEDGMENTS

The work in this study was performed for the Texas Highway Department in cooperation with the Federal Highway Administration under a cooperative research program through the Texas Transportation Institute at Texas A&M University.

The contents of this report reflect the views of the authors, who are responsible for the facts and the accuracy of the data presented. The contents do not necessarily reflect the official views or policies of the Federal Highway Administration. This report does not constitute a standard, specification, or regulation.

REFERENCES

1. G. D. Aitchison, ed. Moisture Equilibria and Moisture Changes in Soils Beneath Covered Areas. Butterworths, 1965.
2. A. T. Bergan and C. L. Monismith. Characterization of Subgrade Soils in Cold Regions for Pavement Design Purposes. Highway Research Record 431, 1973, pp. 25-37.
3. Ray W. Brown. Measurement of Water Potential With Thermocouple Psychrometers: Construction and Applications. USDA Forest Service, Research Paper INT-80, 1970.
4. J. T. Christison. The Response of Asphaltic Concrete Pavements to Low Temperatures. Univ. of Alberta, PhD thesis, 1972, pp. 59-60.
5. B. J. Dempsey and M. R. Thompson. A Heat Transfer Model for Evaluating Frost Action and Temperature-Related Effects in Multilayered Pavement Systems. Highway Research Record 342, 1970, pp. 39-56.
6. H. B. Dillon and O. B. Andersland. Predicting Unfrozen Water Contents in Frozen Soils. Canadian Geotechnical Journal, Vol. 3, No. 2, 1966, pp. 53-60.
7. J. J. Hajek and R. C. G. Haas. Predicting Low-Temperature Cracking Frequency of Asphalt Concrete Pavements. Highway Research Record 407, 1972, pp. 39-54.
8. A. B. Hamilton. Freezing Shrinkage in Compacted Clays. Canadian Geotechnical Journal, Vol. 3, No. 1, 1966, pp. 1-17.
9. K. A. Jackson and B. Chalmers. Freezing of Liquids in Porous Media, With Special Reference to Frost Heave in Soils. Journal of Applied Physics, Vol. 29, No. 8, 1958, p. 1178.
10. R. W. R. Koopmans and R. D. Miller. Soil Freezing and Soil Water Characteristic Curves. Proc., Soil Science Society of America, Vol. 30, No. 6, Nov.-Dec. 1966, pp. 680-685.
11. G. W. Lovell and M. Herrin. SIPRE Report 9. SIPRE, U.S. Army Corps of Engineers, 1953.
12. P. F. Low and C. W. Lovell. The Factor of Moisture in Frost Action. HRB Bulletin 225, 1959, pp. 27-39.
13. N. W. McLeod. Influence of Hardness of Asphalt Cement on Low Temperature Transverse Pavement Cracking. Canadian Good Roads Association, Montreal, 1970.
14. A. J. Peck. Theory of the Spanner Psychrometer: The Thermocouple. Agricultural Meteorology, Vol. 5, 1968, pp. 433-447.
15. A. J. Peck. Theory of the Spanner Psychrometer: Sample Effects and Equilibrium. Agricultural Meteorology, Vol. 6, 1969, pp. 111-124.
16. S. L. Rawlins. Theory for Thermocouple Psychrometers Used to Measure Water Potential in Soil and Plant Samples. Agricultural Meteorology, Vol. 3, 1966, pp. 292-310.

17. B. G. Richards, H. W. Murphy, C. Y. L. Chan, and R. Gordon. Preliminary Observations on Soil Moisture and Dry Compaction in Pavement Design on the Darling Downs, Queensland. Proc., Australian Road Research Board, Vol. 5, Part 5, 1970, pp. 116-146.
18. B. G. Richards. Psychrometric Techniques for Measuring Soil Water Potential. CSIRO, Division of Soil Mechanics, Technical Rept. 9, 1969.
19. M. Y. Shahin and B. F. McCullough. Prediction of Low-Temperature and Thermal Fatigue Cracking in Flexible Pavements. Center for Highway Research, Austin, Texas, Research Rept. 123-14, Aug. 1972.
20. P. J. Williams. Unfrozen Water Content of Frozen Soils and Soil Moisture Suction. Geotechnique, Vol. 4, No. 3, 1964, pp. 231-246.
21. R. N. Yong. Soil Suction Effects on Partial Soil Freezing. Highway Research Record 68, 1965, pp. 31-42.
22. Non Traffic Load Associated Cracking of Asphalt Pavements Symposium. Proc., Association of Asphalt Paving Technologists, Vol. 35, 1966.

ENGINEERING PROPERTIES OF COMPACTED CLAY CONDITIONED BY SATURATION AND FREEZE-THAW CYCLES

Charles A. Pagen,* Mobil Research and Development Corporation; and
Vijay K. Khosla,* Herron Testing Laboratories

This research quantitatively evaluates the effect of saturation and freeze-thaw cycles on the rheological characteristics of a compacted subgrade. Kaolin samples compacted by 25, 40, and 80 blows of a drop hammer were tested over a wide range of moisture contents and densities. The failure and rheological parameters investigated that relate to soil strength are unconfined compressive strength, modulus of elasticity, creep modulus, and complex elastic modulus. Laboratory compacted samples were saturated under controlled boundary stress conditions in a specially designed chamber and were then subjected to nine freeze-thaw cycles before testing. Results show that volumetric swelling, although less than the volume of absorbed water, increases as compaction energy increases and that soil structure also changes under saturation and freeze-thaw cycles. Rheological parameter values seem to be independent of the compaction energy levels used. Results also show that compacted cohesive subgrades exposed to saturation and freeze-thaw cycles in the field will experience major reductions in load-carrying capacity. Therefore, it is recommended that the design of rigid and flexible pavements over cohesive subgrades for areas in which cyclic freezing and thawing occurs should focus greater attention on providing adequate subgrade drainage so that initial saturation of the subgrade is minimized.

•SUBGRADE soils under roadway service conditions frequently experience increases in the degree of saturation because of the capillary rise of groundwater or the infiltration of surface waters. Experience indicates that an increase in moisture content is accompanied by a reduction in dry-unit weight and a coincidental loss of soil strength. This problem is further complicated by seasonal variations in climate. When the ambient temperature falls below freezing, the moisture within the upper reaches of the soil mass freezes and results in a volume increase and the development of ice lenses within the soil matrix, which are reflected as a loss of strength. Of even greater significance to the function and maintenance of highways and airfields is the loss of subgrade strength, which occurs during thaw. As ambient temperatures rise, thawing of the subgrade progresses from the surface downward. Free water from the thawed ice cannot easily drain downward because of the underlying ice barriers, and, in the absence of adequate drainage facilities, it produces highly saturated conditions in the upper parts of the soil and significant loss of strength (5). Consequently, pavement failures frequently occur during the spring thaw as a direct result of the loss of strength of the underlying base course or subgrade soils.

This paper deals specifically with the effects of saturation and subsequent freeze-thaw cycles on the strength characteristics of cohesive pavement subgrades. The

Publication of this paper sponsored by Committee on Frost Action.

*This paper is based on work performed while the authors were with the Ohio State University.

system in which the compacted soil subgrade is first saturated and is then subjected to cyclic freeze-thaw conditions will be designated saturated closed. This system has been used in the laboratory to simulate the complex conditions of adverse water and freezing temperatures affecting subgrade soils in the field. Similar techniques have been used to condition soils to saturation and freeze-thaw cycles in other research programs to evaluate the influence of frost action on compacted soil (17, 18).

OBJECTIVE AND SCOPE

Physical properties such as moisture content and density can be used to analyze the efficiency of the soil compaction process but cannot be directly incorporated in the pavement design methods (10). To realistically define the true nature of soil support, an engineer must know the effects of these parameters on the engineering properties of the soil. Why physical properties fail to give the desired information or even may lead to wrong information has been well demonstrated by Seed and Chan (13). Their investigation showed that, although the same density can be achieved at different moisture contents, the engineering properties will not be the same: Soils compacted to a given density at different moisture contents may exhibit different engineering properties depending on the method of compaction used and the resulting soil structure developed. Considering that physical properties cannot fully satisfy the requirements for pavement design and performance evaluation, a question about other limiting engineering properties that need to be selected has been raised (8, 9). Attempts to answer this question were made by treating the compacted subgrade as a linear viscoelastic material (most traffic loads fall within this range of subgrade materials) (8, 10, 11). The viscoelastic properties can be evaluated by selected rheological tests that are all interrelated by the viscoelastic theory.

An earlier publication (10) used concepts of the viscoelastic theory to investigate the effect of freeze-thaw cycles on the failure and rheological strength parameters of compacted kaolin. We have used these concepts to further evaluate the effect of simulated highway environmental conditions on the engineering properties of compacted soils.

The failure and rheological strength parameters used include the unconfined compressive strength, $\sigma'c$; modulus of elasticity, E; creep modulus, Ec; and complex elastic modulus, $|E^*|$. The unconfined compression test was used to obtain $\sigma'c$ and E, and the unconfined creep test was used to evaluate Ec and $|E^*|$. $|E^*|$ was evaluated by converting the axial creep response of the soil in the time domain to the frequency domain by using Fourier transformations (10).

This investigation was to study the effect of initial compaction energy, molding moisture, content, and degree of saturation on the engineering properties of soils exposed to temperature-induced cyclic freezing and thawing. The fundamental rheological strength parameter used in the study is the linear viscoelastic moduli. This parameter can, more realistically, evaluate the true in-service, stress-strain characteristics and load-carrying capacity of compacted highway subgrades.

MATERIALS AND SAMPLE PREPARATION

Because of its uniformity, low-level swelling characteristics, and absence of thixotropic effects, kaolin was selected to evaluate the effect of compaction, saturation, and freeze-thaw cycles on the rheological characteristics of soil.

Soil samples $1\frac{5}{16}$ in. (3.33 cm) wide and 2.816 in. (7.153 cm) high (Harvard size) were prepared by using the Ohio State University standard drop hammer compactor that has a 3.62-lb (1.64-kg) hammer and a 10-in. (25.4-cm) drop as measured from the top of the sample (7, 10). All samples were prepared by compacting the soil in five layers of equal weight and by applying the desired number of drop hammer blows. The compacted samples were wrapped in plastic bags, completely coated with wax, and stored in a humid room for several days so that they could develop a homogeneous

distribution of moisture throughout. The samples were then conditioned under stringently controlled boundary stress conditions.

Preliminary studies were to select the duration for saturating the soil specimen under controlled boundary stress conditions that simulated a stress field within the subgrades immediately underlying the pavement. Thompson and Thomas (14) suggested a ratio of lateral to vertical stress, K_o, of 0.4. Jaky (3) has shown that K_o can be obtained by the relationship

$$K_o = 1 - \sin \phi$$

where ϕ is the angle of internal friction of the soil. In this relationship $K_o = 0.62$ for the kaolin; a value of 0.6 for K_o was used for the study.

The saturation of the samples was carried out until a steady state degree of saturation of 97 to 98 percent was achieved. Figure 1 shows a plot of the degree of saturation versus time (in days) for a soil sample that had an initial moisture content of 23 percent and that was prepared by drop hammer compaction energy of 40 total blows. Figure 1 shows that the compacted soil will attain 97 to 98 percent saturation within 12 to 18 hours; however, at such saturations the soil swelled excessively, and the resulting moisture content was close to its liquid limit.

Creep data indicated flow characteristics, and nonlinear behavior at test conditions with low stress levels was observed. The test is extremely critical and, in our opinion, does not represent normal highway subgrade conditions. Therefore, so that the complex freezing and thawing phenomenon existing in the field could be approximated, the specimens were saturated to a constant moisture content of 35 to 36 percent, which is close to the plastic limit of the soil. Usually it takes 8 hours or more to attain this moisture state in the saturation device.

The following procedure was adopted to saturate the samples by using specially designed equipment shown in Figures 2 and 3:

1. The sample stored in the humid room is weighed, and the weight recorded.

Figure 1. Degree of saturation versus time in capillary saturation device for identical specimens.

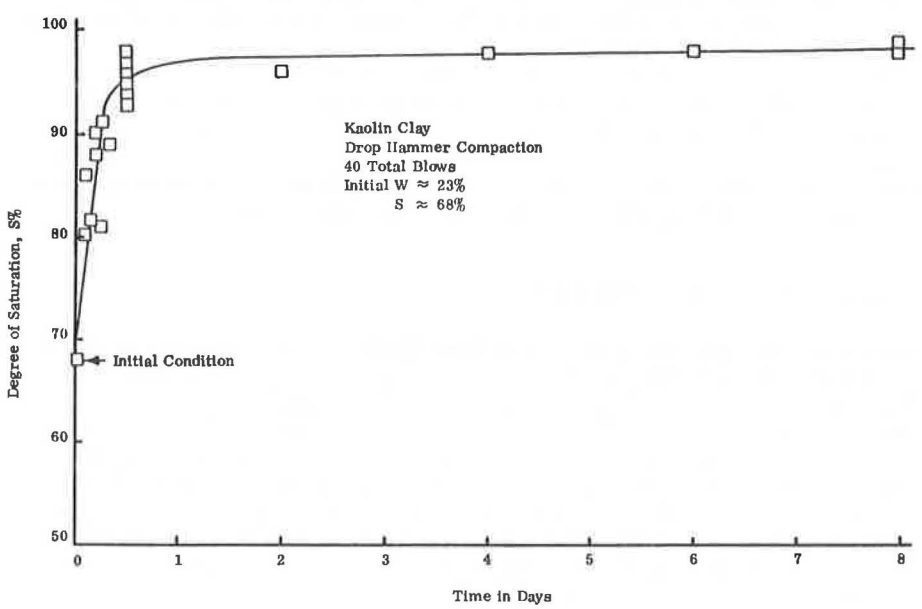

Figure 2. Capillary saturation device for boundary stress conditions.

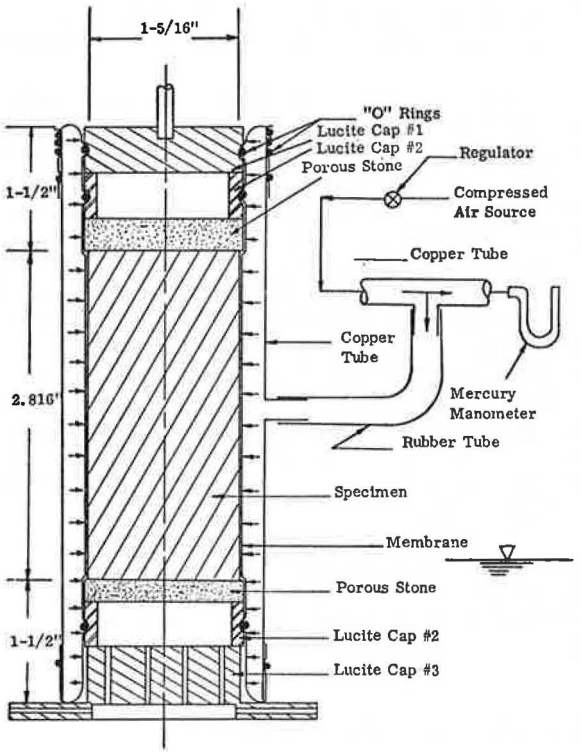

Figure 3. Details of capillary saturation device.

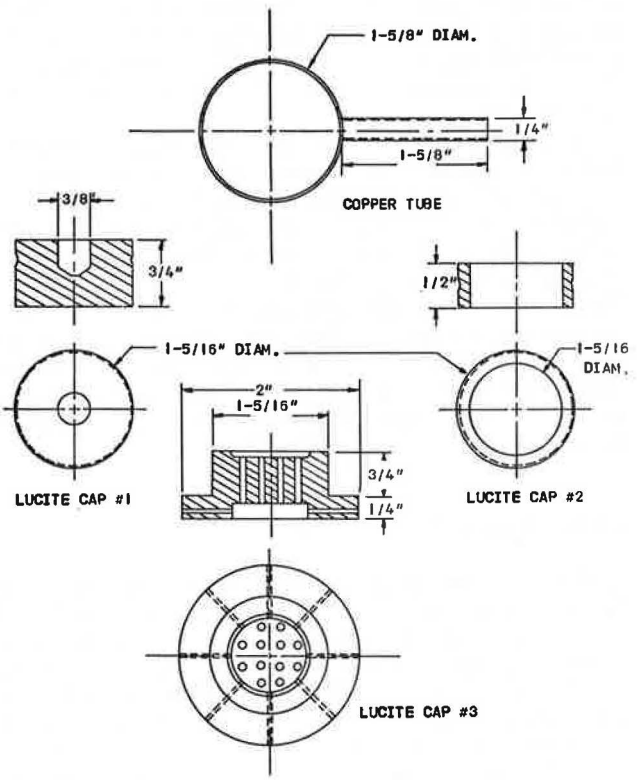

2. The final expected wet weight of the soil specimen is determined and recorded.
3. A stretched membrane on the tube is rolled back, and rubber O-rings are slipped over it.
4. The test specimen, saturated porous stones, and Lucite caps are introduced into the copper tube as shown in Figure 2, and the setup is placed in a tray filled with distilled water to a level about 0.25 in. (0.04 cm) higher than the lower end of the test specimen.
5. Lateral and axial pressures of 1.2 and 2.0 psi (8.3 and 13.8 kPa) are applied respectively to give $K_o = 0.6$.
6. Each end of the sample is exposed to half of the total time required to achieve selected saturation by switching caps 3 and 1, and the copper tube is carefully inverted. Any discrepancy in the final weight is adjusted either by saturating for additional time or by drying.
7. Subsequent to saturation, the sample is wrapped in a plastic bag, is sealed with wax, and is placed in the humid room so that it can be uniformly moisturized.
8. Each specimen is subjected to nine freeze-thaw cycles (10); the freeze cycle consists of 7 hours at a constant temperature of -20 F (-28.9 C), and the thaw cycle occurs overnight in the humid room. The last thaw cycle before creep testing is at least 2 days long.

The system used to condition the soil samples in the laboratory is an approximation of the complex clay-water-temperature system as it exists in nature. Such systems are often used to determine the engineering properties of soils for pavement designs (17, 18).

EXPERIMENTAL PROCEDURE

Unconfined creep and unconfined compression tests were used to find the rheological and strength parameters of a standard soil. The unconfined compression test is used to measure the undrained shear strength. The test was performed according to ASTM D2166-63T at a strain rate of 2.82 percent/min (0.2 cm/min for samples 7.15 cm high). Unconfined compressive strength and modulus of elasticity were also evaluated with this test.

For rheological creep tests, the test procedure consisted of cycling the axial load twice through the load and unload cycle to condition the samples. The third cycle (steady state condition for kaolin) was used to obtain the experimental data and consisted of 30 min of loading and 30 min of creep recovery in the unloaded state (10). Axial strain data, as a function of time, were used to calculate Ec and $|E^*|$ by transferring the experimental results from the time domain to the frequency domain (10). Based on viscoelastic linearity tests, 3.75 psi (25.9 kPa) was used as the axial stress for all creep tests. In the data analysis, $|E^*|$ corresponding to a frequency of $w = 0.1$ rad/s (vehicle speed of 0.065 mph or 0.1 km/h) was selected because subgrade materials loaded by low-speed traffic, as in parking areas, will exhibit greater deformations and fail earlier than high-speed roadway sections of equal design under the same traffic load and environmental conditions.

EXPERIMENTAL RESULTS

Widely used soil parameters such as dry density, unconfined compressive strength, penetration-needle resistance, and California bearing ratio, although convenient, do not exactly reflect the true stress-strain characteristics of the in-service conditions of the compacted soil because they are greatly influenced by environmental and loading conditions. These criteria also are not directly or fundamentally related to the strength and deflection parameters used in the structural design of rigid or flexible pavements; however, rheological parameters seem to describe the soil characteristics more rationally than many parameters currently used.

Moisture content of the subgrade does not generally remain constant subsequent to placement of a pavement, but, with the passage of time, it may increase because of (a) infiltration of rainwater through the permeable surface of the pavement, through cracks in the pavement surface, or at the pavement edges; (b) movement of the liquid or vapor from the water table; and (c) a high water table during the spring months or floods. Though it is possible to reduce the amount of infiltration to a great extent by proper design, most subgrade materials may reach an equilibrium moisture content quite in excess of their initial moisture contents. Final moisture content depends on factors such as soil type, initial moisture content and density, topography, compaction energy, type of compactor, and soil structure.

An increase in the moisture content can cause considerable loss of subgrade strength and support. Greater losses will occur if an increase in the moisture content is followed by periodic freezing and thawing conditions. Therefore, to study the changes in the rheological parameters under these conditions is significant. So that these conditions could be simulated in the laboratory, the as-molded soil samples were saturated to a final moisture content of 35.5 ± 0.5 percent under boundary conditions to produce $K_o = 0.6$, and then were subjected to nine freeze-thaw cycles, as determined from the preliminary studies (10).

Three compaction energy levels of 25, 40, and 80 blows with moisture contents ranging from about 22 to 32 percent were used. Specific molding moisture contents used for each compaction energy level were 22, 25, 29, and 32 percent for 25 and 80 blows; and 22, 25, 26, 29, and 33 percent for 40 blows. The moisture-dry density relationship for kaolin for various compactive efforts is shown in Figure 4.

The experimental results are discussed in the following two sections.

Effects of Saturation

The effect of saturation on swelling characteristics of soils has been investigated by many researchers (1, 2, 4, 6, 12, 13, 16). Ladd (4) points out that swelling characteristics are influenced significantly by (a) clay composition; (b) compaction conditions, i.e., molding water content, dry density, degree of saturation; (c) compaction method; (d) chemical properties of pore fluid; (e) confining pressure; and (f) time allowed for swelling. In this study, with the exception of compaction variables, all parameters were kept constant.

According to Ladd (4), clays compacted at a lower water content, at which the water deficiency in the double layer is high and the degree of saturation is low, will often swell more than clays compacted at a high water content. Lamb (5) points out that swelling based on water inhibition is due almost entirely to an increase in the size of the micelle. Therefore, because clays compacted on the dry side of optimum have a greater water deficiency (water needed to fully develop the double layer) than soils compacted on the wet side, the samples compacted on the dry side of optimum, in the presence of water, would be expected to swell more than those on the wet side of optimum.

According to Seed, Chan, and Lee (13), swelling can be caused not only by osmotic pressures but also by compression of air in the voids as water permeates the soil material. This compression of air is able to produce sufficient pressure to cause an expansion of the soil mass, particularly when the soil structure is too weak to withstand these pressures (Fig. 5). Two observations can be made from Figure 5: (a) Volumetric swelling is always less than the volume of absorbed water; therefore, an increase in the degree of saturation must occur; and (b) for the same water pickup, volumetric swelling increases with an increase in compaction energy (an indication of increase in soil density).

Samples prepared with higher compaction energies have less air voids than those prepared with lower compaction energies. Consequently, for the same amount of water, compression of air will produce greater pressure in samples with low air voids than in samples with high air voids. Physicochemical phenomena and compression of air, however, occur concurrently, and both are significant for producing swell

Figure 4. Dry unit weight versus moisture content for drop hammer compaction.

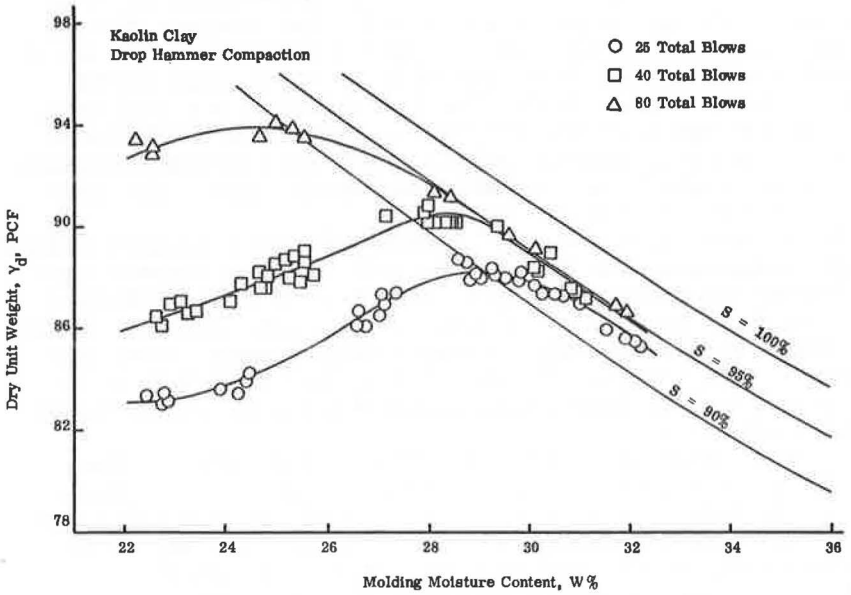

Figure 5. Relationship of volumetric swelling and water pickup for soaking to plastic limit under boundary stress conditions.

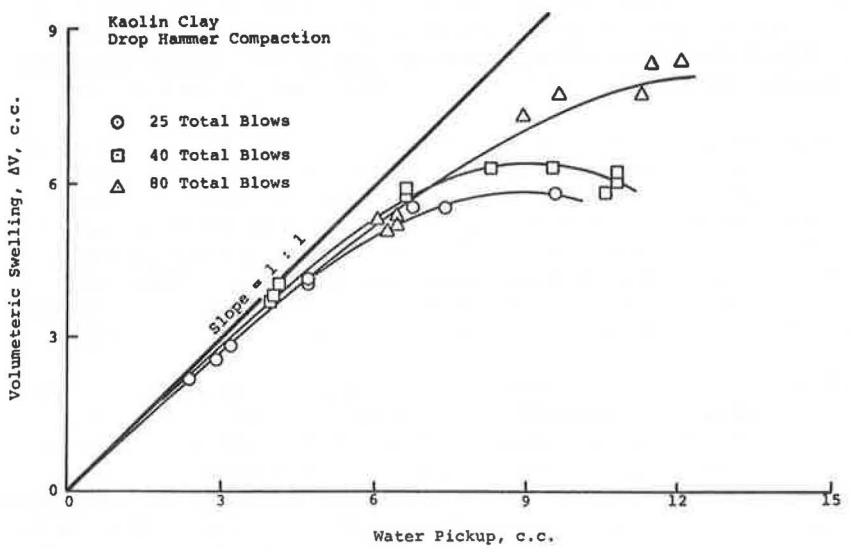

in compacted clays. Figure 6 shows the percentage of volumetric change after saturation versus initial moisture content for three levels of compaction energy. The results from Figures 5 and 6 substantiate the findings of other investigators that for any given dry density swelling decreases with increasing molding water content, whereas for any given molding water content the swelling increases with increasing density (an indication of increase in compaction energy). This conclusion is true mainly on the dry side of optimum because at higher moisture contents on the wet side of optimum the effect of compaction energy is practically negligible (Fig. 4).

From the standpoint of swelling characteristics, although it appears that compacting on the wet side of optimum will be beneficial, it is well known that such water contents will produce compacted materials with lower strength and higher compressibilities. Therefore, the choice of desired molding water content and dry density for a given method of compaction cannot be made merely from a single criterion such as lower swelling characteristics. The final decision should be based on criteria that will ensure a workable range for volume-change and stretch characteristics. This brings us to the effect of saturation and freeze-thaw cycles on the failure and rheological strength parameters of compacted clays.

Effects of Saturation and Freeze-Thaw Cycles

For the design of either rigid or flexible pavements, the modulus of elasticity and complex elastic modulus are the critical factors because they control serviceability, deformation characteristics, and the design thickness of the various structural components of a pavement. Thus, for most economical and structurally safe design, it becomes imperative that the variation of the rheological parameters and changes in the moisture content or degree of saturation be thoroughly investigated.

Figures 7 through 14 show plots of variations in the strength parameters, $\sigma'c$, E, Ec, and $|E^*|$, and initial moisture content and degree of saturation. Because of large scatter indicated on these plots, all data points can generally be approximated by one curve representing an average value, or they can be accommodated within a small band. This indicates that, for samples tested in the saturated closed system, the level of compaction energy does not appreciably affect the soil strength and that only molding moisture content or degree of saturation controls the behavior.

We contend that the large scatter is caused by significant disturbance in the as-compacted soil structure as a result of adverse environmental conditions of saturation and subsequent freeze-thaw cycles.

Studies at Constant Initial Molding Water Content

Figures 7 through 10 show that the in-service creep modulus, modulus of elasticity, and complex elastic modulus of a conditioned-soil roadway decrease with an increase in the initial molding moisture content and that the unconfined compressive strength at failure shows a marginal increase for moisture contents to the dry side of the optimum.

Studies at Constant Initial Degree of Saturation

A given moisture content may be on the dry side of optimum for low levels of compaction energy and on the wet side of optimum for high levels of compaction energy. If one studies the response of the soils at a constant degree of saturation, this drawback can be avoided. Therefore, the variation of the selected strength parameter due to a range of compaction energy inputs was also studied at a constant degree of saturation (Figs. 11-14). Variations in the failure and the rheological parameters of the conditioned samples with initial degree of saturation indicate that, up to initial saturations of about 90 to 95 percent, these parameters for all practical purposes do not reflect

Figure 6. Percentage of volumetric change versus initial molding moisture content.

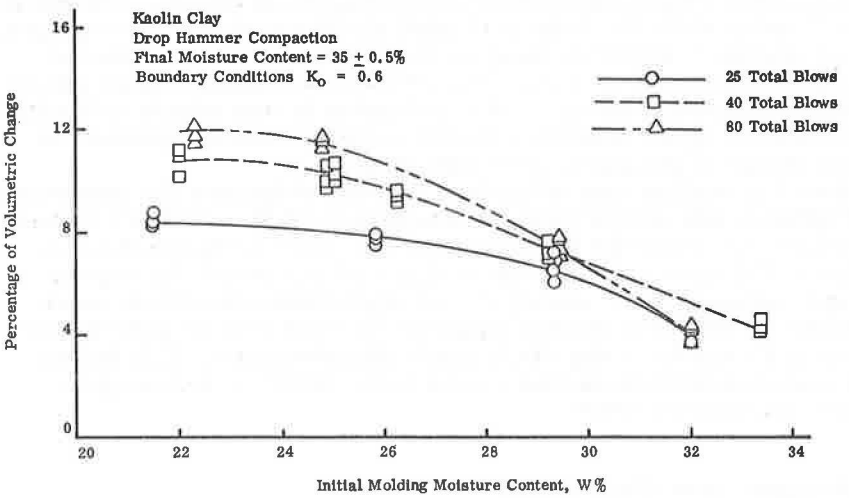

Figure 7. Unconfined compressive strength versus initial molding moisture content.

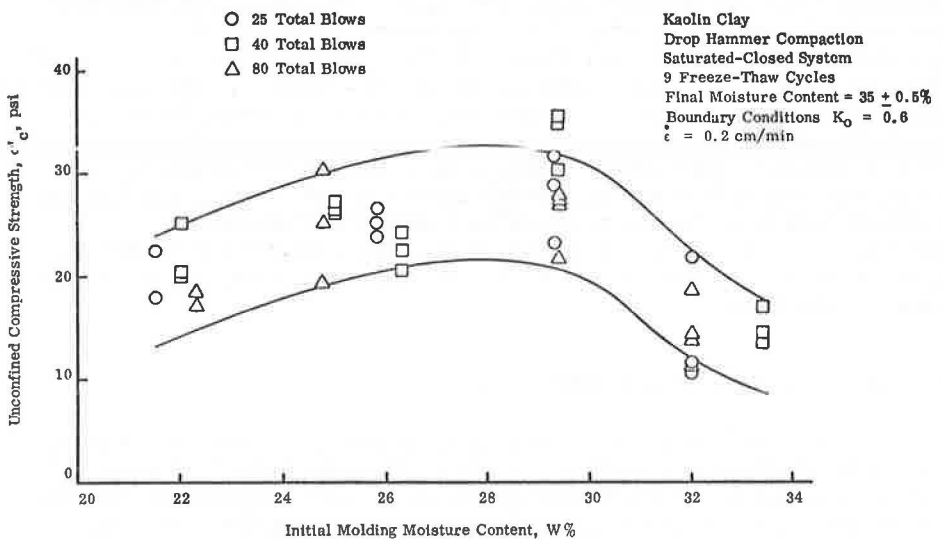

Figure 8. Modulus of elasticity versus initial molding moisture content.

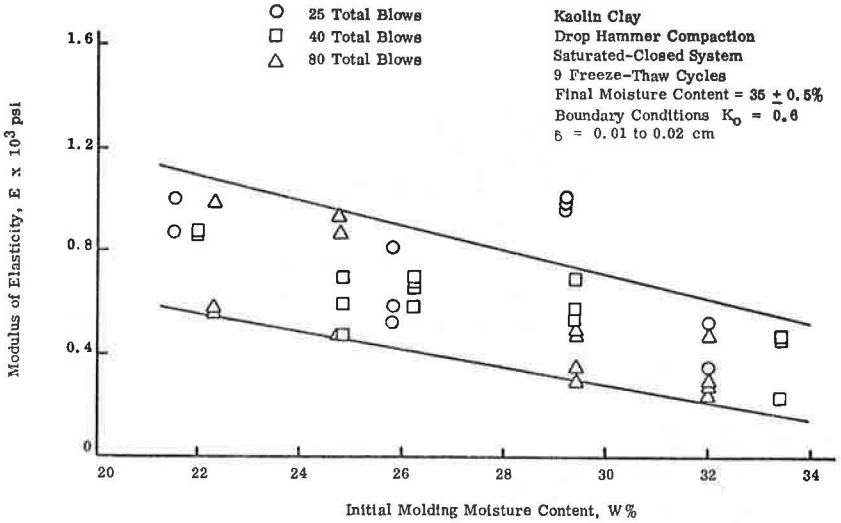

Figure 9. Creep modulus versus initial molding moisture content.

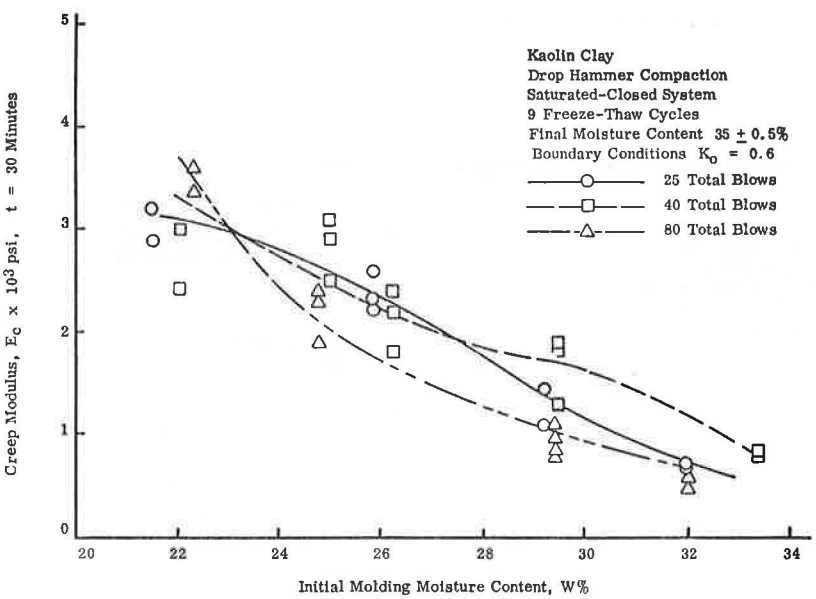

Figure 10. Magnitude of complex elastic modulus versus initial molding moisture content.

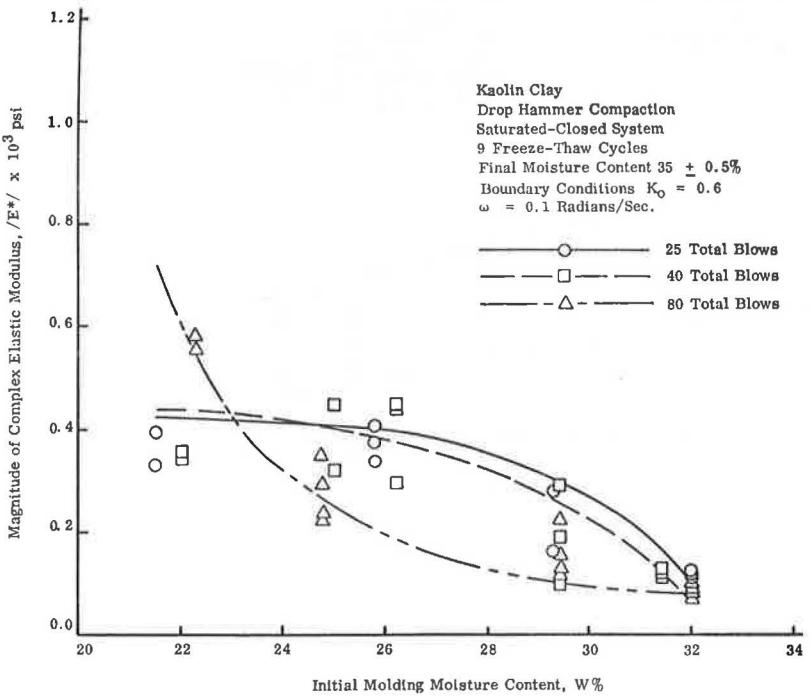

Figure 11. Unconfined compressive strength versus initial degree of saturation.

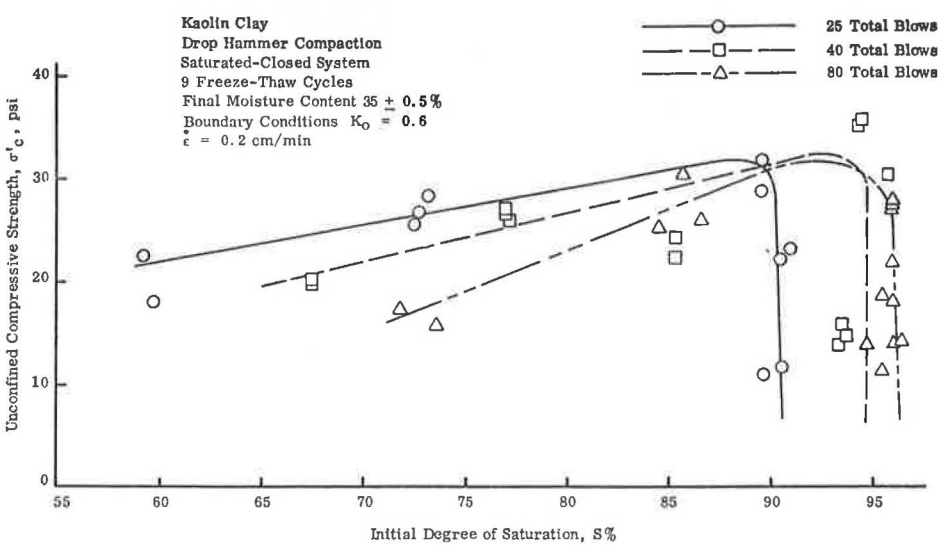

Figure 12. Modulus of elasticity versus initial degree of saturation.

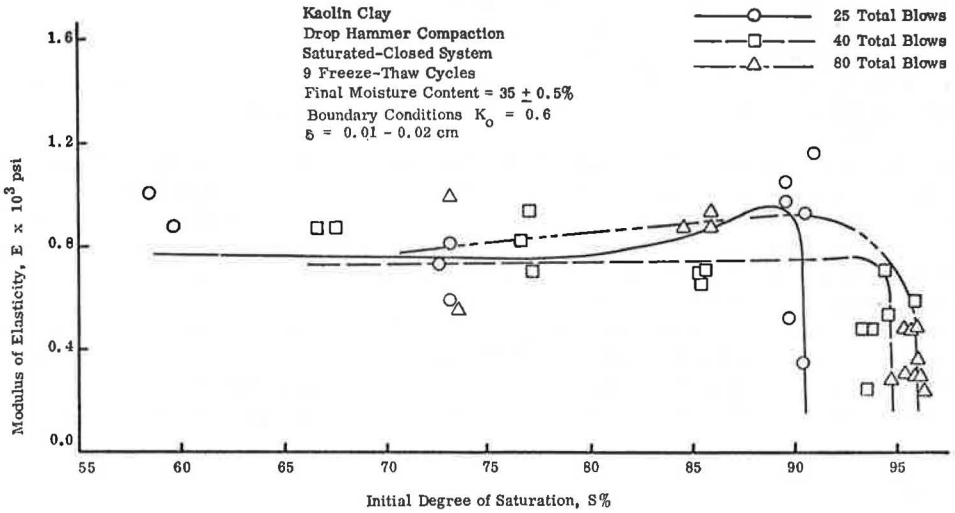

Figure 13. Creep modulus versus initial degree of saturation.

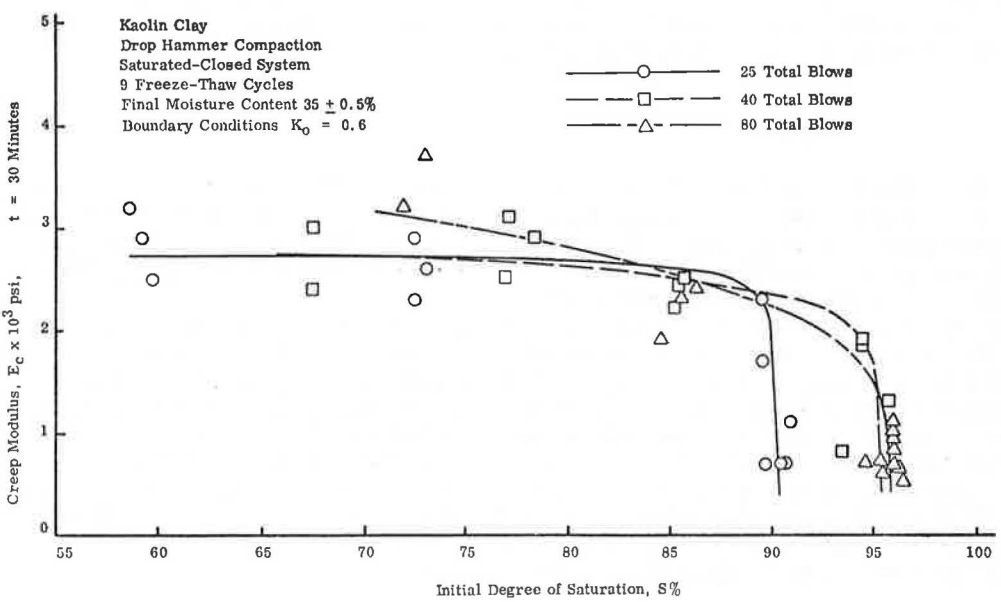

any major changes in their value (the lower limit corresponds to compaction energy of 25 blows, and upper limit to 40 and 80 total blows). Beyond these limits, soil strength falls suddenly and approaches its minimum. Before the limits of 90 or 95 percent initial saturations are achieved, some strength parameters might show a little increase or decrease, but this change is not of any consequence when it is compared to the overall drastic effects of conditioning the compacted samples by saturation and freeze-thaw cycles.

The adverse effects of saturation and freeze-thaw cycles on conditioning compacted subgrade can be better understood by comparing the results of as-compacted state (11) with those of the closed system (10) (in which as-compacted samples were tested after nine freeze-thaw cycles) and with those of the saturated-closed system. This analysis is given in Tables 1 and 2 for 25 and 40 drop hammer blows respectively.

The comparison of the different compaction conditions is not exactly at either a constant molding moisture content or a constant degree of saturation; therefore, discrepancy arises from preparing samples at different times. However, the data indicate that these variations will not significantly affect the overall comparison. The data further indicate the following for the closed system and saturated-closed system.

Closed System

For the closed system, major loss of stretch occurs for conditions on the wet side of the optimum. On the dry side of optimum, the loss of strength is less than about 10 percent, but, while on the wet side at higher moisture contents, strength loss can be as great as 80 percent. The loss, however, seems to decrease with an increase in the compactive effort. The parameter values achieved for the saturated-closed system are also equal to or smaller than those for the closed system for higher molding moisture contents on the wet side of optimum.

Saturated-Closed System

For the saturated-closed system, over most of initial moisture contents investigated, strength loss from about 75 to 90 percent of the as-compacted state occurs. The loss increases somewhat as the compactive effort increases, which directly reflects that, during saturation, volumetric swelling (an indication of reduction in unit weight) increases as the compactive effort increases.

Conclusions for failure strength parameters also hold for rheological parameters of E, Ec, and $|E^*|$. The loss of bearing capacity caused by saturation and freeze-thaw cycles has been reported by Townsend and Csathy (15) who observed a loss in strength as great as 70 percent. In the field, however, this loss in stability may decrease as thawing continues, and shear strength or bearing capacity may approach previous values of the closed system. Regaining strength will be significantly affected by the final state of the compacted soil structure before it is damaged by factors such as saturation and freeze-thaw cycles; frequency of such cycles; reduction in saturation, which will be directly influenced by draining ability of the subgrade soil; and the frequency and intensity of traffic during the thawing period.

PAVEMENT DESIGN CONSIDERATIONS

In the field, soils are seldom compacted at saturations less than about 80 percent. As such, more emphasis should be placed on investigating the changes in the rheological strength parameters of the pavement subgrade at saturations exceeding this limit. As noted, for saturations in excess of about 85 percent both the failure and the rheological parameters for the saturated-closed system drop to values between about 10 and 25 percent of the as-compacted state. This reflects proportionate reduction in the load-carrying capacity. If such conditions are allowed to develop in the field, they will

Figure 14. Magnitude of complex elastic modulus versus initial degree of saturation.

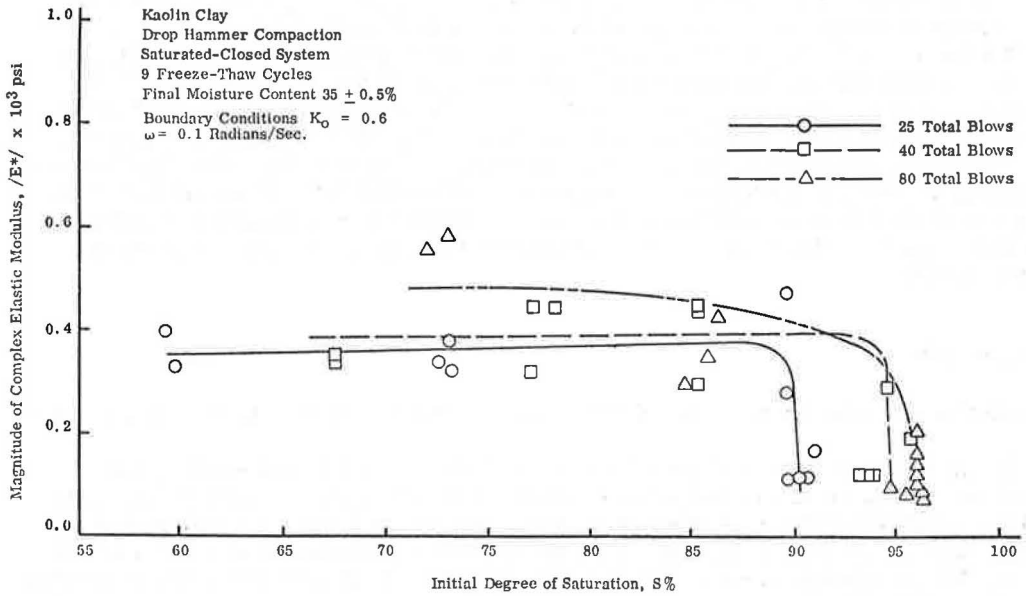

Table 1. Comparison of strengths in as-compacted state, closed system, and saturated-closed system for 25 drop hammer blows.

As-Compacted State		Closed System		Saturated-Closed System		Unconfined Compressive Strength (psi)			Ratio of Closed System to As-Compacted State (percent)	Ratio of Saturated-Closed System to As-Compacted State (percent)
Moisture Content (percent)	Saturation (percent)	Moisture Content (percent)	Saturation (percent)	Moisture Content (percent)	Saturation (percent)	As-Compacted State	Closed System	Saturated-Closed System		
22.02	59.5	22.02	59.5	21.5	59.16	135	125.3	20.2	92.80	14.97
25.50	72.5	25.50	72.5	25.8	72.78	156	145.5	26.7	93.24	17.13
29.30	89.1	29.30	89.1	29.2	88.3	147	103.6	35.7	70.47	20.28
32.61	92.0	32.61	92.0	32.0	90.5	80	16.1	14.8	20.11	18.50

Note: 1 psi = 6.9 kPa.

Table 2. Comparison of strengths in as-compacted state, closed system, and saturated-closed system for 40 drop hammer blows.

As-Compacted State		Closed System		Saturated-Closed System		Unconfined Compressive Strength (psi)			Ratio of Closed System to As-Compacted State (percent)	Ratio of Saturated-Closed System to As-Compacted State (percent)
Moisture Content (percent)	Saturation (percent)	Moisture Content (percent)	Saturation (percent)	Moisture Content (percent)	Saturation (percent)	As-Compacted State	Closed System	Saturated-Closed System		
22.09	66.8	22.09	66.8	22.0	67.2	180	173.3	21.7	96.26	12.07
24.72	76.5	24.72	76.5	24.91	77.0	201	182.3	26.4	90.68	13.11
26.24	85.7	26.24	85.7	26.20	85.3	201	167.6	21.4	83.36	10.67
30.24	92.5	30.24	92.5	29.40	94.4	135	38.4	33.6	28.44	24.90

Note: 1 psi = 6.9 kPa.

make a highway or airport pavement practically incapable of supporting heavy traffic loads. Even for the closed system, rapid loss of the carrying capacity of the compacted subgrade was observed for saturations in excess of about 85 percent (10).

On the basis of the reported research results for closed and saturated-closed systems, it is recommended that greater attention be given to the design of pavements constructed over cohesive subgrades in areas where seasonal temperature variations cause cyclic freeze-thaw conditions to occur. The proper design of surface and subsurface drainage facilities would minimize increases in the initial degree of saturation and subsequent loss of strength in the subgrade. Optimizing the soil compaction conditions will also reduce the influence of adverse environmental conditions, improve the pavement performance, and produce subgrades with better in-service strength characteristics.

CONCLUSIONS

The following are concluded for the materials and experimental conditions investigated:

1. Volumetric swelling is always less than the volume of water absorbed, i.e., an increase in the degree of saturation must occur. For any given compactive effect, an increase in saturation of the as-compacted soil state brings about a corresponding volume increase; the amount of increase depends on molding saturation or water content. However, the percentage of volumetric change decreases with increasing initial molding moisture content. In addition, for any given molding moisture content, percentage of volumetric change increases (an indication of reduction in the unit weight) as compactive effort increases.
2. Data indicate that significant changes in as-compacted soil structure may be anticipated when the soil is subjected to saturation and subsequent freeze-thaw cycles. For these simulated critical climate conditions the soil's rheological parameters decrease significantly and are almost independent of the compaction energy levels used.
3. Rheological parameters for saturations up to 90 to 95 percent do not seem to show any significant variations. The parameters values fall suddenly and approach their minimum after these critical saturations.
4. Irrespective of initial molding moisture content or degree of saturation investigated, values of rheological parameters for the saturated-closed system are approximately 75 to 90 percent lower than those of the as-compacted state. These are also equal to or smaller than the parameter values in the closed system for higher molding moisture contents on the wet side of the optimum at which reductions up to approximately 80 percent of the as-compacted state can occur. This quantitatively indicates the severity of environmental conditions where the compacted soil is first saturated and then subjected to freeze-thaw cycles.

ACKNOWLEDGMENTS

This research was sponsored by the Ohio Department of Transportation in cooperation with the U.S. Department of Transportation, Federal Highway Administration. The interest and cooperation of these agencies are gratefully acknowledged. The opinions, findings, and conclusions expressed in this publication are those of the authors and not necessarily those of the Ohio Department of Transportation or the Federal Highway Administration.

REFERENCES

1. W. G. Holtz. Expansive Clays—Properties and Problems. Colorado School of Mines Quarterly, Vol. 54, No. 4, 1959, pp. 89-125.

2. W. G. Holtz and H. J. Gibbs. Engineering Properties of Expansive Clays. Trans., American Society of Civil Engineers, Vol. 121, 1956, pp. 641-677.
3. J. Jaky. The Coefficient of Earth Pressure at Rest. Journal of the Society of Hungarian Architects and Engineers, 1944, pp. 355-358.
4. C. C. Ladd. Mechanisms of Swelling by Compacted Clay. HRB Bulletin 245, 1960, pp. 10-26.
5. T. W. Lamb. Modification of Frost-Heaving of Soils With Additives. HRB Bulletin 135, 1956, pp. 1-23.
6. T. W. Lamb. The Engineering Behavior of Compacted Clay. Journal, Soil Mechanics and Foundations Engineering Division, American Society of Civil Engineers, Vol. 84, No. 2 SM2, 1958.
7. C. A. Pagen and B. N. Jagannath. Fundamentals of Soil Compaction. Engineering Experiment Station, Rept. EES 248-1, Ohio State Univ., July 1966.
8. C. A. Pagen and B. N. Jagannath. Evaluation of Soil Compaction by Rheological Techniques. Highway Research Record 177, 1967, pp. 22-43.
9. C. A. Pagen and B. N. Jagannath. Mechanical Properties of Compacted Soils. Highway Research Record 235, 1968, pp. 13-26.
10. C. A. Pagen and V. K. Khosla. Effect of Freeze-Thaw on Rheological Characteristics of a Compacted Clay. Transportation Research Record 497, 1974, pp. 1-17.
11. C. A. Pagen, B. N. Jagannath, and C. L. Wang. Effect of Compaction and Increase of Saturation After Compaction on the Engineering Properties of Compacted Clay. Engineering Experiment Station, Rept. EES 248-6, Ohio State Univ., July 1968.
12. H. B. Seed and C. K. Chan. Structure and Strength Characteristics of Compacted Clays. Journal, Soil Mechanics and Foundations Engineering Division, American Society of Civil Engineers, Vol. 85, No. SM5, 1958, pp. 87-128.
13. H. B. Seed, C. K. Chan, and C. E. Lee. Resilience Characteristics of Subgrade Soils and Their Relation to Fatigue Failures in Asphalt Pavements. Proc., International Conference on the Structural Design of Asphalt Pavements, Univ. of Michigan, Ann Arbor, 1962, pp. 611-636.
14. L. J. Thompson and J. P. Thomas. Optimization of Clay Subgrade Compaction in Arid Regions. Highway Research Record 91, 1965, pp. 36-47.
15. D. L. Townsend and T. I. Csathy. Soil Type in Relation to Frost Action. Department of Civil Engineering, Queen's Univ., Kingston, Ontario, Canada, Rept. 15, 1963.
16. H. E. Wahls, W. T. Buchanan, G. E. Futrell, and S. P. Lucas. Distribution and Engineering Properties of North Carolina Soils. Highway Research Program, North Carolina State Univ. at Raleigh, Project ERD-110-W, 1964, p. 118.
17. K. Majidzadeh, H. R. Guirguis, and G. G. Ilves. Rapid Method of Subgrade Compaction and Performance Evaluation. Transportation Research Record 501, 1974, pp. 1-13.
18. B. J. Dempsey and M. R. Thompson. Vacuum Saturation Method for Predicting Freeze-Thaw Durability of Stabilized Materials. Highway Research Record 442, 1973, pp. 44-57.

CASE STUDIES OF VARIATIONS IN SUBGRADE MOISTURE AND TEMPERATURE UNDER ROAD PAVEMENTS IN VIRGINIA

N. K. Vaswani, Virginia Highway and Transportation Research Council

Changes in moisture under uncovered ground and in the subgrades of pavements were evaluated. The pavements ranged from new to about 10 years old. Moisture content was determined by a nuclear probe to determine moisture depth. The findings were as follows: (a) the higher the compaction and dry density of the subgrade soil were, the lower the moisture content would be; (b) subgrade moisture content increased sharply from the beginning to the end of construction; (c) for 1 or 2 years from the date of the subgrade construction, moisture content increased because of precipitation and after this time the rate of increase in moisture decreased; and (d) after about 10 years, there was little increase in the subgrade moisture content.

•PAVEMENT strength is greatly influenced by the moisture content of the subgrade. It is, therefore, essential to determine the changes in subgrade moisture and the factors contributing to these changes.

A comparison was made between the results of temperature and moisture measurements taken under uncovered ground and in subgrades under pavements. On new projects, moisture content was also measured during construction. In grounds covered with pavements, the effect of age of the cover was determined. The pavement projects, therefore, varied from new to about 12 years.

DATA COLLECTION

Precipitation and air-temperature data near the test sites were obtained from the monthly bulletin for Virginia supplied by the U.S. Department of Commerce. A nuclear method for measuring subgrade moisture contents was adopted. The subgrade temperatures were measured by thermistors. Data collected for precipitation, temperature, and moisture content are described in the following.

Measurement of Precipitation

Rainfall data from 1970 and 1971 for test sites at Charlottesville, Culpeper, and Fredericksburg were plotted and are shown in Figure 1. Precipitation data for Charlottesville are applicable to sites 2, 3, 4, 5, 6, 7, and 9; those for Culpeper to site 1; and those for Fredericksburg to site 8.

Data about snow on the ground for 1970 and 1971 show traces in December (for maximum of 5 days), 6 to 10 in. (15 to 25 cm) in January (for maximum of 31 days), about 1 in. (2.5 cm) in February (for maximum of 4 days), and 7 to 9 in. (18 to 23 cm) in March (for maximum of 9 days).

Publication of this paper sponsored by Committee on Subsurface Soil-Structure Interaction.

Measurements for Underground and Subgrade Moisture and Temperature

The moisture content below uncovered ground and under roadway shoulders and pavements was determined with a nuclear depth probe. These measurements were usually made at 1, 2, and 3 ft (0.3, 0.6, and 0.9 m) below the uncovered ground or below the bottom of the shoulder or the pavement.

The determinations of moisture content below uncovered ground were taken for locations 1 through 9 as given in Table 1. Table 1 also gives the physical analysis of the soil. Moisture contents from May 1, 1970, to May 1, 1971, for these nine locations are graphically shown in Figures 2, 3, and 4.

Moisture contents below the pavement or shoulder were recorded for locations 13 through 17 as given in Table 1. On each of these five locations, four sites were chosen: under the shoulder of a cut, under the pavement of a cut, under the shoulder of a fill, and under the pavement of a fill. The measurements on these locations were made over a period of 18 to 24 months. Subgrade moisture contents for these five locations are given later.

Temperatures and temperature gradients under the pavement or shoulders in the subgrade or below uncovered ground were determined by means of thermistors embedded at 0-, 1-, 2-, and 3-ft (0.3-, 0.6-, and 0.9-m) intervals.

Air and subgrade temperatures were continuously recorded for two satellite pavements and occasionally were recorded for other projects. Temperature versus time for location 15 (from March 1969 to November 1969) and for location 14 (from January 1969 to November 1971), for both the fills and cuts, are shown graphically in Figures 5 and 6 respectively.

EVALUATION OF SUBGRADE TEMPERATURE

The following conclusions were drawn from the evaluation of the subgrade temperatures. The minimum subgrade temperature was higher than the average temperature of the 5 previous days, as shown in Figures 5 and 6. For a few days in January, the average of the 5 previous days' temperature was slightly below the freezing point. During these few days, subgrade temperatures below the pavements and the shoulders of project 14 were taken. The subgrade temperature below the pavement was slightly above the freezing temperature, but the subgrade immediately below the shoulder was frozen. Frozen subgrades under the shoulders may occur because (a) snow is pushed from the pavement and collected on the shoulders, and (b) the untreated aggregate is 6 in. (15 cm) deep, is porous, and has higher thermal conductivity than does asphalt concrete.

Changes in the subgrade soil temperature followed changes in the air temperature (Figs. 5 and 6). Thus, during spring and summer, the temperatures in the upper part of the subgrade were higher than those in the lower part; this trend changed during autumn and winter. Figure 7 shows the temperature gradient recorded during summer and winter, the air temperature at the time of testing, the average of 5 previous days' air temperatures, and the subgrade temperatures for 2 days in summer and winter.

Because of the temperature gradient in the subgrade soil, there would be a moisture flow in the subgrade; for example, the moisture would move from the lower part to the upper part of the subgrade in autumn and winter and reverse its movement during spring and summer.

Figures 5 and 6 show that the subgrade temperatures in fills were lower than those in cuts. The variation was from 2 to 10 F (1 to 18 C) depending on the air temperatures: The higher the air temperature was, the higher the variation was.

Figure 1. Precipitation data.

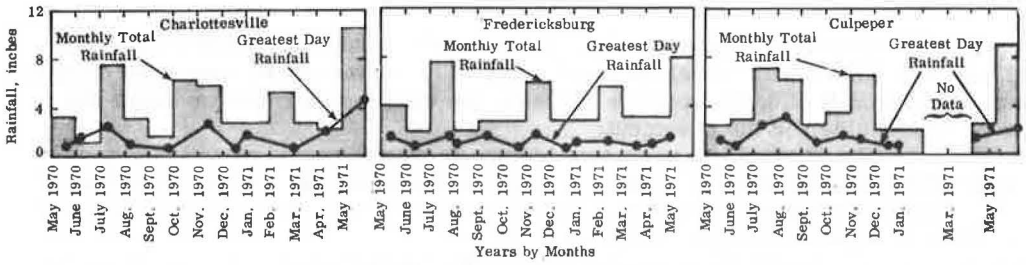

Table 1. Analysis of soil.

Location Number	Physical Condition	Aggregate Gradation (percent passing sieve size) No. 10	No. 20	No. 40	No. 60	No. 80	No. 100	No. 200	Silt (percent)	Clay (percent)	Atterberg Limits (percent) Liquid Limit	Plastic Limit
1	Uncovered ground	100	98.2	96.7	95.3	94.3	93.6	90.9	40	45	53	38
2	Uncovered ground	100	91.7	85.4	—	73.1	67.9	54.8	25	31	0	0
3	Uncovered ground	100	97.1	93.1	87.7	85.7	83.7	76.9	31	41	41	28
4	Uncovered ground	100	96.8	95.2	90.0	86.5	82.9	73.0	34	37	54	36
5	Uncovered ground	100	96.0	87.6	77.2	71.0	66.3	52.0	29	24	41	35
6	Uncovered ground	100	95.8	85.1	77.5	70.3	70.0	61.8	29	33	46	30
7	Uncovered ground	100	98.2	96.2	92.4	89.2	86.6	78.8	20	57	58	36
8	Uncovered ground	100	85.2	62.3	61.5	23.2	21.4	00.0	0	0	—	—
9	Uncovered ground	100	96.0	93.0	89.4	86.6	84.5	77.4	26	41	52	32
13	Pavement, fill	100	97.2	90.9	79.6	71.5	69.9	54.7	23	29	—	—
	Pavement, cut	100	89.0	57.1	57.1	5.6	5.6	0.0	—	—	—	—
14	Pavement and shoulder	100	93.9	88.2	83.4	80.1	78.0	69.8	27	41	53	34
15	Pavement and shoulder	—	—	—	—	—	—	—	—	—	—	—
16	Pavement and shoulder, fill	100	91.2	83.8	72.8	70.3	66.4	54.1	25	16	31	26
	Pavement and shoulder, cut	100	87.0	79.6	73.6	68.2	63.6	42.9	23	13	29	23
17	Pavement and shoulder, fill	100	85.8	73.9	—	60.9	58.2	50.7	—	—	—	—
	Pavement and shoulder, cut	100	90.0	80.0	—	66.5	63.3	54.3	—	—	—	—

Figure 2. Moisture content below ground level at locations 1, 2, and 3.

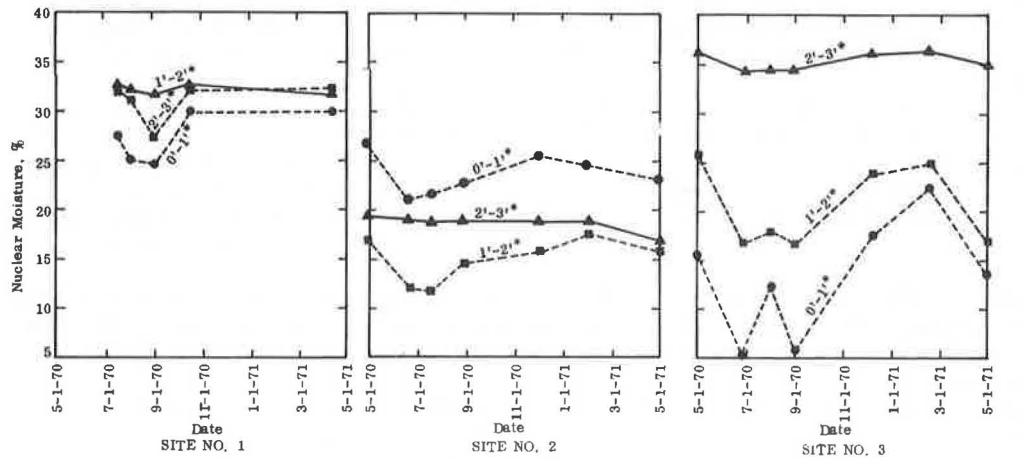

Figure 3. Moisture content below ground level at locations 4, 5, and 6 (*denotes depth below ground level).

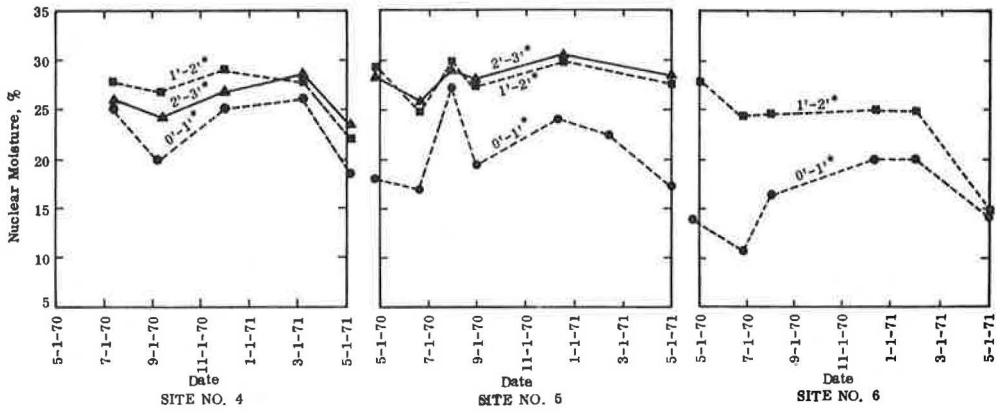

Figure 4. Moisture content below ground level for locations 7, 8, and 9 (*denotes depth below ground level).

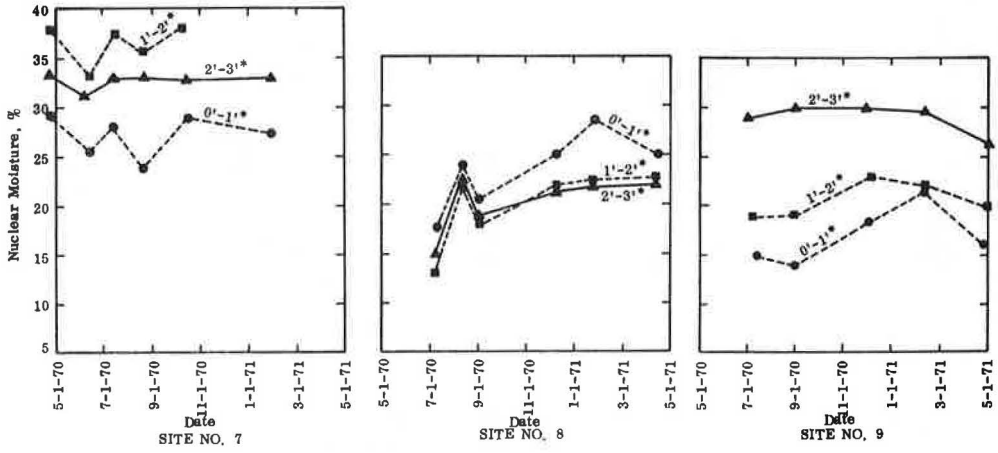

Figure 5. Air and subgrade temperatures at location 15.

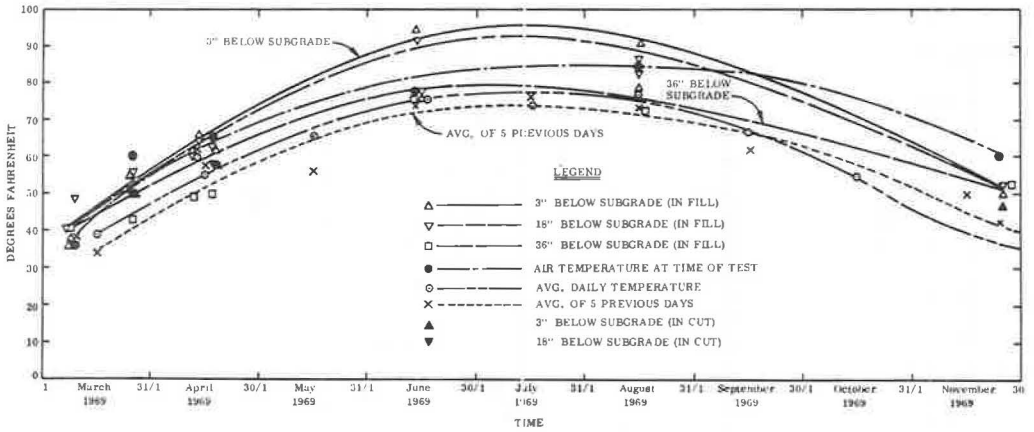

Figure 6. Air and subgrade temperatures at location 14.

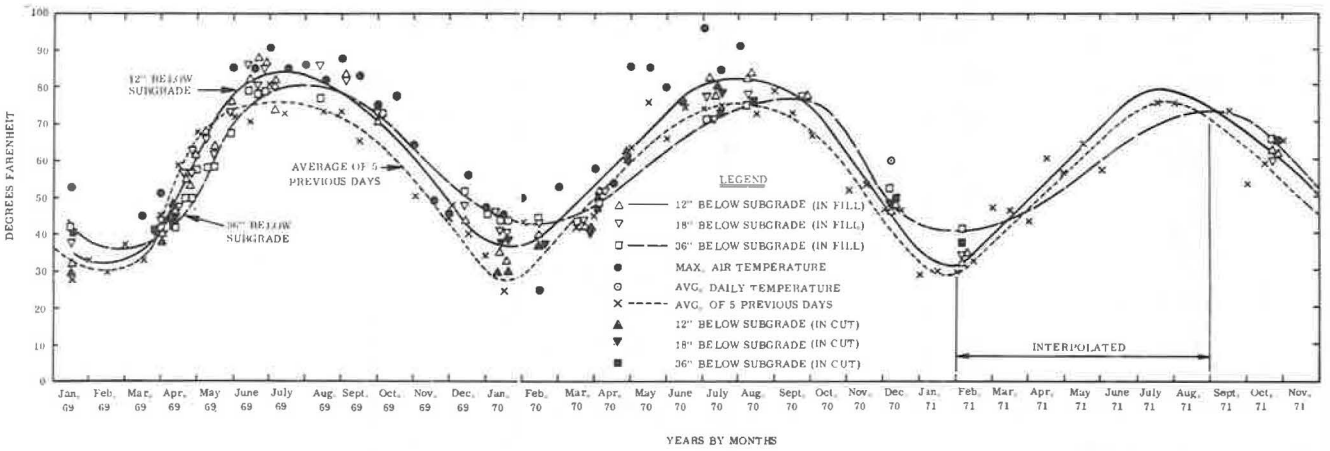

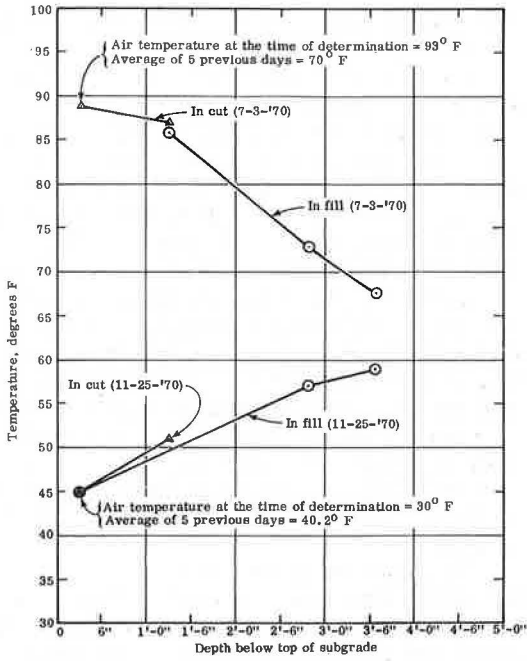

Figure 7. Typical summer and winter day temperatures at location 17.

EFFECTS OF PRECIPITATION AND TEMPERATURE GRADIENT ON UNDERGROUND MOISTURE CONTENT WITHOUT COVER MATERIAL

The moisture contents for nine sites without cover are shown in Figures 2, 3, and 4. There was a high precipitation in July and November 1970 and May 1971 (Fig. 1). Sites 2 through 8 show that the underground moisture content increased in July and then, in most cases, continued to be high through January 1971, after which it decreased. This trend occurred in spite of the low precipitation in September and December and, in two cases, during October and August.

Because no snow was on the ground until the end of November and a trace of snow appeared in December, the only possible reason for the high subsoil moisture contents, even during the low precipitation periods, would be the decrease in air temperature from August 1970 through January 1971. This resulted in thermal gradients with lower temperatures near the top of the ground and high temperatures farther down. The reduction of the temperature near the top of the ground from August through the end of January is evident from the data in Figures 5 and 6.

Evidently, the factors contributing to high moisture contents for uncovered ground are precipitation and low temperatures during autumn and winter. November through March may, therefore, be a period of high moisture contents for uncovered ground.

EFFECTS OF PRECIPITATION, TEMPERATURE GRADIENT, AND TOPOGRAPHY ON SUBGRADE MOISTURE CONTENTS

Data from five locations are discussed to illustrate the effects of precipitation, temperature gradient, and topography on subgrade moisture contents.

Project Location 14

The subgrade on the project at location 14 was completed in April 1969, and the pave-

ment in December 1969. The precipitation and temperatures for this project are shown in Figures 1 and 6.

The project is located in fill and cut areas. The fill is over a deep creek; hence, the subgrade moisture has a tendency to drain away unless held by other forces. The cut has a rocky foundation except for a leveling fill for the subgrade. The ground in the cut slopes away from the road area and provides subsoil drainage away from the pavement. The subgrade soil contains 41 percent clay and 27 percent silt (Table 1).

Figure 8 shows the subgrade moisture at three levels for four sites under the shoulder or pavement in a cut or a fill. The moisture data were taken from April 1969 until 1 year after completion of the pavement. In the fill area during the construction, i.e., the time of completion of the subgrade, the pavement, and the shoulder, the range of the moisture contents rose by about 20 percent, from 7 to 10 percent in April at the time of subgrade completion to 25 to 30 percent in December at the time of pavement completion. After construction, the rate of increase in the moisture content was so low that it was almost unnoticeable.

Figure 8 also shows that, in the cut area during construction, the moisture content rose by about 3 to 5 percent, from 7 to 10 percent in April at the time of subgrade completion to 8 to 15 percent in December at the time of pavement completion. After construction, the rate of increase, as in the fill area, was so low that it was almost unnoticeable.

The high rate of increase in the moisture content during construction may have been the direct effect of precipitation that entered the subgrade treatment, subbase, base, and shoulder much more easily during construction (when the subgrade was more exposed and porous) than after construction.

The higher increase in the moisture content in the fill area may have been caused by the lower density and higher moisture holding power of the soil in the fill area than in the rocky ground in the cut area. Also subgrade soil is better compacted on rocky foundations and, therefore, is more dense than the same soil compacted on weaker foundations.

Temperature gradients in autumn and winter tend to raise the subgrade moisture toward the top from the lower levels. In the case of rocky foundations like the one in the cut, there is little moisture in the foundation, and, therefore, the rise of moisture is proportionately less.

Figures 8a, b, and d show that in the cut as well as in the fill during construction the moisture content at 0 to 2 ft (0.3 to 0.6 m) was higher than at 2 to 3 ft (0.6 to 0.9 m) by about 5 percent. This trend reversed itself in all three cases immediately after construction was over. The reason for this change may have been (a) the reduced effect of increasing moisture from the top because of precipitation immediately after the construction, (b) the temperature gradient of autumn and winter reversed itself, which made the moisture move from the upper to the lower layers of the subgrades, and (c) both the cut and fill areas are in a topography that draws the water away from the roadway rather than toward it.

The following conclusions can be made from the previous discussions:

1. The subgrade soil accumulated and held the moisture during the time of construction mostly because of precipitation and low density of the subgrade material; this also depended on the amount of compaction and soil gradation. The moisture accumulation was as high as about 20 percent in the fill.
2. The temperature gradient did affect the amount of subgrade moisture. The variation in moisture content due to the temperature gradient (although this depended on total moisture content) could not have been greater than 5 percent.
3. The moisture content in the upper layer of the subgrade could be less than that in the lower part of the subgrade if the topography were such that it drained the moisture away from the roadway.

Figure 8. Seasonal variation in subgrade moisture at location 14: (a) under pavement in fill, (b) under shoulder in fill, (c) under pavement in cut, and (d) under shoulder in cut.

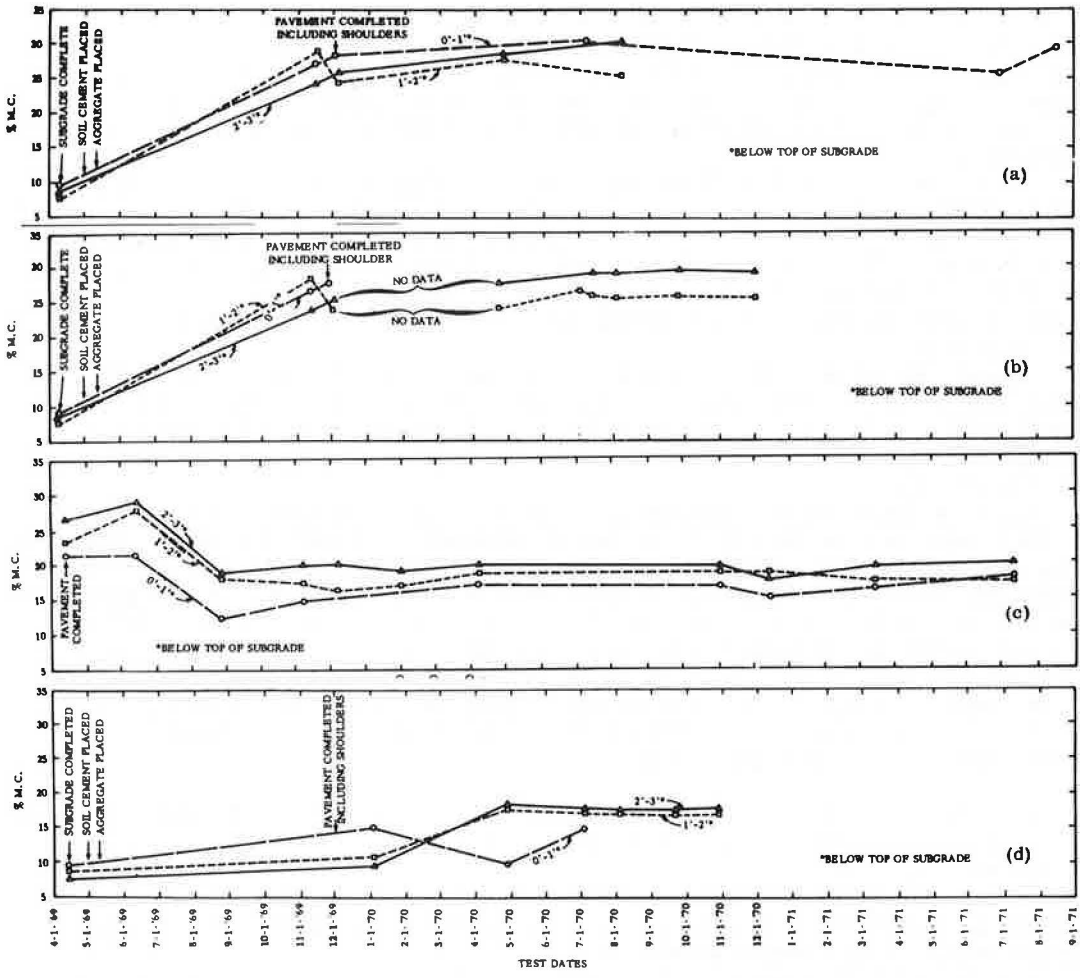

Figure 9. Seasonal variation in subgrade moisture at location 16: (a) under pavement in fill and (b) under pavement in cut.

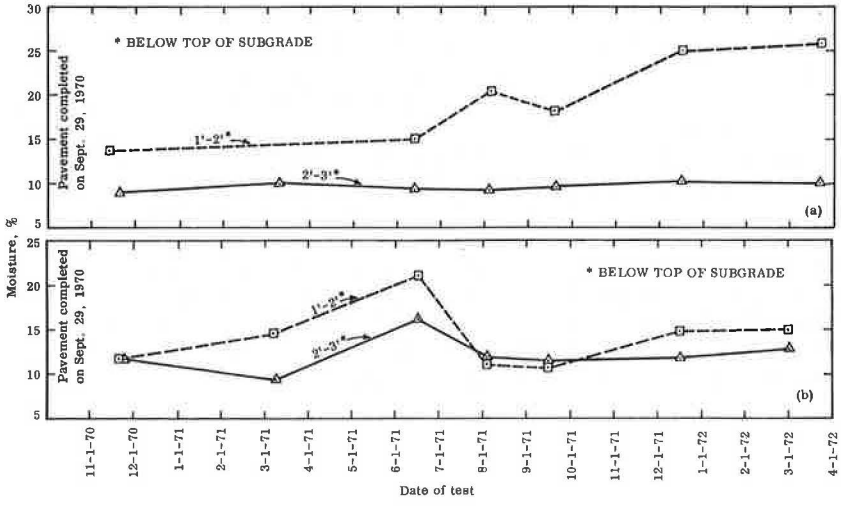

Project Location 16

Pavement on the project at location 16 was completed in September 1970. The project is located between Culpeper and Charlottesville. The precipitation records for it are shown in Figure 1. Because the pavement structure is almost the same as that at location 14, for this evaluation, the air and subgrade temperatures were also considered the same.

The project is located in fill and cut areas. The fills and cuts are not so deep as those at location 14. Similarly, the cut has a rocky foundation except for a leveling fill for the subgrade. The adjacent ground in the cut has a tendency to drain toward the cut, as is evident from the occasional collection of water in the side drains. The fill is over a small creek, and the moisture in the fill subgrade has a tendency to drain away from the pavement. The subgrade soil contains 16 percent clay and 25 percent silt (Table 1).

Figure 9 shows the subgrade moisture under the pavement in the fill and under the pavement in the cut. The subgrade moisture data were taken from November 1970 to April 1972, i.e., for a continuous period of about 18 months. The subgrade moisture content after completion of the project was 10 to 15 percent in the fill and about 12 percent in the cut.

Figure 9 shows that the subgrade moisture in the fill continued to increase from 10 to 15 percent in November 1970, i.e., immediately after completion of the pavement, to 26 percent in the 17-month period after construction. The subgrade seemed to absorb water and hold it in the same way as at location 14. This capacity to absorb precipitation stopped on the project at location 14 when the moisture content reached between 25 and 30 percent. Because the moisture at location 14 also reached 26 percent, it is possible that the rate of increase in the moisture content would now decrease.

Subgrade moisture in the cut increased to about 15 to 20 percent as compared to 8 to 15 percent at location 14 and then decreased in the summer of 1971 (Fig. 9). Therefore, the following observations can be made:

1. In new construction, the subgrade moisture rapidly increased because of precipitation until it reached a certain level. This depends on the density, compaction, and gradation of the soil.
2. After this semisaturated level due to precipitation is reached, the rate of increase in moisture content slows down, and the variations in moisture levels due to temperature gradients become noticeable.
3. After about 10 years, there is almost no change in subgrade moisture and no effect of temperature gradient.

Project Location 13

Location 13 is in the coastal zone and in cut and fill areas with curbs and gutters. The general topography slopes away from the pavement. The subgrade soil in the cut area is sandy with no clay or silt. In the fill area, the subgrade contains 23 percent silt and 29 percent clay. The fill is over a creek.

The pavement was completed in June 1970 and consists of 10.5 in. (27 cm) of full-depth asphalt concrete. After completion of the road, measurements of subgrade moisture were started in October 1970. Data for the subgrade moisture below the pavement in the cut and fill areas are shown in Figure 10.

In the fill area, the subgrade moisture during the 12-month period remained almost constant and ranged from 20 to 25 percent. There were lower percentages of moisture near the pavement than farther from it. This is the same pattern, in which water drained away from the pavement, as was observed for location 14. In this case, curb and gutters also prevented drainage toward the pavement subgrade.

Figure 10. Seasonal variation in subgrade moisture at location 13: (a) under pavement in fill and (b) under pavement in cut.

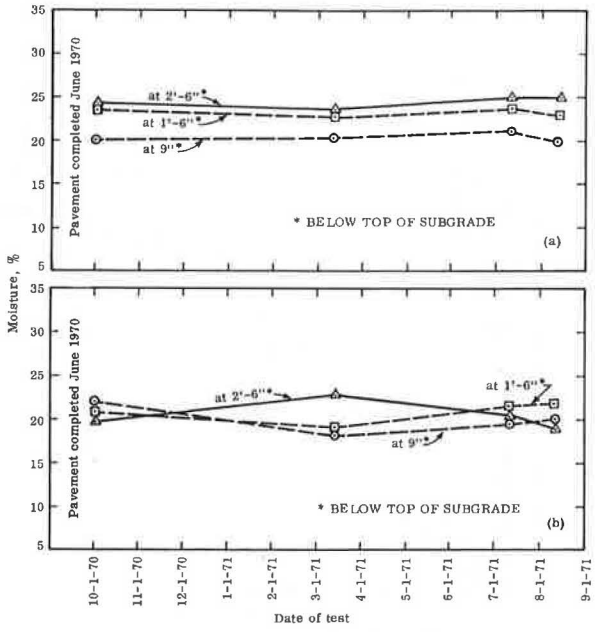

Figure 11. Seasonal variation in subgrade moisture at location 15: (a) under pavement in fill, (b) under shoulder in fill, and (c) under pavement in cut.

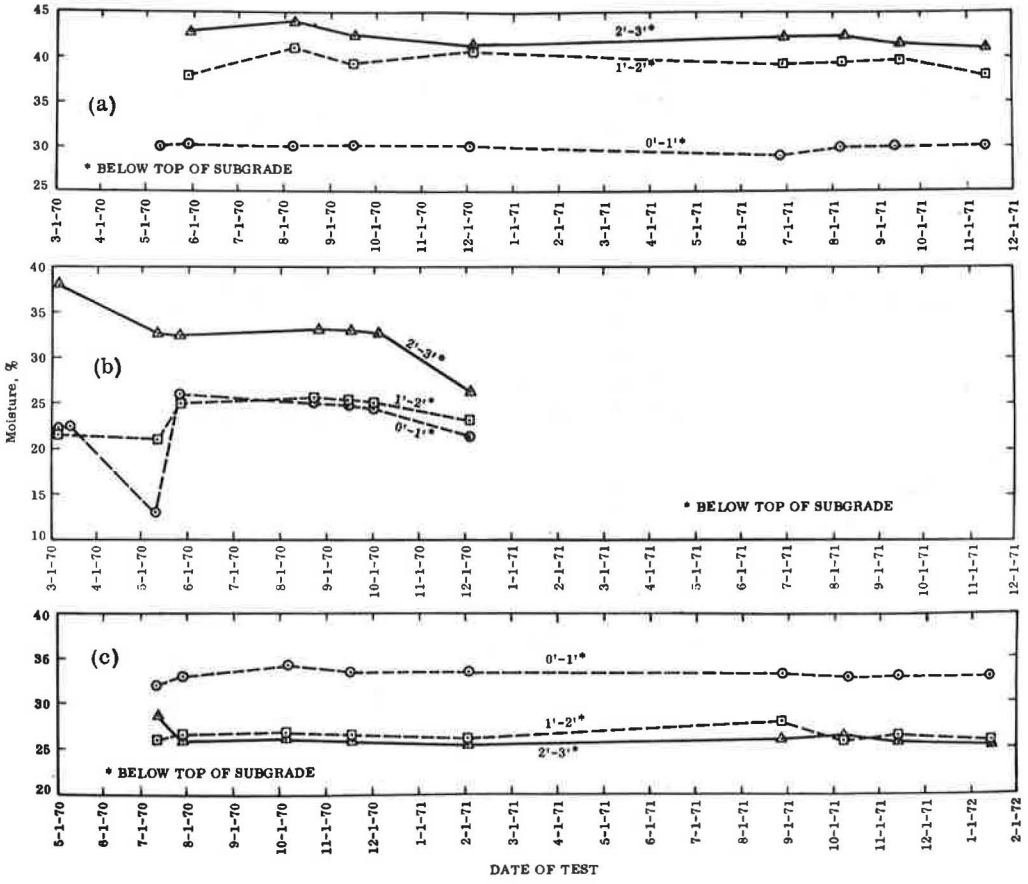

Figure 12. Subgrade moisture variation with time.

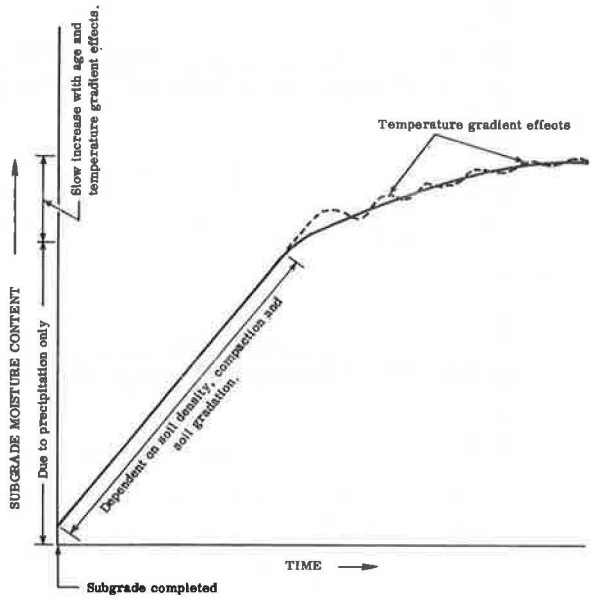

Figure 13. Soil density versus moisture content: (a) for cut and fill at location 17 and (b) by conventional and nuclear tests in laboratory.

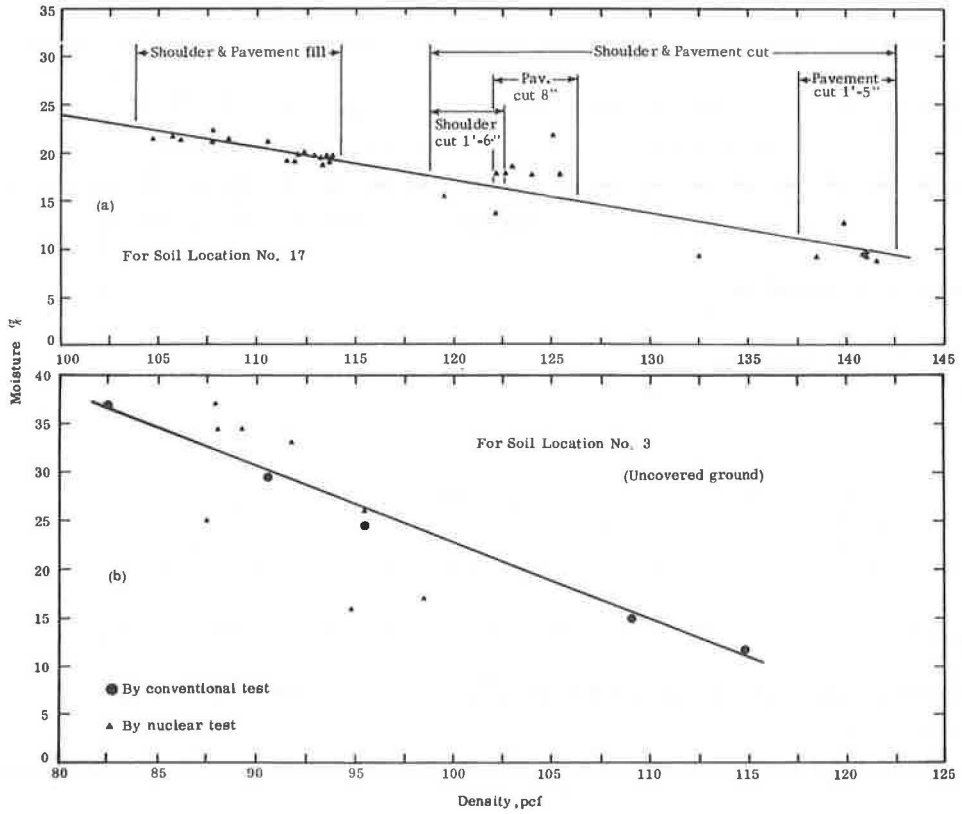

Project Location 15

The project at location 15 is about 12 years old and is located in fill and cut areas. The fill is over a deep depression and, therefore, the subgrade moisture tends to drain away from the subgrade unless it is held by other forces. The cut is over a rocky foundation except for a leveling fill for the subgrade. The side drains of the cut usually collect a lot of water, which indicates that the groundwater is draining toward the cut.

Figure 11 shows the moisture content below the subgrade at three levels: under the pavement and shoulder in the fill area and under the pavement only in a cut area. It shows that the moisture content under the pavement, in the cut, and in the fill remained almost constant. In the cut area, the moisture varied from 25 to 34 percent as compared to 30 to 44 percent in the fill area. This tendency toward lower moisture contents in the cut was observed in projects at locations 14, 16, and 13, although the ground drains toward the cut. The only possible reason for this tendency is the higher density of the subgrade soils on the rocky foundation in the cut.

As stated previously, the subgrade soil moisture content in this cut and fill is much higher than those of the other projects dissussed. This probably proves that after the soil rapidly increases in moisture because of precipitation, the rate of increase in moisture decreases but continues slowly during the life of the pavement and changes with the temperature gradient until it reaches a level at which the temperature gradient loses much of its effect; i.e., the subgrade moisture content follows the pattern shown in Figure 12.

Figure 11 shows that in the fill area, where the drainage slopes away from the pavement, the moisture content near the bottom of the pavement is lower than in the layers underlying it, and, if the drainage slopes toward the pavement, the moisture content is highest near the bottom of the pavement and decreases in the lower layers of the subgrade.

In the fill area under the shoulder (and in uncovered ground), the moisture content seems to have been affected by the climatic conditions (Fig. 11). The shoulder cover in this area consists of gravel less than 4 in. (10 cm) thick. In the three previous cases, the gravel thickness varied from 6 to 9 in. (15 to 23 cm). Because the moisture was draining away, the moisture content was lower in the top layer than in the bottom layer.

Project Location 17

In the four projects discussed, the moisture content of the subgrade soil in the fill was much less than that of the soil in the cut. This was in spite of the few cases in which the ground drainage was toward the cut area rather than away from the fill area. This clearly showed that, in the cut area, because of better compaction, more density, and probably the rocky foundation, the subgrade moisture was less than in the fill.

The moisture versus density relationship was drawn for the project at location 17 so that we could confirm that moisture content was more related to the density of soil than to the rocky cut. This relationship is shown in Figure 13a, which shows that the density of the subgrade soil in the fill varied from about 104 to about 115 pcf (1666 to 1842 kg/m^3), but in the cut it varied from about 118 to 142 pcf (1890 to 2275 kg/m^3). For the same depth, the density in the cut shoulder was less than that in the cut pavement. The same trend was noted for soils with no cover as shown in Figure 13b.

CONCLUSIONS

Based on this investigation, the following conclusions were made:

1. As expected, the higher the compaction and dry density of the subgrade soil were, the lower the subgrade moisture content was.
2. In new construction, the subgrade moisture rapidly increased because of precipitation until it reached a certain level depending upon the density, compaction, and gradation of the soil. After this semisaturated level due to precipitation was reached,

the rate of increase in moisture content slowed down, and the variations in moisture level due to temperature gradients became noticeable. After about 10 years, there was practically no change in subgrade moisture and temperature gradient had no effect.

3. When the drainage was away from the pavement, the moisture content in the top layer of the subgrade was usually lower than that in the lower layers, and, if the drainage was toward the pavement, the moisture content in the top layer was usually higher than that in the underlying layers.

4. The subsoil moisture content in uncovered ground and subgrades of pavement shoulders was greatly affected by climatic conditions such as rain, snow, and temperature. The variation was maximum in uncovered ground, less in shoulders covered by a 4-in. (10-cm) layer of aggregate, and much less in shoulders having 6- to 9-in. (15- to 23-cm) layers of aggregate. The subgrades under the shoulders covered with 6- to 9-in. (15- to 23-cm) layers of aggregate were frozen. This was probably due to (a) the collection of snow over them or (b) the higher thermal conductivity of the porous, untreated aggregate as compared to that of asphalt concrete.

INTERPRETATION OF IN SITU PERMEABILITY TESTS ON ANISOTROPIC DEPOSITS

C. S. Dunn, University of Birmingham, England; and
S. S. Razouki, University of Basrah, Iraq

To caluclate the permeability of a soil from the results of in situ constant- or variable-head tests, one must know the intake factor for the porous tip used. The intake factor for a cylindrical tip of a piezometer is a function of its length and diameter only. No rigorous relationship has yet been derived, but an accurate empirical formula based on the best fit and previously published numerical solutions expresses the intake factor in a dimensionless form as a function of the ratio of the length to diameter of the tip. When tests are carried out in a horizontally bedded cross-anisotropic deposit (e.g., a laminated lacustrine clay), the permeability, calculated by assuming isotropy, will have a value intermediately between the horizontal and vertical permeabilities. If the ratio of these permeabilities is known from laboratory or other tests, a correction factor may be applied to the permeability (assuming isotropy) to determine the coefficients of permeability in the horizontal and vertical directions. The correction factor, which is a function of both the ratio of intake length to intake diameter and the ratio of the coefficient of the permeability in the horizontal position to that in the vertical position, is presented in graphical form to enable quick determination of the directional permeabilities.

THE RATE of consolidation of a layered clay deposit may be significantly affected by horizontal drainage (1), and accurate predictions of rates of consolidation in such deposits require determination of values of vertical and horizontal coefficients of permeability in the horizontal and vertical direction respectively (assuming use of a cross-anisotropic soil).

The notation used in this paper is as follows:

A = cross-sectional area of the standpipe bore,
c_x = coefficient of consolidation in the horizontal direction,
c_z = coefficient of consolidation in the vertical direction,
D = diameter of the intake of the cylindrical piezometer,
F = intake factor for the piezometer in an isotropic deposit,
F_t = intake factor for the piezometer in a cross-anisotropic deposit,
H = excess head in a constant-head permeability test,
k = coefficient of permeability in an isotropic deposit,
k_i = coefficient of permeability assuming isotropy,
k_x = coefficient of permeability in the horizontal direction,
k_z = coefficient of permeability in the vertical direction,
k_e = equivalent coefficient of permeability ($k_e = \sqrt{k_x/k_z}$),
L = length of the intake of the cylindrical piezometer,
m = dimensionless ratio ($m = \sqrt{k_x/k_z}$),

Publication of this paper sponsored by Committee on Subsurface Drainage.

q_∞ = steady state discharge,
T = basic time lag,
z = vertical coordinate,
z' = transformed vertical coordinate, and
λ = dimensionless correction factor ($\lambda = k_x/k_1$).

Most in situ permeability tests are interpreted by assuming isotropy of permeability (3, 8). The permeability of a soil may be calculated from the results of variable-head permeability tests from the standard expression

$$k = \frac{A}{F \cdot T} \tag{1}$$

From the results of constant-head tests more commonly used in the United Kingdom, k may be calculated by using the technique proposed by Gibson (4):

$$k = \frac{q_\infty}{F \cdot H} \tag{2}$$

INTAKE FACTOR FOR ISOTROPIC DEPOSITS

Hvorslev (2) suggested that for isotropic homogeneous soil the intake factor could be calculated from

$$F = \frac{2\pi L}{\ell n\left[\frac{L}{D} + \sqrt{1 + \left(\frac{L}{D}\right)^2}\right]} \tag{3}$$

This was derived on the basis of work by Dachler (5), who studied the flow from a line source for which the equipotential surfaces were semiellipsoids. Hvorslev assumed that the flow lines were symmetrical through the center of the intake of the piezometer, with respect to a horizontal plane, and then he applied Dachler's solution for the upper and lower half of the intake. Therefore, Eq. 3 can only provide approximate values of intake factors when it is applied to a cylindrical intake.

Al-Dhahir and Morgenstern (6) published intake factors for cylindrical piezometers of various L/D ratios. Their analysis was based on the numerical integration of Laplace's equation. They pointed out that the presence or absence of an impervious borehole filling above the seal over the piezometer had an insignificant effect on the value of the intake factor. Therefore, their analysis could be applied to both cases shown in Figures 1a and 1b. They produced solutions for four different ratios of L/D and plotted the results in the dimensionless form of F/D against L/D.

Wilkinson (7) argued that Hvorslev's formula (Eq. 3) underestimated intake factors and suggested that to obtain a more exact equation a cylindrical piezometer could be represented by a spheroid, which had its minor diameter and volume equal to those of the piezometer. The equation derived was

$$\frac{F}{D} = \frac{3\pi \cdot \frac{L}{D}}{\ell n\left[1.5\frac{L}{D} + \sqrt{1 + \left(1.5\frac{L}{D}\right)^2}\right]} \tag{4}$$

In Figure 2, the values of Al-Dhahir and Morgenstern are compared with the curves given by Eqs. 3 and 4. It appears that Hvorslev's method underestimates the intake

Figure 1. Cylindrical intakes.

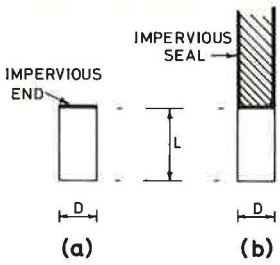

Figure 2. F/D versus L/D for various equations.

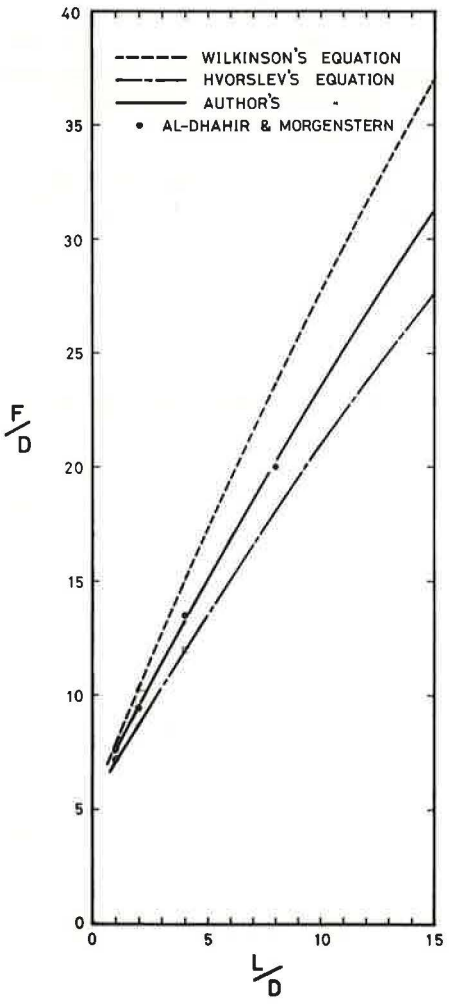

Figure 3. λ versus L/D for six m values.

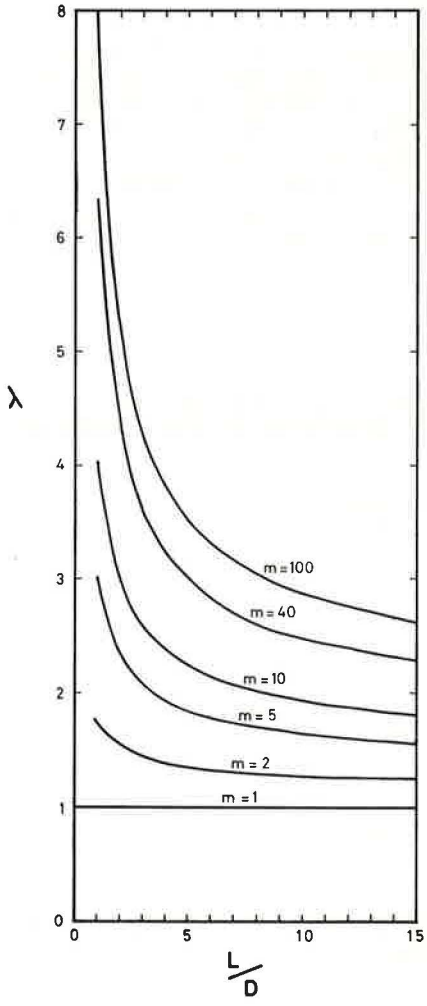

factors and Wilkinson's overestimates them because the numerically derived values of Al-Dhahir and Morgenstern lie almost midway between them.

By retaining the form of Eqs. 3 and 4 and by simply adjusting the constants to give the best fit to the numerical solutions, one obtains

$$\frac{F}{D} = \frac{2.32\pi \frac{L}{D}}{\ell n \left[1.1\frac{L}{D} + \sqrt{1 + \left(1.1\frac{L}{D}\right)^2}\right]} \tag{5}$$

This is likely to be the most precise formula available for determining the intake factors of cylindrical piezometers.

ANISOTROPIC PERMEABILITY

In a laminated clay in which thin layers of clay are interbedded with thin layers of silty or sandy soil, there may be a high degree of anisotropy. If these layers are numerous and make up a uniform structure that is of a thickness significantly greater than the length of the piezometer buried in it, then it is permissible to treat the deposit as homogeneous and anisotropic (7).

Consider the length and diameter of a cylindrical piezometer buried in a thick stratum of cross-anisotropic soil having permeabilities k_z and k_x. By using the standard method of transformation of the vertical scale:

$$z' = mz \tag{6}$$

The problem of flow into the piezometer may be solved by considering a piezometer of length mL in an isotropic soil of permeability:

$$k_e = \sqrt{k_x \cdot k_z} \tag{7}$$

so that

$$k_x = mk_e \tag{8}$$

and

$$k_z = \frac{k_e}{m} \tag{9}$$

The intake factor may be expressed in terms of the transformed dimension, and Eq. 5 becomes

$$\frac{F_t}{D} = \frac{2.32\pi m \frac{L}{D}}{\ell n \left[1.1\, m\frac{L}{D} + \sqrt{1 + \left(1.1\, m\frac{L}{D}\right)^2}\right]} \tag{10}$$

The value of m may not be known at the time that an in situ permeability test is carried out, and the coefficient of permeability will be calculated from Eqs. 1 or 2, assuming isotropic conditions, by using Eq. 5 to determine the intake factor. The value so calculated, k_i, is neither equal to k_z nor k_x.

From Eqs. 1, 2, 5, and 10, it follows that

$$\frac{k_x}{k_i} = \frac{mk_e}{k_i} = \frac{mF}{F_t} = \frac{\ell n\left[1.1\,m\frac{L}{D} + \sqrt{1 + \left(1.1\,m\frac{L}{D}\right)^2}\right]}{\ell n\left[1.1\frac{L}{D} + \sqrt{1 + \left(1.1\frac{L}{D}\right)^2}\right]} \tag{11}$$

Putting $\lambda = mF/F_t$, Eqs. 8 and 9 become

$$k_x = \lambda k_i \tag{12}$$

and

$$k_z = \frac{\lambda k_i}{m^2} \tag{13}$$

Values of λ calculated from Eq. 11 are plotted against L/D in Figure 3 for a range of m values.

The ratio of k_x/k_z may be determined on undisturbed samples in the laboratory. Constant-head permeability tests may be carried out on cube samples (consolidated under the mean in situ effective stress in a triaxial cell) first normal to the bedding planes and then along the bedding planes as described by Chan and Kenney (9). Alternatively, one can perform consolidation tests on large undisturbed samples in a Rowe type of consolidation cell by permitting vertical drainage only and then horizontal drainage only to determine the directional coefficients of consolidation. The permeability ratio is then calculated from the relationship $(k_x/k_z) = (c_x/c_z)$. The actual representative value of k_x/k_z for interpretation of the field tests should be decided on the basis of a total study of the field and laboratory results and a visual study of an undisturbed continuous core taken from a position close to the field test.

It is not the purpose of this paper to discuss sources of error in in situ permeability tests, but spurious results may be obtained if precautions are not taken to avoid smearing of clay soils at the boundary between the porous intake and the soil. Because serious smearing is likely to occur in the case in which the piezometer is pushed directly into the soil, use of the formulas presented is probably unwarranted in such circumstances. Other sources of error are described by Wilkinson (7) and Hvorslev (2).

CONCLUSION

A formula has been derived for calculating the intake factor of any cylindrical intake sealed on its top surface and buried in a homogeneous isotropic soil. When an in situ permeability test is carried out in a horizontally bedded cross-anisotropic deposit, the directional permeabilities may be calculated from the results provided that the ratio of the horizontal to vertical permeabilities is known.

REFERENCES

1. C. S. Dunn and S. S. Razouki. Two Dimensional Consolidation Under Embankments. Journal of Institution of Highway Engineers, London, Vol. 21, No. 9, Sept. 1974.
2. M. J. Hvorslev. Time-Lag and Soil Permeability in Ground-Water Observations. Bulletin 36, U.S. Army Engineer Waterways Experiment Station, Vicksburg, Miss., 1951.
3. R. T. Murray. Embankments Constructed on Soft Foundations: Settlement Study at Avonmouth. Department of the Environment, Great Britain Road Research Laboratory, Crowthorne, RRL Rept. LR 419, 1971.
4. R. E. Gibson. A Note on the Constant Head Test to Measure Soil Permeability In Situ. Geotechnique, Vol. 16, No. 3, 1966, pp. 256-257.
5. R. Dachler. Grundwasserströmung. Wien, Julius Springer, 1936.
6. Z. A. Al-Dhahir and N. R. Morgenstern. Intake Factors for Cylindrical Piezometer Tips. Soil Science, Vol. 107, No. 1, 1969, pp. 17-21.
7. W. B. Wilkinson. Constant Head In-Situ Permeability Tests in Clay Strata. Geotechnique, Vol. 18, No. 2, 1968, pp. 172-194.
8. W. G. Weber. In-Situ Permeabilities for Determining Rates of Consolidation. Highway Research Record 243, 1968, pp. 49-61.
9. H. T. Chan and T. C. Kenney. Laboratory Investigation of Permeability Ratio of New Liskeard Varved Soil. Canadian Geotechnical Journal, Vol. 10, No. 3, Aug. 1973, pp. 453-472.

EVALUATION OF PAVEMENT DRAINAGE SYSTEMS MADE OF LAYERS OF OPEN-GRADED BITUMINOUS AGGREGATE MIXTURES

Shiraz D. Tayabji and Ernest J. Barenberg, Department of Civil Engineering, University of Illinois

This study was aimed at evaluating the performance of pavement drainage systems in Illinois constructed with locally available aggregate sources. The study was limited to investigating the use of open-graded, hot-mixed bituminous aggregate mixtures in pavement drainage systems. A preliminary investigation was carried out in the laboratory to evaluate the permeability and the stability of the open-graded bituminous aggregate mixtures. Specimens were prepared according to the procedures in ASTM D1559. Permeability tests (in which a constant-head test that allowed the measurement of permeability at low heads was used) and stability tests were performed on the same specimen. From the results of the preliminary investigations, six test pavements incorporating different design concepts were tested at the University of Illinois test track. Dynamic loading was applied to the test pavements, and water was passed through the open-graded bituminous aggregate drainage layers to simulate surface and lateral infiltration. Permeability tests at a constant head were carried out regularly on the pavement test sections. The progress of rutting in the test pavements was also recorded. Results of these limited tests indicate that open-graded bituminous aggregate mixtures possess a high order of permeability and that care must be taken to prevent the migration of subgrade fines into these aggregate layers if satisfactory drainage is to be achieved. This paper discusses methods that can be used to ensure satisfactory performance of pavements made of open-graded aggregates.

•WATER is generally accepted as one of the most important factors affecting pavement performance. The primary approach to eliminating water in pavements has been to seal the pavement surface against water infiltration and, if conditions for seepage prevail, to provide sufficient drainage to handle the groundwater. Currently, pavement drainage systems are usually adopted from standards rather than rationally designed. This often leads to uneconomical or poorly performing drainage systems. Only recently, efforts are being made to better understand the concepts of pavement drainage. Cedergren and Lovering (1, 2) and Cedergren (3) have significantly contributed to an understanding of the design process of pavement drainage systems. Recently, several guidelines were published for the design of pavement drainage systems (4, 5), which incorporate asphalt-treated drainage layers made of open-graded aggregates.

Rationally designed pavement drainage systems should satisfy the following requirements. They should

1. Have adequate capacity to drain the pavement rapidly and should retain this capacity for some realistic service life,

Publication of this paper sponsored by Committee on Subsurface Drainage.

2. Be resistant to plugging, and
3. Possess sufficient stability so that the behavior of the drainage system itself does not interfere structurally with the behavior and the performance of the overall pavement system.

STUDY OBJECTIVES

The overall objective of this study was to evaluate the performance of pavement drainage systems that are used in Illinois and that are made of locally available aggregate sources. The study was limited to investigating the open-graded, hot-mixed bituminous aggregate mixtures (OGBAMs) used in the pavement drainage systems.

The primary factors investigated were

1. The permeability of OGBAMs,
2. The behavior of OGBAMs in pavement sections under load, and
3. The tendency of the drainage systems to plug and methods for reducing this tendency.

PRELIMINARY INVESTIGATIONS

General

Laboratory tests to evaluate the permeability and the stability of OGBAMs were designed to enable both characteristics to be measured on the same laboratory specimen. Laboratory specimens were prepared according to ASTM D1559. Certain modifications were made in this procedure to allow for specific, unique characteristics of OGBAMs and their designated use. A constant-head permeameter was developed to measure the permeability of the prepared OGBAMs. The permeameter allows the measurement of permeability at very low heads and satisfies the conditions necessary for valid use of Darcy's law:

1. Laminar flow,
2. Steady state of flow,
3. The 100 percent saturation of the porous material, and
4. No change in volume during the test.

According to Darcy's law

$$Q = \overset{k}{KiA} \tag{1}$$

or

$$k = Q/iA = \frac{Q \times L}{\Delta h \times A} \tag{2}$$

where

Q = discharge per unit time (cm^3/s);
k = coefficient of permeability (hydraulic conductivity), length per unit time (cm/s);
i = hydraulic gradient (dimensionless);
A = cross-sectional area of specimen (cm^2);

L = length of specimen (cm); and
Δh = head causing the flow of water through the specimen (cm).

Test Criteria

Because of the open-graded nature of OGBAMs, permeability had to be measured at very low heads (3, 6). This requirement is based on the assumption in Darcy's law that the inertial force is negligible compared with the viscous force. For this investigation, a head differential of approximately $\frac{1}{16}$ in. (1.6 mm) was used. This corresponds to the hydraulic gradient of 2.5 percent for a specimen 2.5 in. (6.35 cm) high and agrees with the transverse pavement slopes used in practice.

Initial tests showed that permeability was inversely proportional to the compaction effort used in preparing the specimens. Excessively high compaction efforts caused particle breakdown and concomitant changes in particle gradation and, thus, a reduction in the volume of voids in the specimen. During the initial testing, 35 blows with a 10-lb (4.54-kg) mass dropped from a height of 18 in. (45.7 cm) on each face of Marshall specimens produced reasonable densities with a minimum of particle fracture. Therefore, this compactive effort was used throughout the laboratory testing program.

The Marshall method requires the immersion of specimens in water at 140 F ± 1.8 F (60 C ± 0.8 C) for 30 to 40 min before the stability test. Initial tests showed that this was too severe for OGBAMs. In that the drainage layer would be at least 6 in. (15.2 cm) below the surface of the pavement, it was felt that the requirement of 140 F (60 C) would be too severe and unrealistic when compared with actual environmental conditions. According to Straub et al. (7), the temperature observed over 1 year in the model test pavement of dense-graded bituminous mix never exceeded 100 F (37.8 C) at 8 in. (20.3 cm) or more depth and reached about 100 F (37.8 C) at 6 in. (15.2 cm) depth approximately 2 percent of the time. Thus, the specimens were immersed in the water bath at 100 F ± 1.8 F (37.8 C ± 0.8 C) for 30 to 40 min before the stability test. Three specimens were tested for each set to evaluate the variables of aggregate type, aggregate gradation, and asphalt content.

Results of Preliminary Investigations

Aggregate gradations meeting the specifications of Illinois Department of Transportation, CA-7, CA-8, CA-11, CA-13, and CA-15, were evaluated for permeability and stability as was an aggregate gradation recommended for a drainage blanket by the Federal Highway Administration (4). Gradations of the aggregates evaluated are given in Table 1.

Both crushed stone and gravel aggregates were evaluated. The A penetration-grade asphalt cement was used that had a penetration range from 85 to 100.

Results from the evaluation tests for the crushed-stone aggregates are given in Table 1, and those for the gravel aggregates are given in Table 2. All mixes tested had permeabilities in the range of 3,000 to 8,000 ft/day (1.06 to 2.82 cm/s). The Marshall stability values [100 F (37.8 C)] for the crushed-stone aggregates ranged from about 600 to 1,000 lbf (2669 to 4448 N), and the gravel aggregates had stability values ranging from about 300 to 450 lbf (1334 to 2002 N).

Recommended Test Sections

After the results of the preliminary investigations and the availability of construction materials in Illinois were evaluated, it was decided to use open-graded materials having gradations corresponding to Illinois Department of Transportation specifications CA-7 and CA-14.

Table 1. Results of material evaluation of crushed-stone aggregate.

Item	Specification										
	CA-7	CA-8A	CA-8B	CA-8A	CA-11	CA-13A	CA-13B	CA-15A	CA-15B	CA-15A	U.S. DOT
Aggregate gradation, percent passing sieve size											
¾ in.	100	100	100	100	100	100	100	100	100	100	100
½ in.	60	45	65	45	55	100	95	100	100	100	72
⅜ in.	—	—	—	—	—	—	—	90	60	90	—
No. 4	10	5	15	5	10	50	20	15	0	15	0
No. 16	0	0	0	0	0	0	0	0	0	0	0
Asphalt content, percent	2	2	2	1.5	2	2	2	2	2	1.5	2
Average bulk specific gravity	1.89	1.88	1.93	1.88	1.85	1.87	1.89	1.83	1.83	1.86	1.86
Coefficient of permeability, ft/day	3200 to 4100	6600 to 8100	3600 to 4300	4700 to 6600	4300 to 5200	2600 to 3500	2800 to 3300	4000 to 5000	5500 to 6000	3300 to 3900	4900 to 7700
Average Marshall stability, lbf	777	851	806	611	824	806	1000	660	725	612	818

Note: 1 ft = 0.3048 m, 1 lbf = 4.448 N.

Table 2. Results of material evaluation of Pontiac gravel.

Item	Specification		
	CA-8A	CA-15A	U.S. DOT
Aggregate gradation, percent passing sieve size			
¾ in.	100	100	100
½ in.	45	100	72
⅜ in.	—	90	—
No. 4	5	15	0
No. 16	0	0	0
Asphalt content, percent	2	2	2
Average bulk specific gravity	1.82	1.80	1.77
Coefficient of permeability, ft/day	5100 to 6500	3500 to 4900	6100 to 7900
Average Marshall stability, lbf	386	456	328

Note: 1 ft = 0.3048 m, 1 lbf = 4.448 N.

Figure 1. Layout of test track.

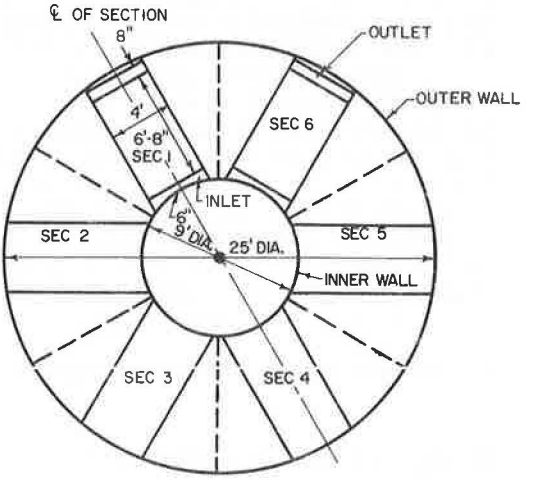

Table 3. Analysis of pavements selected for test sections.

Item	Test Sections					
	1	2	3	4	5	6
Surface course thickness, in.	3	3	3	3	3	3
OGBAM						
Aggregate type	CA-7	CA-7[a]	CA-7	CA-14	CA-7	CA-14
Thickness[b], in.	4	4	4	4	4	4
Sand layer thickness[b], in.	—	—	—	—	2	—
Lime-modified clay layer thickness[b], in.	2.5	—	—	—	—	2.5

Note: 1 in. = 2.54 cm.

[a]The OGBAM layer is to be placed over a filter cloth placed on the subgrade.
[b]These measurements are nominal.

Figure 2. Cross section of test section along centerline.

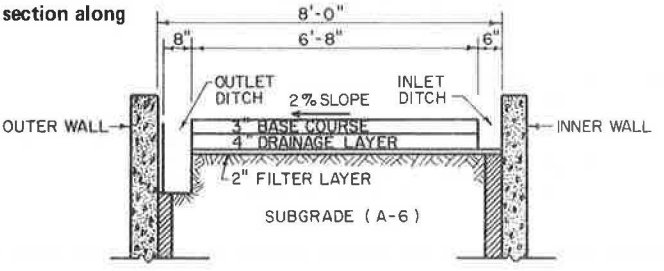

EXPERIMENTAL DESIGN

Test Pavement and Track Layout

The physical characteristics and use of the University of Illinois test track are well-documented in reports by Ahlberg and Barenberg (8) and Barenberg and Thompson (9). In summary, the circular track has an inside diameter of about 9 ft (2.74 m), an outside diameter of approximately 25 ft (7.62 m), and a pavement width of 8 ft (2.44 m). The center of the wheel path has a diameter of 16 ft (4.88 m), and this places it 3.5 ft (1.07 m) from the inside edge and 4.5 ft (1.37 m) from the outside edge of the test pavements. The test pavements rest on a prepared subgrade having a minimum thickness of 3 ft (0.91 m). Because of the physical limitations, the maximum number of test pavements considered practical in one test set is six; for this study, six test sections were chosen. The layout of the six test sections is shown in Figure 1. The pavement systems selected for the six test sections are given in Table 3.

Lime-modified clay layers in sections 1 and 6, a sand layer in section 5, and a filter cloth in section 2 were used to evaluate the functional characteristics of these materials. Sections 3 and 4, in which the drainage layer was laid directly on the subgrade, were used as control sections. All layers were designed to have a transverse slope of 2 percent. A transverse cross section along the centerline of a typical test section is shown in Figure 2.

Materials Used

The materials gradations used in the test track pavements are given in Table 4. Properties of the subgrade are given in Table 5. The physical characteristics of the bituminous aggregate mixtures obtained by using crushed stone are given in Table 6. High-quality, low-permeability asphalt concrete obtained from a local supplier was used in the surface course and placed between the test sections as transitions to ensure no lateral movements of water from one drainage layer to another.

Torpedo sand was tested as a filter layer but failed to satisfy the criteria to prevent clogging of the sand level by the subgrade. However, the satisfaction of this criterion was not relevant for this study, for only surface water drainage was under investigation.

Construction of Test Sections

The subgrade soil, which was already in place in the test pit, was removed to about 1 ft (0.3 m) below the designed level of the subgrade, was partially dried, brought to about optimum moisture content, and pulverized with a soil tiller. Lifts about 4-in.-thick (10-cm) were compacted around the entire track by a J-ram impact tamper.

A 2-in. (5-cm) layer of lime-clay mixture was placed in sections 1 and 6. A silty clay soil (Goose Lake clay) and 2 percent lime were mixed in the pug mill with enough water added to bring the materials up to optimum moisture content (13.0 percent) as determined by AASHO T-99. The mixture was placed in a single, 2-in. (5-cm) lift and was compacted to the desired density by using the J-ram tamper. The lime-clay was allowed to cure for 3 days at room temperature before the OGBAM layer was placed. In section 5, torpedo sand was placed, compacted, and brought to the desired level just before the OGBAM was placed.

Catch basins of galvanized sheet iron were placed adjacent to the outside wall in each section. Pie-shaped layers of dense-graded, hot-mixed asphalt concrete mixtures were placed between each drainage test section to provide impermeable barriers between the drainage sections.

The OGBAM layers were then placed between the impermeable pie-shaped sections. A filter cloth, Mirafi 140, was placed over the subgrade in section 2 before the OGBAM was placed. The OGBAMs were prepared in-house by using a Barber-Greene

Table 4. Aggregate gradation of materials used in test sections.

Sieve Size	Percent Passing					
	CA-7		CA-14			
	Tuscola Stone	Illinois DOT Specimen	Fairmount Stone	Illinois DOT Specimen	Torpedo Sand	Subgrade
1½ in.	–	100	–	–	–	
1 in.	100	90 to 100	–	–	–	
¾ in.	92.5	–	100	–	–	
½ in.	59.7	30 to 60	88.8	80 to 100	100	
⅜ in.	35.7	–	45.7	25 to 65	99.9	100
No. 4	11.5	0 to 10	4.2	0 to 6	96.9	98
No. 16	1.3	–	0.9	–	77.1	–
No. 30	–	–	–	–	54.5	–
No. 40	–	–	–	–	–	92
No. 50	–	–	–	–	9.1	–
No. 100	–	–	–	–	–	85
No. 200	–	–	–	–	1.0	79
0.02 mm	–	–	–	–	–	61
0.005 mm	–	–	–	–	–	39
0.002 mm	–	–	–	–	–	27

Table 5. Physical characteristics of subgrade.

Characteristic	AASHO Designation	Value
AASHO classification		A-6(8)
Optimum moisture content, percent	T 99-57	13.0
Maximum dry density, pcf	T 99-57	120
Liquid limit, percent	T 89-54	25
Plastic limit, percent	T 90-54	14
Plasticity index, percent	T 91-54	11

Note: 1 pcf = 16.02 kg/m^3.

Table 6. Physical characteristics of drainage materials.

Characteristic	Average Values	
	Tuscola Stone[a] (CA-7)	Fairmount Stone[b] (CA-14)
Marshall specimen, 30 blows/face		
Bulk specific gravity	1.91	1.84
Stability, lbf	1570	1086
Flow, (×0.01), in.	10	10
Coefficient of permeability, ft/day	8800 to 11,600	9300 to 9900
Marshall specimen, 40 blows/face		
Bulk specific gravity	1.95	1.89
Stability, lbf	1835	1294
Flow, (×0.01), in.	11	12
Coefficient of permeability, ft/day	6200 to 6700	5900 to 7200
Marshall specimen, 50 blows/face		
Bulk specific gravity	1.95	1.91
Stability, lbf	1737	1550
Flow, (× 0.01), in.	10	9
Coefficient of permeability, ft/day	4200 to 5500	5600 to 6200

Note: Two specimens for each set were prepared. 1 lbf = 4.448 N. 1 in. = 2.54 cm. 1 ft = 0.3048 m.

[a]From the batch used for section 5 (asphalt content = 2.33 percent).
[b]From the batch used for section 6 (asphalt content = 2.00 percent).

Table 7. In situ properties of materials.

Characteristic	Sections					
	1	2	3	4	5	6
Subgrade						
Dry density, pcf	134.8	127.3	130.2	124.7	130.9	130.1
Percentage of standard	103.6	97.9	100.2	95.9	100.7	100.1
Moisture content, percent	10.0	11.7	11.8	10.4	10.7	10.2
Lime-clay layer						
Lime used, percent	2	–	–	–	–	2
Dry density, pcf	107.2	–	–	–	–	107.4
Percentage of standard	91.5[a]	–	–	–	–	91.7[a]
Moisture content, percent	13.3	–	–	–	–	13.7
Drainage layer						
Bulk specific gravity	1.80	–	174	1.75	1.82	1.76
Marshall stability, lbf	387	–	–	528	458	546
Flow, (×0.01), in.	12	–	–	14	14	16
Asphalt used, percent	2.33	2.33	2.00	2.00	2.33	2.00
Surface layer						
Bulk specific gravity	2.37	2.33	2.32			
Marshall stability, lbf	1802	1304	1492			
Flow, (×0.01), in.	16	16	13			

Note: 1 pcf = 16.02 kg/m^3. 1 lbf = 4.448 N. 1 in. = 2.54 cm.

[a]The layers were compacted further with the J-ram after the tests.

Mixall with a drum dryer in batches of about 300 lb (136 kg). The OGBAMs were compacted with the vibrating plate compactor and then were placed in single lifts approximately 4 in. (10 cm) thick. Because of the open texture of the mixtures, compaction effort was controlled to provide optimum density with a minimum fracturing of particles. Four-in.-diameter (10-cm) core samples were taken from each section, except for section 2, in which the OGBAM was laid over the filter cloth. The cores were tested for specific gravity and stability (by using the modified version of ASTM D1559 as described earlier). A 3-in. (7.6-cm) course of dense-graded, high-quality asphalt concrete (which was obtained from a local supplier and which met the Illinois Division of Highways requirements for a high-quality surface course) was placed over the OGBAM and compacted by using the vibrating plate compactor.

Table 7 shows the in situ properties of the materials used. The as-constructed geometrical details of the test sections are given in Table 8. Figure 3 shows the as-constructed test sections.

Test Concepts

Test sections were designed for the water to flow transversely through the drainage layers as shown in Figure 2. The drainage test was designed so that the coefficient of permeability could be obtained by the use of Darcy's equation (Eqs. 1 and 2).

The level of water at the inlet end was kept constant at the interface of the drainage layer and the surface course. This ensured constant flow of water under a constant head. For simplicity of calculations, the following assumptions were made:

1. All head loss was due to flow through the drainage layer,
2. The entire cross section of the drainage layer along the full width of the test section was used for the flow,
3. The hydraulic gradient for the flow was equal to the average gradient or slope of the layer on which the drainage layer was placed,
4. Flow was laminar, and
5. No volume change occurred during the tests.

The water passing through the drainage layer flowed into a collection basin (Fig. 2) and was pumped out continuously during testing. A water meter attached to the pump measured the quantity of water pumped. For measurement of permeability, the flow of water was measured over a period of 10 min. For the first 50,000 load applications, no wheel loads were applied while drainage tests were being conducted. After the first 50,000 applications, continuous moving wheel loading was maintained simultaneously with drainage tests. So that rainfall conditions could be simulated, water was also passed during the interval between the drainability tests for 30 and 60 min per section, and continuous wheel loads were applied. Turbidity of the discharged water was observed for every passage of water so that the severity of infiltration of fines could be evaluated. The time for the flow of water to emerge at the outlet ditch and the time for flow to stop at the end of the test were also noted. In some of the initial tests, after the flow of water had become steady, liquid dye was introduced at the inlet end, and the time taken for the dye to appear at the outlet was measured. This was discontinued after 50,000 load applications. Surface levels and rut depths were measured regularly to evaluate the distress in the test sections.

Dynamic loads were applied to the test sections by a loading frame (9, Fig. 3). Ballast was added to the loading frame to bring its effective mass to about 6,400 lb (2900 kg), i.e., 3,200 lb (1450 kg) per wheel. The loading frame rides on 8.25 × 20 ten-ply truck tires inflated to 80 psi (552 kPa). The speed of the wheels during loading was kept at about 7 to 8 mph (11 to 13 km/h) for most of the experiment. The rate of application was about 25/min. All wheel loads were normally distributed over a wheel path about 30 in. (76 cm) wide.

Table 8. As-constructed geometric details of test sections.

Item	Sections					
	1	2	3	4	5	6
Thickness, in.						
Lime-clay layer	2.2	—	—	—	—	2.6
Sand layer	—	—	—	—	1.7	—
OGBAM drainage layer	4.0	4.1	3.7	4.3	3.9	4.0
Surface course	2.8	2.8	3.2	2.6	2.8	3.0
Cross-sectional area of drainage layer						
Average, ft^2	1.31	1.33	1.23	1.39	1.30	1.30
Average gradient of base of drainage layer, percent	1.6	1.4	1.7	2.1	2.1	1.9

Note: 1 in. = 2.54 cm. 1 ft^2 = 0.09 m^2. Average width of section = 6.40 ft (19.51 m); length of section = 4.0 ft (12.2 m).

Figure 3. As-constructed test track.

Table 9. Water passed through test sections during drainage tests.

Load Applications	Discharge at Outlet End by Section (ft^3/min)						Total Duration (min)
	1	2	3	4	5	6	
224	0.523 A	0.571 A	0.566 A	0.604 A	0.377 A	0.566 A	10
4,040	0.433 A	0.447 A	0.427 A	0.457 A	0.311 A	0.442 A	10
8,200	0.370 A	0.411 A	0.343 A	0.406 A	0.261 A	0.390 A	10
50,000	0.284 A	0.279 A	0.235 A	0.329 A	0.237 A	0.343 A	10
53,000[a]	0.284 A	0.290 D	0.307 C	0.330 B	0.245 A	0.346 A	10
60,000[a]	0.213 A	0.228 D	0.175 C	0.245 B	0.162 A	0.293 A	60
71,000[a]	0.271 A	0.276 E	0.294 D	0.314 C	0.227 A	0.354 A	10
101,000[a]	0.231 A	0.235 E	0.206 D	0.275 C	0.217 A	0.280 A	10
118,900	0.230 A	0.102 B[b]	0.186 A	0.244 A	0.225 A	0.322 A	10
130,000[a]	0.266 A	—	0.171 D	0.238 C	0.182 A	0.222 A	30
144,000[a]	0.222 A	—	0.192 E	0.270 C	0.230 A	0.267 A	30
148,000[a]	0.213 A	—	0.159 E	0.254 A[bc]	0.227 A	0.283 A	10
150,000[a]	0.166 A	—	0.159 E	—	0.205 A	0.232 A	30
164,000[a]	0.240 B	—	0.184 E	—	0.189 A	0.222 A	30
200,000[a]	0.237 B	—	0.129 E	—	0.212 A	0.203 A	30
210,000[a]	0.183 B	—	0.146 E	—	0.189 A	0.210 A	30
233,000[a]	0.168 C	—	0.085 E	—	0.266 A	0.285 B	10
246,074	0.140 B	—	0.059 C	—	0.222 A	0.281 B	10

Note: Turbidity scales for discharge water: A = clear, B = almost clear, C = slightly dirty, D = dirty, and E = very dirty. 1 ft^3/min = 0.0005 m^3/s.

[a]Application of loads during drainage test.
[b]Test conducted before removal of test section.
[c]Water passed through section 4 without load application.

TEST RESULTS

Table 9 gives the records of water that passed through the test sections during the drainage tests. From these data, the coefficients of permeability were calculated for each section by using Eq. 2. These results are given in Table 10. For the calculations of the coefficient of permeability, it was also assumed that the area of the cross section and the average transverse gradient of the drainage layer remained constant throughout the duration of the test. The temperature at which the permeability tests were conducted ranged from 70 F to 80 F (21 C to 27 C).

Section 1

Section 1 was made of an asphalt concrete surface, an OGBAM (CA-7) drainage layer, and a 2.2-in. (5.6-cm) lime-clay mixture layer placed over the subgrade.

The drainage trend, i.e., the change in the drainage of the OGBAM (in terms of rate of discharge and coefficient of permeability, k) with respect to the number of load applications, is shown in Figure 4. The coefficient of permeability of the drainage layer decreased by almost half from the initial value of 37,900 ft/day (13.4 cm/s) to 20,600 ft/day (7.27 cm/s) after 50,000 load applications. The coefficient of permeability stabilized at about 17,000 ft/day (6.0 cm/s) and then started decreasing at an increasing rate after 200,000 load applications to reach a final value of 10,000 ft/day (3.5 cm/s) at 246,074 load applications. As can be seen from Table 9, clear water was discharged up to 150,000 load applications. Up to 230,000, the turbidity of the water remained at almost the clear water level, and, just before the end of the testing program, the turbidity changed to the slightly dirty water level. The turbidity of the discharged water is shown in Figure 5 at 100,000 load applications.

Little rutting occurred in the lime-clay layer. Some consolidation occurred in the surface course and the OGBAM drainage layer.

When the section was opened up at the end of the testing program, the OGBAM matrix had loosened in the region of the wheel path and the particles had been covered with infiltrated fines from the lime-clay mixture. The OGBAM had penetrated into the lime-clay mixture layer to a depth of about ½ in. (13 mm).

Section 2

Section 2 was made of an asphalt concrete surface course and an OGBAM (CA-7) drainage layer placed over a filter cloth directly on the subgrade.

The drainage trend of the drainage layer is shown in Figure 4. The coefficient of permeability of the drainage layer decreased by almost half from an initial value of 46,200 ft/day (16.3 cm/s) to 22,600 ft/day (7.98 cm/s) after 50,000 load applications. The drainage performance of this section deteriorated rapidly with the continuous application of load and water, and dirty water was discharged almost immediately. The coefficient of permeability dropped to 8,300 ft/day (2.93 cm/s), and the turbidity of water increased rapidly to the very dirty water level (Table 9). Figure 5 shows the extent of the washing of the subgrade fines at 100,000 applications.

After 50,000 load applications, rutting progressed at an increasing rate and was 2.5 in. (6.4 cm) deep at the point of maximum rutting after 118,900 load applications. Transient deflections under wheel load became apparent to the observer at about 60,000 load applications, and the magnitude of these deflections increased when there was further loading. Faint cracks appeared in the region of the wheel path at about 75,000 load applications and propagated as there was more loading. During the drainage tests, some water was forced up to the surface through these cracks. Most of the rutting occurred in the subgrade, apparently because of consolidation and piping of the fines.

Section 2 was removed after 118,900 load applications. When the section was opened up, the OGBAM matrix in the region of the wheel path had loosened and could be removed with only a shovel. Also, the OGBAM particles had become coated with dirt.

Table 10. Coefficient of permeability of layers of open-graded bituminous aggregate mixtures.

Load Applications	Coefficient of Permeability by Section (ft/day × 1000)					
	1	2	3	4	5	6
224	37.9	46.2	39.5	33.2	20.9	36.3
8,200	26.8	35.7	23.9	22.3	14.5	25.0
20,000	24.8	32.2	27.0	20.5	16.0	24.1
50,000	20.6	22.6	15.1	18.1	13.1	21.9
101,000[a]	16.7	19.0	14.4	15.1	12.0	17.9
118,900	16.7	8.3[b]	13.0	12.3	12.5	20.6
148,000[a]	15.4	—	11.1	13.9[bc]	12.6	18.1
246,074	10.1	—	5.1	—	12.3	18.0

Note: 1 ft = 0.3048 m.

[a]Application of loads during drainage test.
[b]Test conducted before removal of test section.
[c]Water passed through section 4 without load application.

Figure 4. Coefficient of permeability versus load applications.

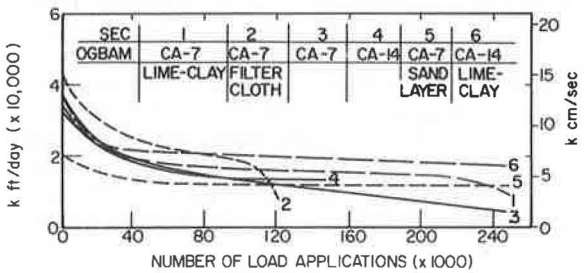

Figure 5. Turbidity of discharge water at 100,000 load applications.

The state of the filter cloth could not be determined because it had been damaged during removal of the OGBAM layer. However, it appeared to have withstood, without damage, the high temperature [about 300 F (150 C)] to which it was subjected during placement of the OGBAM.

Section 3

Section 3 was made of an asphalt concrete surface course and an OGBAM (CA-7) drainage layer placed directly over the subgrade.

The drainage trend of the drainage layer is shown in Figure 4. The coefficient of permeability of the drainage layer decreased by almost half from an initial value of 39,500 ft/day (13.9 cm/s) to 21,000 ft/day (7.4 cm/s) at 50,000 load applications. It continued to decrease at an almost constant rate with further load applications to 5,100 ft/day (1.8 cm/s) at the end of the testing program. Slightly turbid water was discharged when loading was initiated simultaneously with the drainage test. The discharged water became quite turbid during further load applications, and, by 138,000 applications, very dirty water was discharged (Table 9). The level of turbidity of the discharge water at 100,000 load applications can be seen in Figure 5.

Little rutting took place in this section, and the maximum rut depth was about ¼ in. (6 mm) at the end of testing.

When the section was opened up at the end of the testing program, the OGBAM matrix in the region of the wheel path was loose and was covered substantially with dirt to the extent that the OGBAM looked as if it were almost clogged with fines. The OGBAM between the wheel path and the outlet end was also covered with fines from a depth of about 3 in. (7.6 cm) near the wheel path to about 2 in. (5.0 cm) near the outlet end.

Section 4

Section 4 was made of an asphalt concrete surface course and an OGBAM (CA-14) drainage layer placed directly over the subgrade.

The drainage trend of the drainage layer is shown in Figure 4. The coefficient of permeability of the drainage layer decreased by almost half from an initial value of 33,200 ft/day (11.7 cm/s) to 18,100 ft/day (6.4 cm/s) at 50,000 load applications and decreased gradually with further load applications to a value of 13,900 ft/day (4.9 cm/s) at 145,940 load applications when the section was removed from test because of excessive rutting. As can be seen in Table 9, some fines washed out with the discharged water when the first loading was applied simultaneously with water for the drainage test. As there were further load applications, the quantity of fines washing out increased, and at the time of removal of the section the turbidity of the discharge water had reached a level of slightly dirty water. Figure 5 shows the turbidity levels at 100,000 load applications.

Rutting progressed rapidly in this section, and the rut depth at the point of maximum rutting progressed from $1\frac{3}{16}$ in. (30 mm) at 90,000 load applications to 2 in. (50 mm) at 145,940 load applications. A faint crack appeared in the middle of the section at about 140,000 load applications, and some water was forced to surface during subsequent drainage tests. Transient deflections were observable after about 144,000 load applications. Most of the rutting in this section occurred in the subgrade.

The section was removed after 145,940 load applications. When the section was opened up, the OGBAM was loose in the region of the wheel path and could be shoveled out. The OGBAM particles were covered with dirt.

Section 5

Section 5 was made of an asphalt concrete surface course, an OGBAM (CA-7) drainage layer, and a sand filter (torpedo sand) placed over the subgrade.

The drainage trend of the drainage layer is shown in Figure 4. The coefficient of permeability of the drainage layer decreased by about a third from an initial value of 20,900 ft/day (7.4 cm/s) to 13,000 ft/day (4.6 cm/s) at 50,000 load applications. There was no significant decrease in the rate of discharge with further load applications, i.e., the coefficient of permeability stabilized at about 12,700 ft/day (4.5 cm/s). Because the lip of the catch basin was formed over the sand filter layer, the turbidity data may not be relevant; however, clear water was discharged throughout the testing program.

Rutting progressed gradually as there was more loading from $\frac{3}{4}$ in. (19 mm) at 90,000 load applications to $1\frac{1}{2}$ in. (3.8 cm) at the point of maximum rutting at 246,074 load applications. Rutting occurred primarily in the sand layer and was apparently due to consolidation.

When the section was opened up at the end of the test, the OGBAM matrix was loose in the region of the wheel path. Sand had filtered from about $\frac{1}{2}$ in. (13 mm) to $\frac{3}{4}$ in. (19 mm) into the OGBAM layer.

Section 6

Section 6 was made of an asphalt concrete surface course, an OGBAM (CA-14) drainage layer, and a 2.6-in. (6.6-cm) lime-clay mixture layer placed over the subgrade.

The drainage trend of the drainage layer is shown in Figure 4. The coefficient of permeability of the drainage layer decreased by about 40 percent from an initial value of 36,300 ft/day (12.8 cm/s) to 21,900 ft/day (7.7 cm/s) at 50,000 load applications and decreased gradually with further load applications to 18,000 ft/day (6.4 cm/s) at 246,074 load applications. As can be seen from Table 9, clear water was discharged until almost the end of the test. Some fines washed out with the discharge water after about 230,000 load applications. The clearness of the discharge water at 100,000 load applications can be seen in Figure 5.

Rutting progressed gradually to a maximum rut depth of $1\frac{1}{16}$ in. (27 mm) at the end of the testing program (246,074 load applications). The surface layer consolidated, and some rutting occurred in the lime-clay mixture layer.

When the section was opened at the end of the test, the OGBAM matrix was loose within the region of the wheel path; however, the dirt covering the particles was confined only to the lower region of the drainage layer, and the upper region seemed relatively free of the dirt cover. About $\frac{1}{2}$ in. (13 mm) of the drainage layer had penetrated into the lime-clay mixture.

DISCUSSION OF RESULTS

From previous experience on the test track, we feel that the test track loading on the OGBAM layer is significantly more severe than the expected loading on an OGBAM layer used as a subbase for concrete pavements. Similarly, the stresses in the OGBAM layer and the subgrade of the typical test section, which were caused by a 3,200-lb (145-kg) wheel load, were significantly higher than the stress levels expected in the OGBAM layer and the subgrade when they were used as a subbase for a concrete slab on which typical highway loading had been applied. Other factors also contributed to the severity of loading. The loads in the test track are applied at a greater frequency; therefore, the recovery time between loads is decreased. The twisting action of the tire on pavement as the loading frame revolves around the track probably adds an additional component of stress to the pavement. Thus, the structural and drainage distress levels (washing out of fines) were relatively higher in the test sections than were expected under a typical concrete slab pavement.

As can be observed from the test results, all the drainage layers started out with a high coefficient of permeability that decreased substantially during initial loading. Figure 4 shows the trend of the change in coefficient of permeability with respect to loading for all sections. The initial changes in the coefficients of permeability are similar in all the sections except for section 5, which started out with a lower coefficient

value. It appears likely that these changes were due to initial consolidation and rearrangement of the particle matrix in the OGBAM layers. This phenomenon should be greatly reduced in a typical pavement installation because of much lower anticipated stress levels and lower levels of deflection.

The experimental design was formulated to allow the comparison and the evaluation of the effects of different variables with various replications. By comparing the responses of sections 1 and 6 and sections 3 and 4, one can see that the effect of aggregate gradation, the CA-7 type of gradation as compared to the CA-14 type of gradation, seems not to be significant in regard to permeability. However, as can be seen from Table 9, sections 1 and 3, which had OGBAM layers with CA-7 aggregate gradation (slightly coarser gradation than that of the CA-14 aggregates), exhibited a more pronounced tendency for washing out the subgrade fines. Consequently, they also had a greater tendency to plug than did their corresponding sections 6 and 4.

The effect of the different design variables can be evaluated by comparing the response of the 4 sections that had OGBAM layers made of CA-7.

Section 2, which had the OGBAM layer on a filter cloth, gave the poorest performance. It appears that the repeated dynamic loadings caused the subgrade fines to filter through the openings of the filter cloth (average size opening equal to that of a No. 140 mesh sieve). The fines subsequently washed out. Section 3 gave a poor performance in terms of drainage, but for some reason little rutting occurred. Sections 1 and 5 showed stable behavior in terms of drainage capacity. After the initial decrease in the permeability, a gradual decrease took place as more loads were applied.

Because of the open-graded nature of the OGBAM, sufficiently accurate measurement could not be made of the degree of compaction achieved during construction of the OGBAM layers. Therefore, the correlation between the amount of voids in the OGBAM and the drainage characteristics cannot be made with any confidence. The measured bulk specific gravity of the OGBAM layers ranged from 1.74 to 1.82. The average voids content in the OGBAM was 29.1 percent, and the time required to fill up these voids after inflow was initiated was 10 min. However, in most sections, water appeared at the outlet end after about 2 min 30 s, and the steady state of the flow was attained within 1 additional min. Therefore, it is possible that for most of the length of flow only a part of the cross-sectional area of the OGBAM layer was used for the flow of water. If this is true, higher values for the coefficients of permeability than indicated earlier would result. Consequently, the coefficient of permeability values presented in this paper should be considered conservative.

The modification of the characteristic of subgrade clay soil with small quantities of lime (2 percent) can be highly beneficial in lime-reactive soils. The cohesive nature of the lime-modified clay restricted the washing out of the subgrade fines; however, the behavior of lime-modified clay when the pavement is subjected to a high degree of groundwater seepage or significant frost action will need further investigation.

At the end of the testing of each section, it was observed that the OGBAM matrix within the region of the wheel path had become unbound and could be shoveled out of most sections. This may have been due to an inadequate asphalt cement film covering the aggregate particles, which resulted in the fatigue of the asphalt cement bond between the particles, which was caused by the heavy repeated wheel loads. In a rigid pavement, the looseness of the OGBAM may pose few problems, but in a flexible pavement this loss of bond may cause a loss in pavement performance. For in-service pavements, this problem can possibly be reduced by imposing a maximum allowable stress on the OGBAM layer and restricting the total resilient deformation. It is probable that the use of softer and slightly increased amounts of asphalts could be effective in securing a more lasting bond between the aggregate particles.

This study was designed to evaluate the performance of drainage sections by the consideration of only surface water inflow, and this fact should be remembered when the results of this study are used.

CONCLUSIONS

In terms of the objectives of the study, the following conclusions can be drawn from the results. OGBAM layers possess a high order of permeability. No significant difference was observed in the drainage behavior of OGBAM with CA-7 aggregates and that with CA-14 aggregates. For design purposes, the coefficient of permeability values for either gradation of OGBAM can be conservatively estimated at 10,000 ft/day (3.5 cm/s). The use of OGBAMs in a properly designed pavement structure is not detrimental to the overall performance of the system. The limited results show that

1. Satisfactory performance can be obtained by incorporating a sand filter with the OGBAM drainage layer.
2. OGBAM drainage layers placed on modified clay subgrades can be expected to perform at a higher level than those placed directly on natural clay subgrades.
3. Use of a filter cloth in a structural drainage section subjected to heavy wheel loads and high inflows of water into the pavement section may be detrimental to the performance of the pavement system.

ACKNOWLEDGMENTS

Information for this paper was collected as a part of an Illinois Cooperative Highway Research Program project (10). The study was conducted by the Department of Civil Engineering at the Engineering Experiment Station, University of Illinois, under the sponsorship of the Illinois Department of Transportation.

The opinions, findings, and conclusions expressed in this paper are those of the authors and are not necessarily those of the Illinois Department of Transportation.

The help of the Illinois Association of Aggregate Producers in supplying the aggregates used in this study is appreciated.

REFERENCES

1. H. R. Cedergren and W. R. Lovering. The Economics of and Practicability of Layered Drains for Roadbeds. Highway Research Record 215, 1968, pp. 1-7.
2. W. R. Lovering and H. R. Cedergren. Structural Section Drainage. Proc., International Conference on the Structural Design of Asphalt Pavements, Ann Arbor, Mich., Aug. 1962.
3. H. R. Cedergren. Seepage, Drainage and Flow Nets. John Wiley and Sons, New York, 1967.
4. Implementation Package for a Drainage Blanket in Highway Pavement Systems. Office of Development, Federal Highway Administration, U.S. Department of Transportation, May 1972.
5. H. R. Cedergren and Ken O'Brien and Associates. Development of Guidelines for the Design of Subsurface Drainage Systems for Highway Pavement Structural Sections. Office of Research, Federal Highway Administration, Final Rept. FHWA-RD-73-14, Feb. 1973.
6. R. E. Collins. Flow of Fluids Through Porous Materials. Reinhold Publishing, New York, 1961.
7. A. L. Straub, H. N. Schenck, Jr., and Frank E. Przybycien. Bituminous Pavement Temperature Related to Climate. Highway Research Record 256, 1968, pp. 53-78.
8. H. L. Ahlberg and E. J. Barenberg. The University of Illinois Test Track—A Tool for Evaluating Highway Pavements. Highway Research Record 13, 1963, pp. 1-21.
9. E. J. Barenberg and O. O. Thompson. Behavior and Performance of Flexible Pavements Evaluated in the University of Illinois Pavement Test Track. Civil

Engineering Studies, Univ. of Illinois, Urbana, Highway Engineering Series 36, Jan. 1970.

10. E. J. Barenberg and S. D. Tayabji. Evaluation of Typical Drainage Systems Using Open Graded Bituminous Aggregate Mixture Drainage Layer. Civil Engineering Studies, Univ. of Illinois, Urbana, Transportation Engineering Series 10, May, 1974.

CAPACITANCE SENSOR FOR SOIL MOISTURE MEASUREMENT

Ernest T. Selig and Darold C. Wobschall, State University of New York at Buffalo; Sundru Mansukhani, Law Engineering Testing Company, Birmingham, Alabama; and Arif Motiwala, Stromberg-Carlson, Rochester, New York

Moisture content is an important parameter that controls the performance of earth materials. Because satisfactory techniques were not available, this study was undertaken to develop new instrumentation that could be permanently installed in highway substructures for long-term monitoring of moisture content. Moisture content determination requires that the amount of water and the dry weight in a given volume of soil be obtained. This study considered only the amount of water. A concept that involved the relationship between the amount of water in soil and the dielectric constant, an electrical property, was investigated. The electrical capacitance (C) of a pair of electrodes with moist material between them is related to the dielectric constant (K) by $C = (\alpha\epsilon_o)K$, where α is a constant based on the geometry of the electrodes and ϵ_o is the permittivity of the vacuum. So that instrumentation problems encountered in the measurement of capacitance and dielectric constant with laboratory methods used in the field could be overcome, the sensor electrodes and soil were incorporated in the resonance circuit whose frequency of oscillation is a function of the circuit components. The measured output is the difference between the frequency in soil and in an electronic reference substituted for the soil. The circuit design was first tested with the electrodes forming a container into which soil could be placed. Several configurations of the embedded sensor were designed and tested. The capacitance concept was useful for sensing change in the amount of moisture per unit volume of soil.

•MOISTURE CONTENT is one of the most important factors influencing the performance characteristics of earth materials. Insufficient or excessive moisture in the components of a highway system adversely affects the service behavior. Changes in moisture not only produce undesirable volume changes, but also increasing moisture reduces strength and traffic-supporting capability of materials used in the construction of bases, subgrades, and embankments.

Currently, engineers are hampered in their efforts to predict performance because of the lack of suitable instrumentation and techniques for adequate moisture measurement. One or more of the following limitations apply to monitoring moisture content: no remote readout capability, high cost, site disturbance, long-term instability, and inadequate response to moisture change. The development of an instrument that does not have these limitations is the objective of this paper.

A concept that appeared to be promising for fulfilling the objectives involves the relationship between soil moisture content and soil capacitance, which are sensed by a pair of embedded electrodes. An important part of this approach is that soil is used as the dielectric; i.e., it is part of the measurement circuit. This is believed to be a distinct improvement over previous approaches that depended on absorbing water from the soil into either a dielectric or resistive element and that used sensors that were highly influenced by placement conditions. It was also noted that the amount of water

Publication of this paper sponsored by Committee on Environmental Factors Except Frost.

absorbed depends on the soil type, unit weight, and the water content of the soil and that considerable hysteresis takes place during wetting and drying cycles.

At the outset of the study a literature review was conducted, which supplemented a previous review (1) so that information could be obtained on relevant past research related to capacitance methods for moisture determination. This information formed the basis for the sensor design and evaluation of the results.

After the literature reveiw, a preliminary, capacitance-measuring system was designed and constructed to evaluate the proposed electronic concepts and to obtain initial performance data for a range of soil types and moisture contents. Results from the initial tests led to an improved circuit design with a change in configuration of the sensor. A more extensive investigation was then made of the influence on sensor output of variables such as soil composition, soil density, soil moisture content, soil and sensor temperature, and electronic circuit characteristics. These tests resulted in further circuit modifications that improved the sensor performance.

The final task involved the selection of suitable configurations for the embedded sensor. The effects of geometry and size on sensitivity, accuracy, and placement techniques were examined. On the basis of the results, three final prototype sensor configurations containing printed electronic circuit boards were designed and fabricated. The evaluation of these sensors was conducted primarily in the laboratory by using a variety of prepared soil samples.

BASIC CONCEPTS

The two electrical properties of soil involved in the capacitance sensor concept are dielectric constant (K) and conductivity (σ). For most solid components of soil alone K lies in the range of 2 to 4, and the water component alone has the much higher value of 78 to 81. Therefore, K of a soil sample is expected to vary primarily with the amount of water present per unit volume of soil, which for our purposes is termed moisture density (m_v expressed in g/cm^3). This is in contrast to the conventional moisture content defined as the ratio of weight of water to the weight of dry soil (w) expressed as a percentage. These two definitions of the amount of moisture are, of course, related to each other by the dry density of the soil (γ_d) in g/cm^3 as follows

$$w = \frac{100\ m_v}{\gamma_d} \tag{1}$$

It is not possible with any method to determine soil moisture without measuring the amount of water present and the weight of a given quantity of soil. This study concerns the means of determining the amount of water present per unit volume of soil. Other methods, a variety of which already exists, are needed for determining the soil density so that conventional moisture content can be computed.

The capacitance (C) of a sensor consisting of a pair of electrodes embedded in soil is related to dielectric constant by

$$C = \alpha \epsilon_o K \tag{2}$$

where

α = electrode geometry constant, and
ϵ_o = permittivity of the vacuum.

Similarly the electrical conductance (g) of the embedded electrodes is related to the soil conductivity (σ) by

$$g = \alpha \sigma \tag{3}$$

Conductance is the reciprocal of the resistance measured across the pair of electrodes, and the soil resistivity is the reciprocal of the conductivity.

In most previous studies, C and g have been measured by an impedance bridge that operates at various alternating current frequencies. K and σ may then be computed separately by using Eqs. 2 and 3. For soil, these values will depend on the oscillator frequency of the bridge at which C and g were measured and on the moisture content. We used an alternate measurement method that is based on the frequency shift of an oscillator circuit, which incorporates the soil electrodes as one component. For a given pair of electrodes, the frequency shift is a function of the nominal oscillator frequency and both K and σ.

The electrical measurement most commonly used in the past for moisture determination has been conductance (or its reciprocal, resistance). However, instead of incorporating the soil directly, one usually measured the conductance of a sensor that absorbs moisture from the soil. This approach has generally been too inaccurate for engineering use.

The capacitance or dielectric constant approach has been investigated with a wide variety of materials including coal; glass; paper; fiber-reinforced plastics; concrete; rock cores; soil types such as clay, silts, sands, and gravel; and agricultural products such as wheat, peas, and oats (2). Moisture contents from 0 to 450 percent have also been considered, depending on the type of material. The values over 100 percent are primarily montmorillonites. Many investigators have correlated C or K with w rather than with m_v. This has suggested much greater composition effects than actually exist. Reported experimental results clearly indicate that the electrical parameters should be correlated with m_v rather than w.

A variety of electrode configurations have been used in past studies (2). These basically may be classed as (a) containers in which the material being measured is placed in a device whose sides form the electrodes (Fig. 1), or (b) fringing probes in which the electrodes are placed against or inserted into the material (Fig. 2). The fringing probes are required for in situ measurements.

A range of measurement frequencies from 1000 Hz to 1.5 GHz has been used in the past. From instrumentation and composition considerations, the radio frequency range of 10 to 100 MHz seems to be best for soil applications.

Generally, K increases nonlinearly as m_v increases. For a given electrode configuration at a specific oscillator frequency, K, unlike σ, is primarily a function of m_v; secondary variations are caused by soil composition (Fig. 3). This trend is believed to be partly a result of the difference in electrical properties of free and absorbed water.

In addition K decreases with increasing frequency, and σ increases with increasing frequency (Fig. 4). This phenomenon is termed electrical dispersion. The frequency effect is present even though the values of K and σ for the individual solid and liquid components of soil (e.g., saturated illite Grundite) do not depend on frequency. These characteristics have been explained by the fact that the electrical equivalent circuit for soil consists of a network of parallel-series combinations of resistance and capacitance elements (4).

In summary, the capacitance method is promising and better than conductance methods for measuring m_v. Soil composition appears to be a secondary factor, which can be accounted for by calibration. The technique should work in most soils over any desired moisture content range if the sensor is properly designed; however, the measurement systems used in past studies are generally only suitable for laboratory use with short-term monitoring. Therefore, the main objective of this research was to develop an electrical circuit and sensor configuration for field use that can achieve the desired technical requirements.

SENSOR DESIGN AND RESULTS

A capacitance bridge used as a measurement device is not satisfactory as is a buried sensor, where remote readout is required. A better approach is to incorporate the electrodes containing the soil dielectric as part of a resonance circuit, which oscillates at a frequency based on the magnitude of the circuit components. A simple example of such a circuit is shown in Figure 5. In this example as the soil capacitance (C_s)

Figure 1. Device for studying soil electrical properties (3, 4).

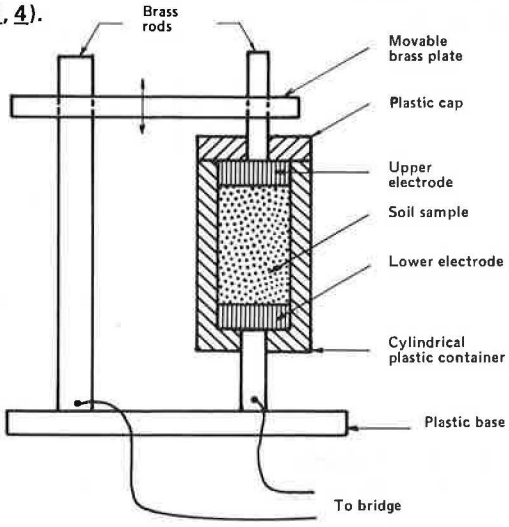

Figure 2. Probe for soil moisture measurement (5).

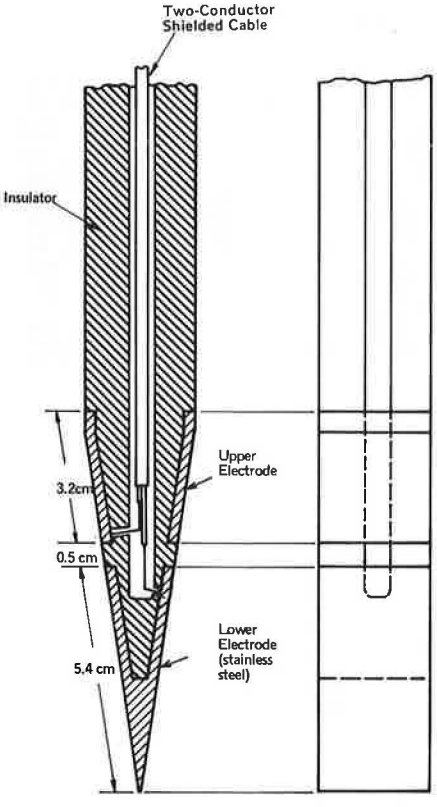

Figure 3. Relationship between capacitance and moisture density for a variety of soils (5).

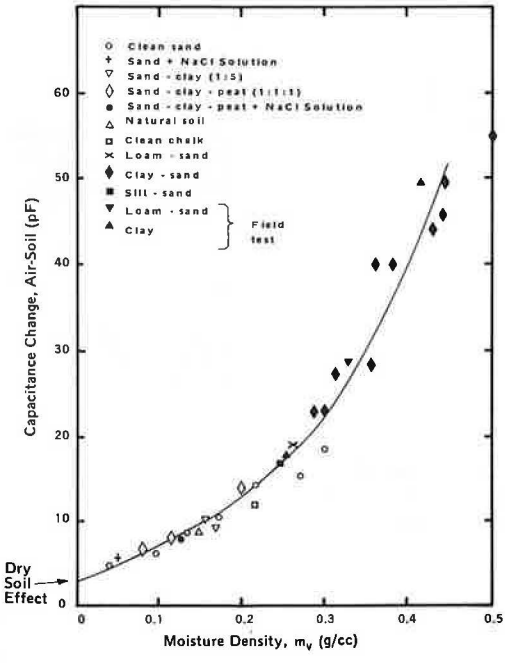

Figure 4. Dielectric and conductivity dispersion characteristics of saturated illite Grundite (3).

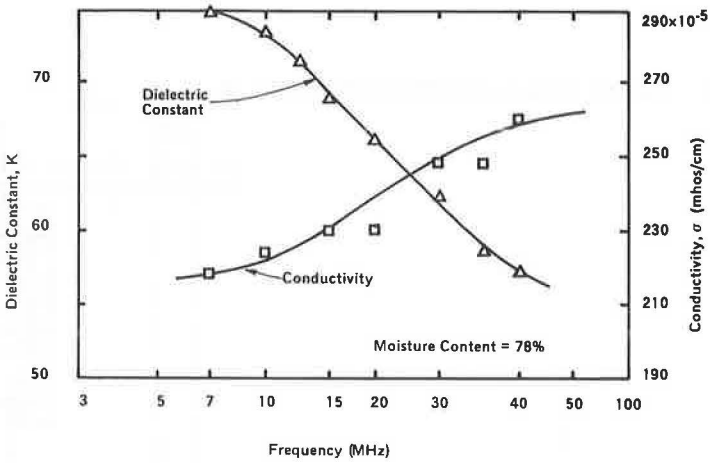

Figure 5. Simplified apparatus for resonance frequency shift.

$$f = \frac{1}{2\pi\sqrt{L\,(C_s+C_o)}}$$

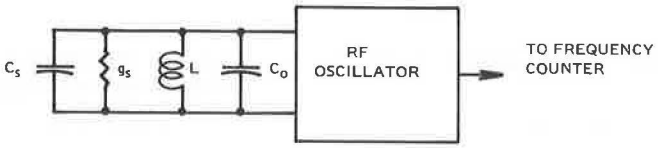

Figure 6. Rectangular container apparatus.

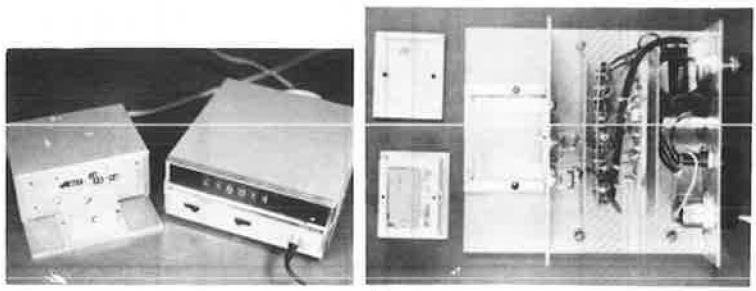

(a) assembled as in test (b) disassembled

Figure 7. Cross section of rectangular container for laboratory tests.

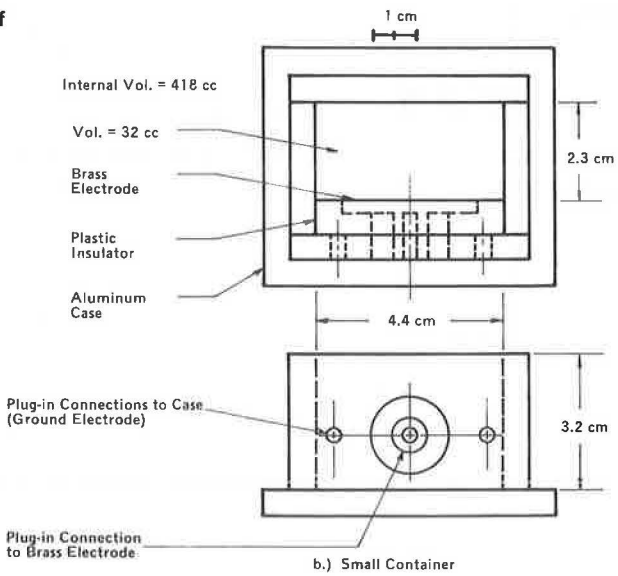

changes, the measured frequency (f) changes. The frequency change with respect to dry soil (Δf_d) or an electronic reference (Δf_r) can be accurately measured from a remote station.

For a particular electrode, nominal frequency, and soil type, a calibration curve can be prepared relating Δf to m_v; however, the soil conductance (g_s) may be high enough to also affect Δf. The choice of nominal frequency and circuit component values can be selected to minimize this adverse effect of g_s for a particular soil. By use of the capacitance bridge approach, C_s and g_s can each be determined because they are independently measured; however, by use of the frequency shift method, in which only one parameter is measured, the effect on Δf of g_s changes cannot be distinguished from the effects of C_s changes. Preliminary experiments showed that circuit changes to minimize the effects of g_s also reduced the sensitivity of the system to m_v changes. Therefore, a compromise is needed between sensitivity and composition effects because the differences in g_s values among soils to be tested is expected to be the primary cause of calibration curve changes. It may not be possible to eliminate the effect of g_s sufficiently by the choice of circuit so that one calibration curve will be achieved for all soils.

The first sensors constructed were containers for evaluating various circuit designs and for studying the influence of soil conditions on system performance (Figs. 6 and 7). A conventional frequency counter was used as the readout device. At first, oscillator instability occurred in the bentonite clay at all moistures and at the higher frequencies and moistures tested for the other soils. This was believed to be a result of high conductivity; however, sensitivity in terms of $\Delta f/\Delta m_v$ also increased significantly as nominal frequency increased up to frequencies at which the circuit stopped functioning.

Improved performance was obtained through a long series of design changes and trials in which rectangular plug-in containers were used. The nominal operating frequencies obtained with this apparatus ranged from 15 to 40 MHz. The following conclusions were drawn from these tests:

1. Δf_r increased as m_v increased; however, the rate often decreased again at moisture densities above $m_v = 0.6$ to 0.8 g/cm^3 (Fig. 8). This latter trend is correctable by circuit component changes, but a reduction in sensitivity will also occur.
2. In the final set of tests with the rectangular container (at 21 MHz), most soils had approximately a common calibration curve (Fig. 9). Only bentonite departed significantly from this trend. All curves had a common intercept at $m_v = 0$.
3. Temperature change had little effect on the results as long as freezing was avoided.
4. The standard deviation of the Δf_r measurement variation was 0.1 to 0.2 kHz for the electronics over a 2-day period. Short-term variability with soil samples ranged from 0.2 to 1.4 kHz. The m_v values corresponding to these standard deviations are about 0.002 to 0.03 g/cm^3, which is equivalent to moisture content variation from 0.1 to 1.5 percent. However, most of this variation in soil was believed to be caused by specimen preparation rather than instrumentation.
5. If the container size was geometrically scaled up or down, then the calibration relationships remained essentially unchanged.
6. Void ratio or dry unit weight of a soil sample had little effect on the Δf_r-m_v calibration curve. Varying the amounts of specimen compaction for a constant w changed m_v, but Δf_r changed correspondingly.
7. The insensitivity to compaction made the container apparatus useful for rapid moisture determination of soil samples in the laboratory or field. So that w could be obtained the soil was uniformly tamped into the container, and the sample weight and Δf_r were measured.

After the system was evaluated with the rectangular container, the research effort was directed toward developing a fringing-probe type of sensor. Four sensors representing three configurations (cylindrical, parallel plate, and disk) were designed and tested (Figs. 10, 11, and 12). The electronic circuit used in these sensors (2) was

Figure 8. Sensor response for tests on clays at three frequencies.

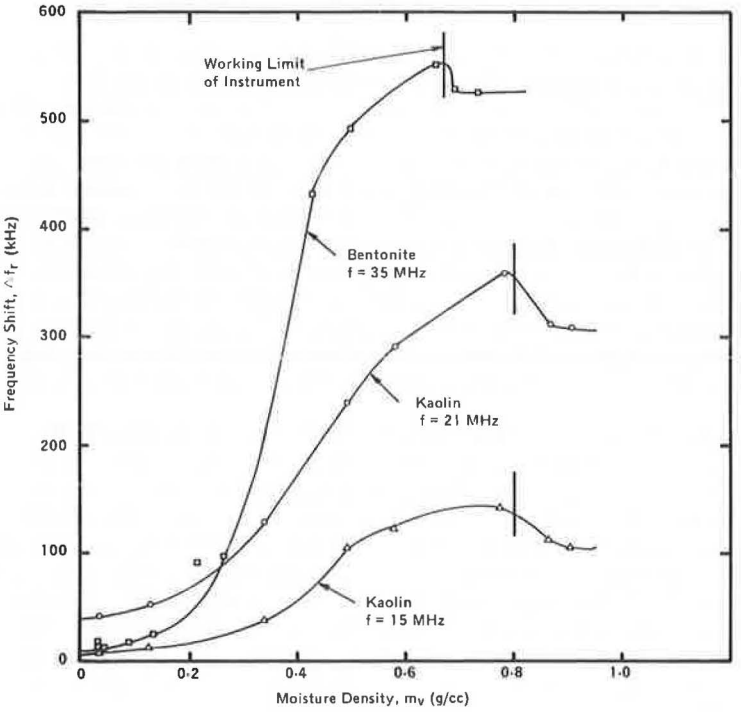

Figure 9. Calibration curves for a range of soils tested with rectangular container at 21 MHz.

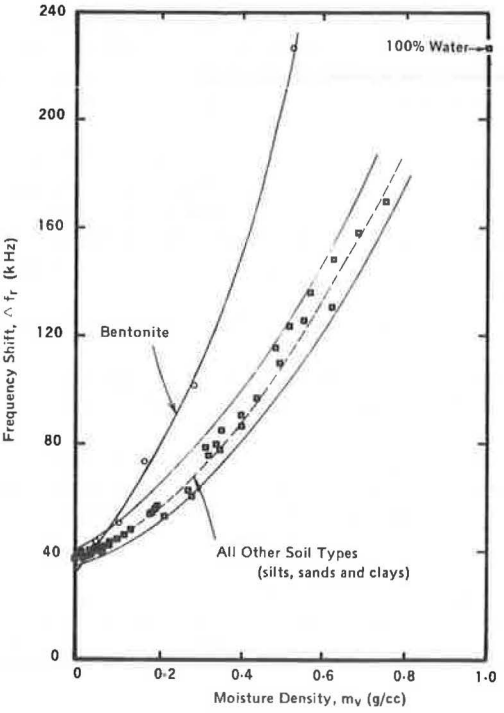

Figure 10. Prototype of cylindrical embedded sensor.

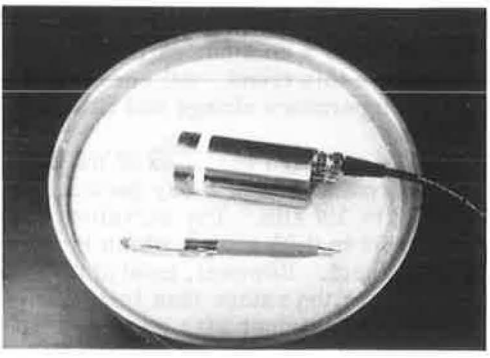

Figure 11. Cross section of prototype of cylindrical embedded sensor.

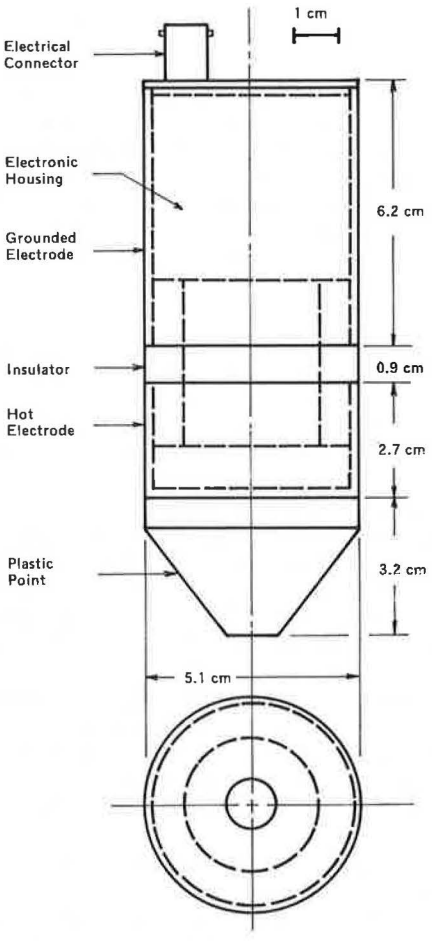

Figure 12. Alternate configurations for embedded sensor.

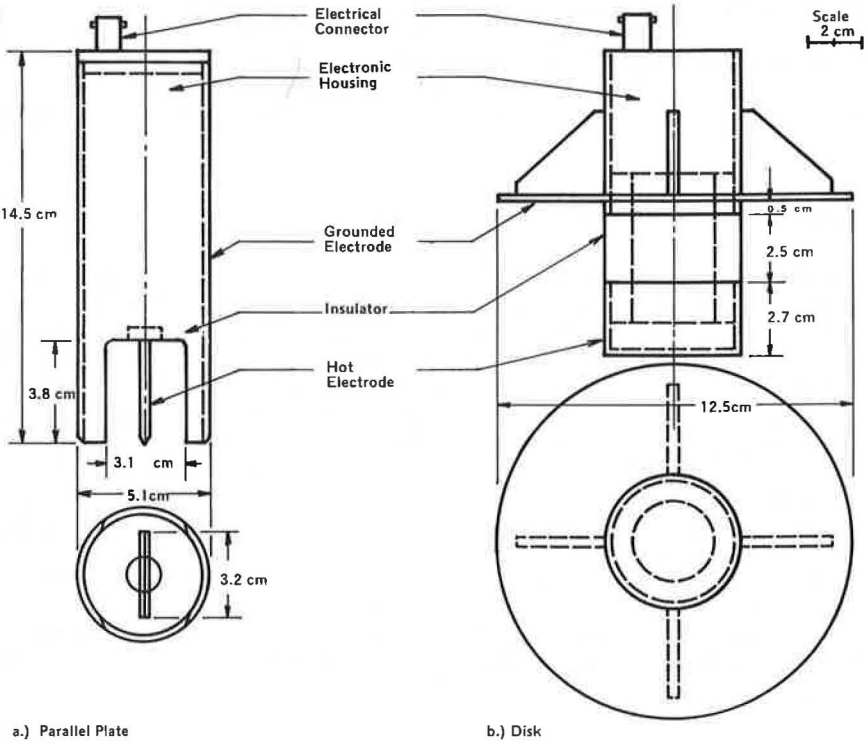

essentially the same as the final version for the rectangular container. Printed circuit boards holding most of the electronic components were placed inside the sensors. A coaxial cable connected the sensor to the remote readout station, which consisted of a power supply, control switch, and frequency counter. The nominal operating frequency was 25 MHz. The approximate fringing fields indicating the zone of soil influencing the reading in each case are shown in Figure 13.

The following conclusions were drawn from the evaluation tests done with an embedded sensor:

1. The frequency shift increase was approximately proportional to the moisture density increase (measured with cylindrical, disk, and parallel-plate sensors) for the coarse-grained soils (Figs. 14, 15, and 16). The frequency shift with the kaolin was higher than that for any of the other soils tested, and it increased as moisture density increased. The extension of the curves for the coarse-grained soils corresponded with the Δf_r values in water alone.
2. The three configurations had about the same sensitivity to moisture change and the same intercept at zero moisture. The choice of sensor used, therefore, was primarily dictated by the type of application and method of installation.
3. The soil types involved in the sensor evaluation included clay up to 100 percent moisture content, silt, sand, and gravel up to 1 in. (2.54 cm). Although no single sensor was satisfactory over this entire range of conditions, the results suggested that sensors can be designed to handle all of these conditions.
4. For coarse-grained materials, the minimum sensor size is limited by the particle size of the material. Sensor electrode spacing should probably be at least as great at the D_{90} particle size (size below which 90 percent of the sample falls). The maximum associated sensor dimensions will depend on the sensor geometry.
5. The output appeared to be sensitive to changes in salt concentration and soil composition.
6. The short-term variability of the electronic system expressed as standard deviation of Δf_r was about 0.15 kHz for the small cylindrical sensor and 0.75 kHz for the large cylindrical sensor. These values correspond to standard deviation errors in m_v of about 0.002 g/cm^3 and 0.005 g/cm^3 and in w of about 0.1 and 0.3 percent for the small and large cylinders respectively. A few repeated tests in soil with the small cylindrical sensor gave Δf_r standard deviations of 0.5 to 1.7 kHz, which correspond to 0.002 to 0.01 g/cm^3 variation in m_v and 0.1 to 1.5 percent variation in w. Sample preparation variability probably was the main reason for the larger errors with soil.
7. Field installation techniques can be expected to have a big effect on the results. This may be the major source of error in determining m_v with the frequency shift sensor concept.

SUMMARY OF SENSOR CAPABILITIES

The frequency-shift sensor can be designed to operate in almost any soil type including highly plastic clays and gravelly materials. The sensor can be monitored from a remote station and can be permanently sealed to operate when it is submerged. It can easily be made rugged enough to withstand shock and, by proper case design, it can withstand the loading intensity involved in highway applications: The case must be rigid enough to avoid geometry change under loading. Of the configurations tested, the cylindrical sensor is best. There should be no inherent hysteresis in the calibration curve during moisture fluctuations because the sensor monitors the soil moisture directly. Although moisture measurements in frozen soil are quite different from those in unfrozen soils, the sensor electronics can be selected to remain operative at any anticipated temperature.

Difficulty with sensor stability over many weeks, encountered in the early stages of this study, has been overcome. Although long-term performance tests have not yet been conducted, it is expected that, if reliable electronic components and printed circuit boards are used and the sensor is permanently sealed, 1- to 5-year operation periods are feasible.

Figure 13. Fringing fields for sensors.

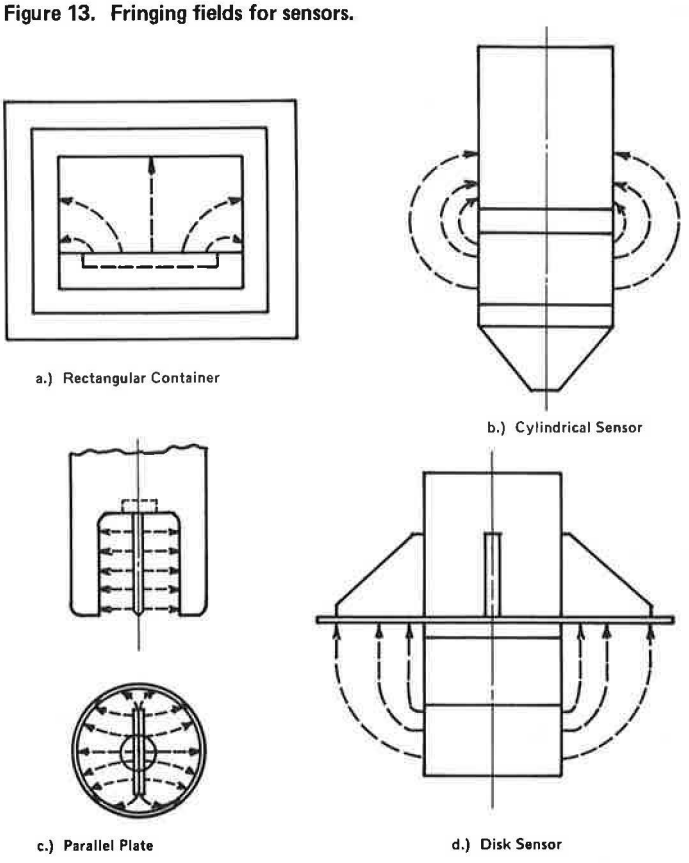

Figure 14. Calibration curve for cylindrical sensor.

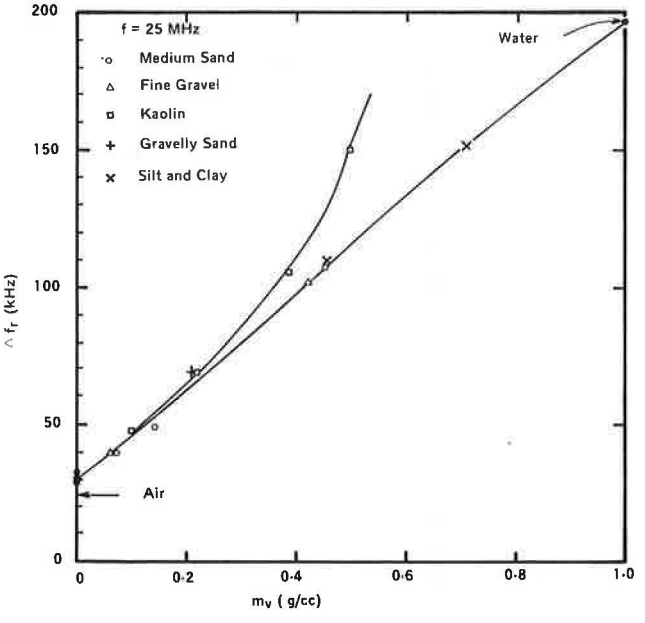

Figure 15. Calibration curve for disk sensor.

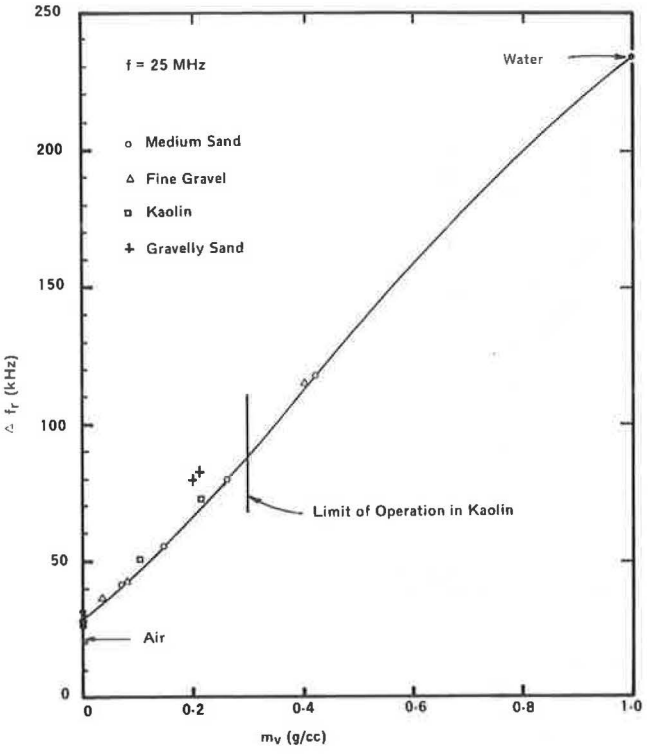

Figure 16. Calibration curve for parallel-plate sensor.

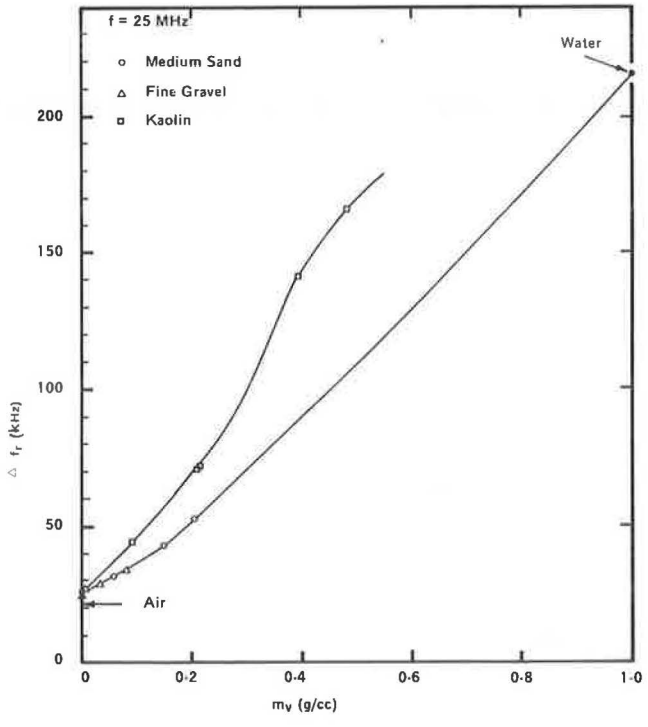

Sensor readout at a single oscillator frequency can be accomplished with a readily available battery-operated frequency counter. However, proper interfacing components, which are inexpensive and simple to construct, are needed. Special purpose readouts will simplify the process and permit multiple frequency readout. This latter arrangement may make it possible to eliminate the soil composition effect on the sensor calibration.

The sensor concept is scalable so that almost any size is possible. The smallest size, governed by the degree of circuit miniaturization for the electronic components within the sensor, is about 1½ in. (3.8 cm) long. The desired size will primarily be dictated by the soil conditions. The smallest size will be for silts and clays with uniform moisture content, and the largest size will be for gravelly materials and soils with heterogeneous moisture conditions. In these cases, the electrode spacing probably will need to be at least equal to the D_{90} size or the dimensions of the heterogeneity. However, disturbance of soil conditions by sensor installation is also determined by the sensor configuration and installation procedures. The sensor concept can easily provide the variety of configurations needed for optimum results over the range of desired highway applications.

The sensor can be designed to operate over almost any range of moisture content in any soil. However, there are several qualifying factors for meeting this objective: (a) A single circuit design will not be optimum for all possible conditions, (b) more than one calibration curve may be needed for each sensor geometry and circuit design to account for composition effects, and (c) the best sensor size and configuration will vary with the soil and application conditions. In addition, it must be recognized that the sensor only measures moisture content in terms of weight of water per unit volume of soil. Density measurements are also needed to compute moisture content in terms of ratio of weight of water to weight of dry soil. This is a limitation of all methods, however.

If a nominal dry unit weight of soil of 1.6 g/cm^3 (100 lb/ft^3) is assumed, then a 1 percent moisture change is equivalent to 0.016 g/cm^3 change in water per unit volume. The frequency-shift concept has the sensitivity to detect such moisture changes; however, accuracy depends not only on this sensitivity (precision) but also on such factors as long-term instrument stability, calibration curve accuracy, and placement conditions. Thus, overall accuracy is hard to assess. The sensor circuit design incorporates an internal reference to minimize errors caused by changes in the electronic system. (More experience is needed to determine the effectiveness of this technique.) Other sources of error must be controlled by the user.

In addition to the system capabilities described, one other useful application of the capacitance system for moisture determination has developed from this research. This application concerns disturbed soil samples such as those obtained in laboratory soil classification and compaction tests or in moisture control for field compaction. In these situations, a rapid method for moisture determination is desirable. The capacitance method can provide this capability by constructing a sensor in the form of a container in which to put the sample. This approach involves, first, uniformly tamping the soil into the container by hand. The electrical reading is then taken to get moisture per unit volume, and the sample weighed to get the wet weight per unit volume. These two immediate measurements will permit calculation of moisture content. This method can be used in the field as well as in the laboratory because the instrumentation system is portable. The electronic circuit is the same as that used in the embedded sensor system. By use of the proper calibration curves and size of container, essentially any soil type and moisture range can be tested.

ACKNOWLEDGMENTS

This research was performed by E. T. Selig and D. C. Wobschall at the State University of New York at Buffalo. A. Motiwala conducted the electronic development work, and S. Mansukhani performed the laboratory tests. Y. T. Kao participated in the final prototype evaluation. Throughout the project H. A. Smith of the National Cooperative Highway Research Program provided helpful comments and suggestions.

The opinions and conclusions in this paper are those of the authors and not necessarily those of the Transportation Research Board, Federal Highway Administration, American Association of State Highway and Transportation Officials, or of the individual states participating in the National Cooperative Highway Research Program.

REFERENCES

1. L. F. Ballard. Instrumentation for Measurement of Moisture—Literature Review and Recommended Research. NCHRP Rept. 138, 1973.
2. E. T. Selig, D. C. Wobschall, S. Mansukhani, and A. Motiwala. Capacitance Instrumentation for Measurement of Moisture in Bases, Subgrades and Earth Materials. State University of New York at Buffalo, Final Rept., NCHRP Project 21-2 (2), July 1974.
3. K. Arulanandan, R. Basu, and R. J. Scharlin. Significance of the Magnitude of Dielectric Dispersion in Soil Technology. Highway Research Record 426, 1973, pp. 23-33.
4. K. Arulanandan and S. S. Smith. Electrical Dispersion in Relation to Soil Structure. Journal, Soil Mechanics and Foundations Division, American Society of Civil Engineers, No. SM12, Dec. 1973, pp. 1113-1133.
5. A. M. Thomas. In-Situ Measurement of Moisture in Soil and Similar Substances by Fringe Capacitance. Journal of Scientific Instruments, Vol. 43, 1966.

NUCLEAR MAGNETIC RESONANCE SENSORS FOR MOISTURE MEASUREMENT IN ROADWAYS

G. A. Matzkanin and C. G. Gardner, Southwest Research Institute

The feasibility of practical instrumentation based on the nuclear magnetic resonance method was investigated to address the need for accurate, reliable moisture measurements in highway systems. A prototype of an implantable sensor that uses the pulsed nuclear magnetic resonance spin-echo technique was developed and subjected to laboratory verification. The sensor is 3 by 2 by 2¼ in. (7.6 by 5.1 by 5.7 cm) and weighs about 3 lb (1.35 kg). It directly measures the mass of moisture present; to obtain the percentage of moisture requires that soil density be determined by an auxiliary method. Experiments with bentonite, silica flour, and topsoil indicated that the sensor operated reliably, with an accuracy of approximately ±1 percent up to 25 percent moisture, ±2 percent up to 100 percent moisture, and ±4.5 percent up to 200 percent moisture. A dependence of sensor response on soil type necessitated calibration for each soil type. Organic matter and dissolved salt did not affect the sensor readings for bentonite, but organic matter had an effect for silica flour. All of the results obtained were qualitatively accounted for in terms of a simple moisture adsorption and bonding model.

•SERVICE behavior of a highway system strongly depends on the moisture content of the system's components. Despite recognition of this relationship, progress in highway construction and maintenance practices related to control of moisture and its effects has been impeded by lack of adequate instrumentation and methodology for measuring moisture under conditions and constraints of highway practice. The economic significance of the problem is proved by the large annual investment aimed at removal of excess water that causes loss of supporting capacity of subgrade soils and aggregate bases, instability of embankments, and deterioration of pavements.

The techniques currently used in the highway field for measuring moisture content in situ are generally inadequate to meet researchers' needs. Instrumentation is specifically needed for remote readout of local sensing, for remote sensing of subsurface conditions, for high-precision measurements, and for long-term continuous monitoring. Devices that can be installed permanently and portable devices for sampling at random locations are needed to provide data to allow for development of new designs and use of new materials.

A moisture sensor based on the detection of hydrogen nuclei by the nuclear magnetic resonance (NMR) spin-echo method has been developed. A prototype of a sensor was fabricated and subjected to a laboratory verification program to determine its suitability for highway applications. Currently, a field evaluation program is under way, during which a number of replicate sensors will be tested for 1 year in actual highway field installations. This report describes the basic principles of operation of the NMR sensor and the results of the laboratory verification program. More complete details have been documented elsewhere (1).

Publication of this paper sponsored by Committee on Environmental Factors Except Frost.

PRINCIPLES OF NUCLEAR MAGNETIC RESONANCE

Many atomic nuclei possess nonzero spin angular momentum and an associated magnetic dipole moment. As a top spins in a gravitational field, the spinning nucleus precesses about the direction of an applied steady magnetic field (Fig. 1). The precession frequency is proportional to the strength of the magnetic field, and the proportionality constant (the gyromagnetic ratio) has a value characteristic of the specific nuclear species. For the hydrogen nucleus, the gyromagnetic ratio has the value $2.67 \times 10^4\ S^{-1}G^{-1}$ ($2.67 \times 10^8\ S^{-1}\ T^{-1}$). A resonance condition can be achieved by applying a second magnetic field, which alternates at a frequency corresponding to the precessional frequency of the nuclei of interest, in a direction orthogonal to that of the steady field. For appropriate values of steady and alternating fields, the spin axis of the nucleus can be reoriented; this is the phenomenon of NMR. The NMR detection of moisture involves the hydrogen nuclei (protons) in the water molecules. For fields of around 700 Oe (56×10^3 A/m), the NMR frequency for hydrogen nuclei is in the radio-frequency (RF) region, i.e., 3 MHz.

Although several methods of producing and detecting NMR signals are possible (2), the approach used in the moisture sensor described in this report is the pulsed NMR spin-echo technique. If the RF field is applied in a short burst, or pulse, of the proper duration, the nuclear magnetization vector can be made to rotate 90 deg into the plane orthogonal to the direction of the constant field H_o, which is measured in Oe or A/m (Fig. 2). At the termination of the pulse, the magnetization vector precesses in the plane perpendicular to H_o and induces a voltage in the RF coil that then serves as a sensor. This voltage is proportional to the number of nuclei within the effective volume of the RF coil. However, two effects must be taken into consideration: (a) Interactions between the nuclei in the specimen tend to diminish the amplitude of the precessing transverse magnetization, and (b) inhomogeneities in the applied static field gradually destroy the coherence among the individual nuclear spins that compose the net magnetization and cause a fanning out of the precessing nuclear magnetic moments. As a consequence of these two effects, the voltage induced by the precessing magnetization gradually decays to zero; this is called free induction decay. If, now, a second RF pulse is applied to the specimen at a suitable time following the first pulse, i.e., after the initial voltage has decayed because of the fanning out of the nuclear magnetic moments but before the amplitude of the transverse magnetization has diminished to zero because of internal interactions, then the nuclear magnetic moments can be refocused into a spin echo, which manifests itself as an induced voltage following the second applied pulse. This is shown in Figure 3.

The amplitude of the spin-echo signal is related to the magnitude of the nuclear magnetization (M_o), which in turn is proportional to the number of nuclei within the detection coil. Figure 4 shows an oscilloscope photograph of spin echoes from bentonite specimens containing different amounts of water. The echo amplitude also depends, of course, on a number of other parameters such as NMR frequency (which in turn depends on the magnetic field), temperature, and pulse spacing. These dependencies are so well-known that, once the calibration is established between a particular instrumentation and the amount of moisture present, corrections can be made for changes in these parameters.

The essential elements of an arrangement used to implement the NMR spin-echo method are shown in Figure 5. The specimen is encircled by an RF induction coil. A static magnetic field of strength H_o is applied by a magnet. An RF oscillator supplies pulses of RF energy of the proper duration and separation to the coil to produce spin echoes. The induced voltage is increased by the amplifier, demodulated by the detector, and displayed as a function of time on a cathode ray oscilloscope. A digital readout of the amplitude of the spin echo is carried out by a sampling gate and a digital voltmeter.

Figure 1. Precession of nuclear magnetic moment in static magnetic field.

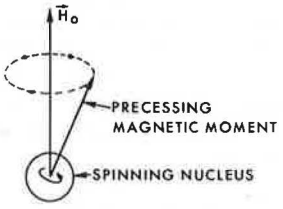

Figure 2. Rotation of nuclear magnetization by radio-frequency pulse followed by free induction decay.

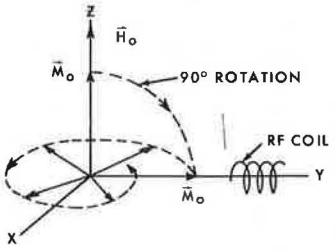

Figure 3. Free induction decay and spin echo associated with two-pulse sequence.

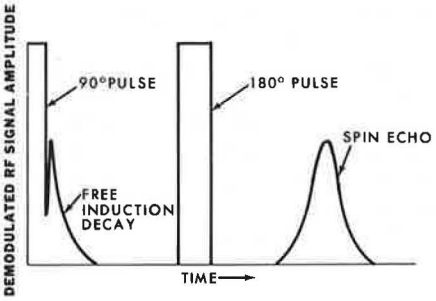

Figure 4. Pulsed nuclear magnetic resonance spin echoes from moisture in bentonite.

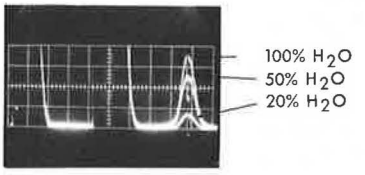

Figure 5. Essential elements of arrangement for pulsed nuclear magnetic resonance measurements.

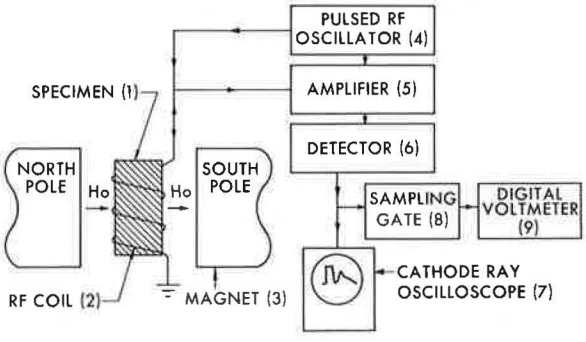

Figure 6. Prototype of implantable nuclear magnetic resonance moisture sensor.

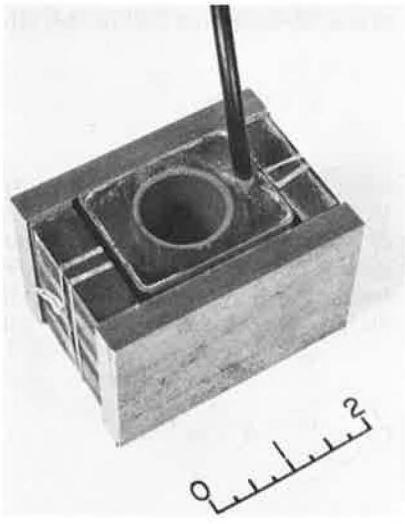

IMPLANTABLE NUCLEAR MAGNETIC RESONANCE MOISTURE SENSOR

Most laboratory work on NMR is done by using large electromagnets to produce strong, homogeneous fields. This, of course, is unfeasible for the desired highway applications; therefore, initial design efforts centered around developing a miniaturized sensor that is made with a permanent magnet and an RF transmission and detection coil, small enough to be buried. This necessitates a smaller, weaker magnet than is ordinarily used, and a consequent loss in signal amplitude results (the NMR signal is proportional to the square of the magnetic field). However, initial tests showed that, when magnetic fields were as low as 700 Oe (56×10^3 A/m), spin-echo signals could still be measured down to a moisture density of 0.1 g/cm^3 for specimen volumes of 10 cm^3. This corresponds to a dry weight moisture percentage of 5.5 for a soil with a dry density of 112 lb/ft^3 (1.82 g/cm^3).

One version of a buriable prototype NMR moisture sensor is shown in Figure 6. For achieving a sufficiently strong magnetic field with as little magnet material as possible and with acceptable homogeneity over the specimen volume, the Watson magnet design was used (3). In the design in Figure 6, the magnets are cast Alnico VIII, and the plates are $^3/_8$-in.-thick (0.95-cm) mild steel. The overall dimensions of the structure are 3 by 2 by $2^1/_4$ in. (7.6 by 5.1 by 5.7 cm), and the magnet gap (separation of the plates), in which a field of approximately 600 Oe (48×10^3 A/m) is developed, is $1^1/_2$ in. (3.8 cm). The sensor, as photographed, weighs $3^1/_4$ lb (1.5 kg).

The RF transmission and detection coil is approximately 1 in. (2.54 cm) long and is wound on a plastic tube with an inside diameter of 0.875 in. (2.2 cm). This provides an active specimen volume of 0.6 in.^{3} (9.8 cm^3). The coil and tube are permanently cast with an epoxy-like material into a thin-walled rectangular copper case that serves as a RF shield. A coaxial cable serves as the connection between the coil and the detection and readout instrumentation. In laboratory tests, cable lengths from 2 to 66 ft (0.6 to 20 m) have been used without serious degradation of signals.

LABORATORY VERIFICATION

Calibration

The measured NMR (spin-echo) signal amplitude, ξ (in volts), is proportional to the mass of moisture within the effective volume of the detection coil, that is

$$\xi = Cm_vV \tag{1}$$

where m_v (in g/cm^3) is the moisture density, V (in cm^3) is the volume of the coil, and C (in V/g) is a proportionality factor between the measured NMR signal and the mass of water. The value of C depends on the size and geometry of the detection coil, the filling factor, the gain of the detection electronics, the strength of the applied magnetic field, the magnitude of the nuclear magnetic moments, and the temperature. Moisture density is related to the conventional dry weight moisture fraction (m) by the expression

$$m_v = \frac{m}{1 + m} D \tag{2}$$

where D is the density (in g/cm^3) of soil plus moisture. Thus the NMR signal amplitude is related to the dry weight moisture fraction by the equation

$$\frac{\xi}{D} = K\frac{m}{1+m} \tag{3}$$

where K is a proportionality factor. Thus, for a series of specimens of various moisture content, volume, and density, ξ/D is expected to be linearly related to the quantity $m/(1 + m)$.

So that the capabilities of the prototype of a NMR sensor could be established, a set of specimens was prepared and placed in glass tubes that could be inserted into the sensor cavity. A portion of each specimen was weighed and oven-dried to determine gravimetrically the moisture percentage. The density of each specimen was determined by directly weighing and measuring the volume of each specimen. Three soil types were investigated: (a) bentonite clay, (b) silica flour, and (c) a local, organic, silty clay topsoil. Specimens were prepared at various dry weight percentages up to 213 percent for bentonite, 24 percent for silica, and 55 percent for the topsoil.

The results for bentonite are shown in Figure 7; $\mu = m/(1 + m)$ and is the wet weight moisture fraction. The data are linear within experimental error, except for the observation of a nonzero intercept. A least squares fit results in the equation

$$\xi/D = [2.288\mu - 0.291]\ V \cdot\ cm^3/g \tag{4}$$

Figure 8 shows the sensor readings for bentonite replotted against the dry weight moisture percentage, m × 100 percent. The solid curve is a graph of Eq. 4 and essentially constitutes the sensor calibration curve for bentonite.

The failure of the observed data for bentonite to extrapolate through zero (in accordance with Eq. 3) may be interpreted in terms of a model based on the adsorption and binding of water molecules in the soil system. In the preceding analysis, all hydrogen nuclei in the water molecules in the sample were assumed to be sensed. However, the NMR spin-echo method is sensitive to the physical state of the detected nuclei. Atomic and molecular interactions affect the decay time of the transverse nuclear magnetization shown in Figure 2. Generally speaking, tight molecular binding, as in solids, causes a fast decay time, whereas looser molecular coupling, as in liquids, produces longer decay times. Thus, a spin-echo signal associated with the water molecules in the liquid state may be produced by appropriately choosing the time interval between the two RF pulses. If some of the water molecules present are adsorbed on the surface of soil particles, or are chemically bonded to solid constituents (e.g., water of hydration), thus effectively removing them from the liquid state, the hydrogen in the molecules so affected will generally not be detected by the NMR spin-echo technique when the instrumentation is adjusted for optimum detection of hydrogen in liquid water. If this situation exists, ξ in Eq. 1 should be modified as follows:

$$\xi = C(m_v V - \Delta_{wc}) \tag{5}$$

where Δ_{wc} is the mass of water (in g), within the effective volume of the detection coil, which does not contribute to the observed NMR signal. Letting m' be the dry weight moisture fraction for this bound moisture, the following modification of Eq. 3 is obtained:

$$\frac{\xi}{D} = K(1 + m')\frac{m}{1+m} - Km' \tag{6}$$

If the adsorption (or binding) of water molecules by the solid constituents of the sample

Figure 7. Nuclear magnetic resonance moisture sensor signal versus wet weight moisture fraction for bentonite.

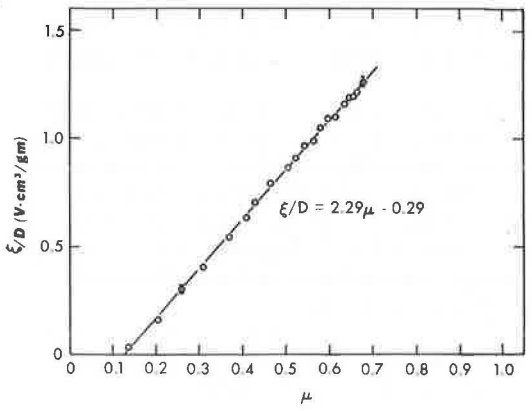

Figure 8. Nuclear magnetic resonance moisture sensor signal versus percentage of moisture for bentonite.

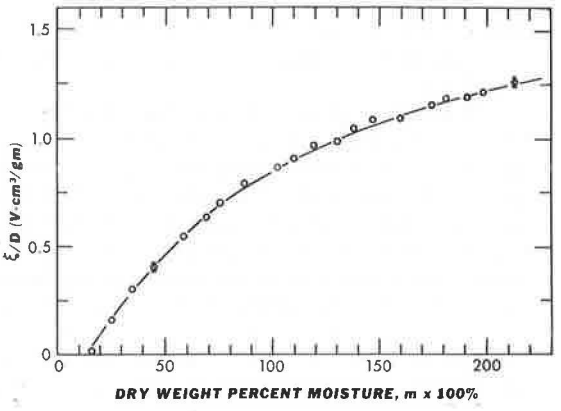

Figure 9. Theoretical dependence of pulsed nuclear magnetic resonance response on moisture content (based on adsorption model).

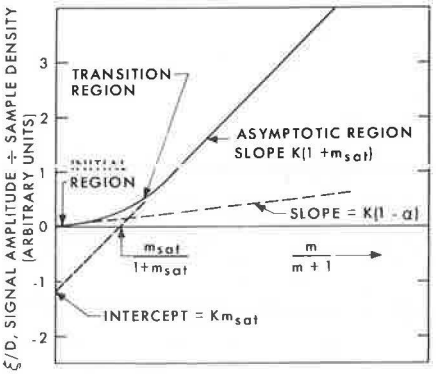

Figure 10. Nuclear magnetic resonance sensor signal versus percentage of moisture for bentonite, silica flour, and organic silty clay.

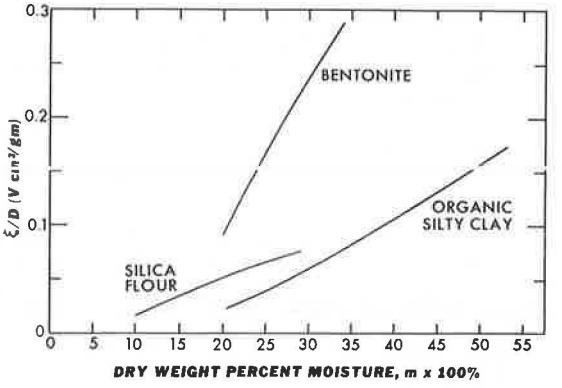

Table 1. Comparison of nuclear magnetic resonance sensor and gravimetric moisture determinations.

Specimen Number	Density (g/cm^3)	Moisture (percent)		Deviation	
		NMR Sensor	Gravimetric	Amount	Percent
1	1.184	19.8	20.4	-0.6	2.9
2	1.224	22.8	23.1	-0.3	1.3
3	1.200	22.2	23.4	-1.2	5.1
4	1.334	29.6	31.4	-1.8	5.7
5	1.405	29.8	32.3	-2.5	7.7
6	1.476	33.1	35.2	-2.1	6.0
7	1.579	42.5	45.1	-2.6	5.8
8	1.429	54.2	52.5	+1.7	3.2
9	1.231	81.3	82.6	-1.3	1.6
10	1.247	106.9	105.8	+1.1	1.0
11	1.176	160.9	158.7	+2.2	1.4
12	1.085	214.7	221.4	-6.8	3.1

eventually saturates at some moisture fraction, as seems physically plausible, then beyond that moisture fraction, m' is a constant, denoted by m_{sat}. Thus for $m > m_{sat}$, Eq. 6 predicts that ξ/D is again a linear function of the variable $m/(1 + m)$ and has slope $K(1 + m_{sat})$. When this straight line is extrapolated backwards ($\xi/D = 0$), it crosses the $m/(m + 1)$ axis at $m_{sat}/(1 + m_{sat})$, and when further extrapolated to $m/(m + 1) = 0$, it intercepts the ξ/D axis at $-Km_{sat}$. This behavior is shown in Figure 9.

When the moisture content of the specimen is below the value for which the adsorption (or binding) of water molecules is fully saturated, m', the bound-water mass fraction, is not a constant but depends on m, the total-water mass fraction. In fact, for sufficiently small values of m, m' must be directly proportional to m; i.e., $m' = \alpha m$ as $m \to 0$, where α is the proportionality constant between the bound-water mass fraction and the total-water mass fraction. In this moisture range, Eq. 6 reduces to

$$\frac{\xi}{D} = K(1 - \alpha)\frac{m}{1 + m}, \quad m \to 0 \tag{7}$$

Thus, near the origin, ξ/D is again a linear function of $m/(1 + m)$ and has slope $K(1 - \alpha)$ as shown in Figure 9. If the value of K can be inferred from the $m > m_{sat}$ region of the curve, then α can, in principle, be determined from the slope near the origin.

By comparing Figures 7 and 9, one can see that results in bentonite at least qualitatively agree with the foregoing adsorption model. From Eqs. 4 and 6 one can obtain, for bentonite, the following parameters: $K = 2.0$ V cm^3/g and $m_{sat} = 0.145$ (14.5 percent moisture by dry weight). Parameter α was not determined because moisture levels below 14 percent were not measured.

For further verification of the reliability of the prototype sensor for measuring moisture in soil, a second, independent series of bentonite specimens was prepared at nominal moisture percentages ranging from 20 to 220 percent. These specimen materials were also loaded into glass vials for insertion into the sensor cavity. From the measured spin-echo signal amplitude, the moisture percentage was obtained by using the bentonite calibration curve shown in Figure 8. After the measurement with the prototype sensor was completed, the specimen material was removed from the glass vial, and the moisture content determined gravimetrically. A comparison of these results and the deviations and percentage of deviations between the NMR sensor and gravimetric moisture determinations are given in Table 1. As can be seen by comparing columns 3 and 4 of Table 1, the agreement between the moisture content obtained with the NMR sensor and the gravimetrically determined moisture content is quite good over the entire moisture range investigated. The average deviation in percentage of moisture between the sensor and gravimetric results is 2.0.

Dependence on Soil Type

Results of investigations with the silica and topsoil specimens indicated that the sensor response depends on soil type. Figure 10 shows the calibration curves experimentally obtained for each of the three soils studied, and individual data points are omitted for clarity. Only the initial part of the bentonite calibration curve is shown. Although the exact cause of this dependence on soil type is not understood, it may tentatively be interpreted in terms of the previously described moisture adsorption model, as follows. In bentonite, at moisture levels above 14 percent, the adsorption-bonding mechanism is saturated, and all additional moisture is sensed; in silica flour and topsoil, the adsorption mechanism is not saturated up to the investigated moisture levels, and not all added moisture is detected. Therefore, the observed calibration curves depend on the particular details of water adsorption in given soil types. This interpretation is supported by experimental results showing that larger NMR signals are obtained from pure water than are obtained from a comparable amount of water mixed with silica or topsoil.

From the practical standpoint, this dependence of calibration on soil type necessitates calibrating the sensor for each particular soil type in which it is to be used.

Influence of Organic Matter

The influence of organic matter was investigated by mixing peat, up to 20 percent by dry weight, into bentonite and silica specimens. The results for bentonite are shown in Figure 11, in which the solid curve is the sensor calibration curve for pure bentonite already shown in Figure 8. Within the limits of experimental error, the data points for the peat specimens fall on the previously established calibration curve for pure bentonite. This indicates that for bentonite there is no observable influence attributable to the added organic matter; however, for silica, there is an influence due to the organic matter as shown in Figure 12.

The results for the silica-peat specimens may be understood in terms of the adsorption model by recalling that previously not all of the moisture in the silica specimens was being detected because of an adsorption-bonding mechanism. The addition of organic matter to the silica provides capillary storage of free water, all of which is sensed. Therefore, the net fraction of water adsorbed or bound in silica flour that contains organic matter is less than that for a pure silica specimen at the same nominal moisture content. This results in a correspondingly larger signal. As the percentage of peat is increased, the observed moisture signals from the silica-peat specimens also increase (Fig. 12).

Influence of Dissolved Salts

The influence of dissolved salt was determined by preparing some bentonite specimens with water containing NaCl at concentrations up to 2,000 ppm by weight. These salt concentrations were chosen to conform to those found in runoff water along roadways (4). The results of sensor readings plotted against the gravimetrically determined moisture content are shown in Figure 13. The solid curve is the bentonite calibration curve previously shown in Figure 8. The good agreement between the sensor readings for the specimens containing dissolved salts and the calibration curve shows that the dissolved NaCl presents no significant effect on the NMR spin-echo signals from bentonite. The influence of dissolved salt was not investigated in soil other than bentonite; however, it is not expected to affect the sensor response, as long as it does not contribute to the number of hydrogen atoms present.

Effect on Moisture Distribution

The question of whether the presence of the buried sensor disturbs the free-field distribution of moisture in the soil was briefly addressed. This was done by selective coring and gravimetrically determining the distribution of moisture in a container of silica flour into which water was allowed to permeate, both with and without the sensor being present. These results indicated that the free-field distribution of moisture was not significantly altered by the presence of the buried sensor, at least for silica flour. Further studies of this question are planned during the field evaluation program.

SUMMARY

The basic feasibility of using the pulsed NMR spin-echo method for measuring soil moisture has been demonstrated, and a prototype of an implantable sensor has been developed. Because sensor response depends on soil type, calibration of the sensor for each soil in which it is to be used will generally be necessary. The sensor response was unaffected by the organic matter and the dissolved salt that were mixed into bentonite

Figure 11. Nuclear magnetic resonance moisture sensor signal versus percentage of moisture for organic peat with bentonite.

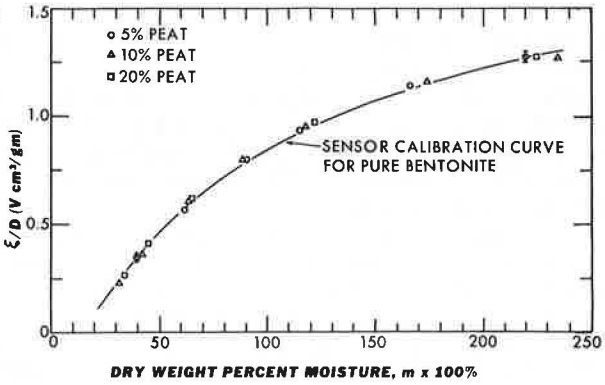

Figure 12. Nuclear magnetic resonance moisture sensor signal versus percentage of moisture for organic peat with silica flour.

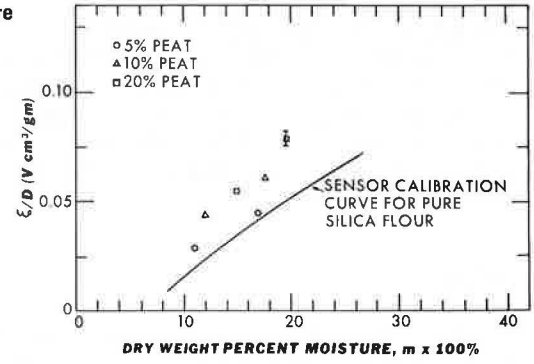

Figure 13. Nuclear magnetic resonance moisture sensor signal versus percentage of moisture for bentonite with sodium chloride aqueous solutions.

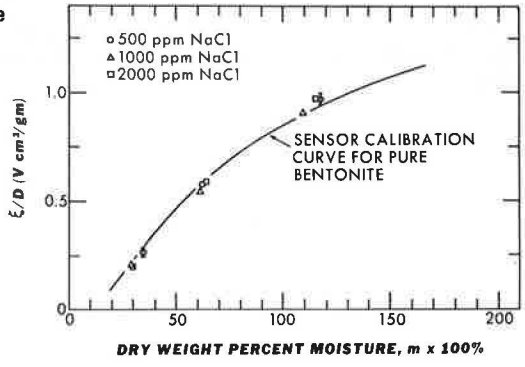

clay. For the silica flour, the sensor output was affected by organic matter in a qualitative agreement with a model of adsorption of water molecules in pure silica flour. The accuracy of the prototype version of the sensor was at least ±1 percent moisture over the 6 to 25 percent moisture range, ±2 percent moisture over the 25 to 100 percent moisture range, and ±4.5 percent moisture over the 100 to 200 percent moisture range. The sensitivity (resolution of change in moisture percentage) was at least 0.5, 1.5, and 2 percent moisture respectively for the corresponding ranges of percentage of moisture.

A program is currently in progress to develop a fieldworthy version of the NMR moisture sensor with portable readout instrumentation and to conduct a field evaluation of the system. Plans call for the implantation of about 30 sensors in 4 or 5 test sites in various locations around the country. The system will be evaluated during 1 year for reliability, accuracy, and suitability for measuring moisture in highway-related applications. This project is expected to be completed by December 1976.

ACKNOWLEDGMENTS

Consultation on problems of highway-related applications throughout the research was provided by J. D. Michie. The suggestion for using the Watson magnet design in the final prototype sensor was made by W. L. Rollwitz, and technical assistance in conducting the laboratory verification experiments was provided by E. S. Riewerts.

The work on the prototype of the NMR sensor described in this report was performed at Southwest Research Institute and was sponsored by the National Cooperative Highway Research Program.

REFERENCES

1. C. G. Gardner, G. A. Matzkanin, and J. R. Birchak. Instrumentation for Moisture Measurement—Bases, Subgrades, and Earth Materials (Sensor Development). Southwest Research Institute, Final Rept., NCHRP Project 21-2, Aug. 1974.
2. A. Abragam. The Principles of Nuclear Magnetism. Clarendon Press, Oxford, 1961.
3. E. Watson. Proc., International Conference on Magnet Technology, 1967.
4. R. E. Hanes, L. W. Zelazny, and R. E. Blaser. Effects of Deicing Salts on Water Quality and Biota—Literature Review and Recommended Research. NCHRP Rept. 91, 1970.

INVESTIGATION OF FILTRATION CHARACTERISTICS OF A NONWOVEN FABRIC FILTER

William J. Rosen, Marks-Rosen, Inc.; and
B. Dan Marks, Department of Civil Engineering, University of Tennessee

The purpose of this study was to investigate the behavior of a nonwoven fabric filter in subdrainage applications. Experiments were restricted to a single fabric, Mirafi 140. Conventional aggregate filters were tested under compatible conditions to provide a basis of performance behavior. Experimental results indicate that the nonwoven fabric provides desirable performance under a relatively wide range of soil conditions. Hypotheses that relate to mechanisms controlling the behavior of the nonwoven fabric in subdrain applications are discussed. These mechanisms are, in turn, related to induced filtration and internal grading of the soil near the soil-fabric contact surface.

•MANY problems that occur both during and after construction are related to the flow of subsurface water or seepage. Hydrostatic pressures associated with seepage may produce instability within a soil mass. Unstable soil conditions may often be corrected or improved by subsurface drainage systems. Mechanisms involved in seepage and subsurface drainage are complex because they are related to both the physical and physicochemical characteristics of the soil.

Regardless of application, subsurface drainage systems must meet two divergent design criteria: (a) The subdrain must be sufficiently permeable so that seepage can be removed without buildup of excessive hydrostatic pressures, and (b) the subdrainage system must protect the soil against piping, i.e., the subsurface erosion of the soil mass. Consequently, subsurface drains or underdrains are often referred to as protective filters.

The basic criteria for the selection or design of fabric subdrainage systems must be the same as those for conventional filters. The primary difference arises because the gradation of the aggregate to be used as the filter is selected to provide the optimum of the two divergent criteria, whereas the filter criteria must be satisfied by the fabric structure and its effect on gradation of the soil immediately adjacent to the fabric.

LITERATURE REVIEW

Traditionally, the problems of seepage and subsurface drainage have been analyzed on the basis of empirical relationships. Although Darcy's law, formulated in 1856 (1), was based on a macroscopic investigation of the flow of water through fine-grained soils, the relationship was applicable to a majority of the seepage problems falling within the range of laminar flow.

Bertram (2) studied the filter design criteria suggested by Terzaghi. Experimental results indicated that, for an aggregate filter to provide sufficient permeability without development of excessive hydrostatic pressure, the 15 percent size of the aggregate must be four to five times the 15 percent size of the protected soil. Tests also revealed that the 15 percent size of an aggregate must not be greater than four to five times the

Publication of this paper sponsored by Committee on Subsurface Drainage.

85 percent size of the protected soil so that piping could be prevented. The work of Bertram was subsequently expanded by the U.S. Army Corps of Engineers (3) and the Bureau of Reclamation (4). These investigations substantiated the criteria for selection of aggregate gradation for use in subdrains; however, additional requirements have been suggested for gradation requirements. One such requirement recommended by both studies was that the aggregate filter gradation be as nearly parallel to the protected soil gradation curve as possible.

During the past decade, the availability of synthetic fabrics and filter cloths has produced increased interest in seepage control by subsurface drainage systems. Healy and Long (5) conducted laboratory and field tests on prefabricated subdrainage systems by using woven filter cloth. The subdrainage system was successful under several site conditions, one of which was the drainage of an unstable slope in glacial till where the installation of conventional aggregate drains would have been virtually impossible.

Because of the increasing interest and availability of fabric filter materials, the U.S. Army Corps of Engineers, through the Waterways Experiment Station, conducted an investigation to develop design criteria and acceptance specifications for fabric filter materials (6). Filtration tests and clogging tests were conducted to determine head losses across the fabric during filtration and soil loss through the fabric. A clogging ratio based on the hydraulic gradients measured across the fabric and across the system was used as a basis of comparison of performance. Flow measurements taken during the clogging tests were considered inconclusive; however, the clogging ratio did indicate the relative susceptibility of fabrics to clogging.

Barrett (7) has presented numerous examples of fabric use under a wide variety of field conditions. Although many of the applications of fabrics were in coastal structures, much information is presented about the ability of fabrics to prevent soil piping or clogging.

TEST PROCEDURES AND MATERIALS

Filtration tests were conducted in 1-ft (30.5-cm), square, plexiglass, constant-head permeameters equipped with a manometer to measure head losses at various points in the soil and across the fabric filter. The permeameters were constructed in two sections that bolted together after placement of conventional aggregate filters or fabric filter systems in the lower portion. For testing, 4 in. (10.2 cm) of soil were placed over the filter system. Flow measurements were obtained periodically as were head loss readings. Filtration tests were continued for 21 to 28 days or until the flow through the system became constant. All tests were conducted under a constant hydraulic gradient for the entire system of three.

The fabric filter system consisted of 8 in. (20.3 cm) of river gravel, which passed the U.S. standard $\frac{3}{4}$-in. (19.0-mm) sieve and was retained on the U.S. standard $\frac{1}{2}$-in. (12.5-mm) sieve. This was overlaid with a single layer of Mirafi 140 fabric.

Conventional aggregate filter systems were designed according to the procedure recommended by the U.S. Army Corps of Engineers. Conventional 8-in. (20.3-cm) filters were used beneath the soil to be tested.

In this experimental investigation, 12 soils were tested. All soils were produced from a basic soil that was an alluvial deposit found in the floodplain of the Holston River near Knoxville, Tennessee. The base soil was produced by removing material finer than the No. 100 sieve.

Three groups or series of soils were produced by adding various fine fractions to the base soil. These groups were designated the S, K, and M series to indicate the addition of silt, kaolinite, and montmorillonite fractions respectively. A particular soil was identified by a series designation followed by a number representing the percent of the particular fines added to the base soil. Physical properties of the 12 soils tested are given in Table 1. Grain size distribution curves for the three series of soils tested are shown in Figures 1, 2, and 3.

The nonwoven fabric tested in filtration tests is produced by randomly distributing both monofilament and heterofilament fibers. The monofilament fiber is a polypro-

Table 1. Physical properties of soils tested.

Soil Type	Liquid Limit (percent)	Plastic Limit (percent)	Plasticity Index (percent)	Effective Grain Size, D_{10} (mm)	Uniformity Coefficient	Soil Classification	
						AASHTO	Unified
Natural	28.3	19.7	8.6	0.010	15.2	A-2-4(0)	SC
S-0	24.5	20.0	4.5	0.025	6.8	A-2-4(0)	SM
S-5	23.8	18.0	5.8	0.020	8.0	A-2-4(0)	SM
S-15	25.1	20.3	4.8	0.014	10.7	A-4(0)	ML
S-25	26.0	16.8	9.2	0.010	11.0	A-4(3)	ML-CL
S-35	28.4	19.6	8.8	0.007	12.2	A-4(5)	CL
S-50	29.7	20.6	9.1	0.007	8.6	A-4(6)	CL
K-0	22.75	21.05	1.70	0.059	4.2	A-2-4(0)	ML
K-10	23.50	18.45	5.05	0.0070	27.1	A-2-4(0)	ML-CL
K-20	26.25	20.60	5.65	0.00061	303.3	A-2-4(0)	ML-CL
K-30	27.8	17.2	10.6	0.00063	214.3	A-4(1)	CL
M-2	30.0	22.3	7.7	0.046	4.35	A-2-4(0)	CL
M-4	39.1	24.1	15.0	0.0175	11.1	A-2-4(0)	CL

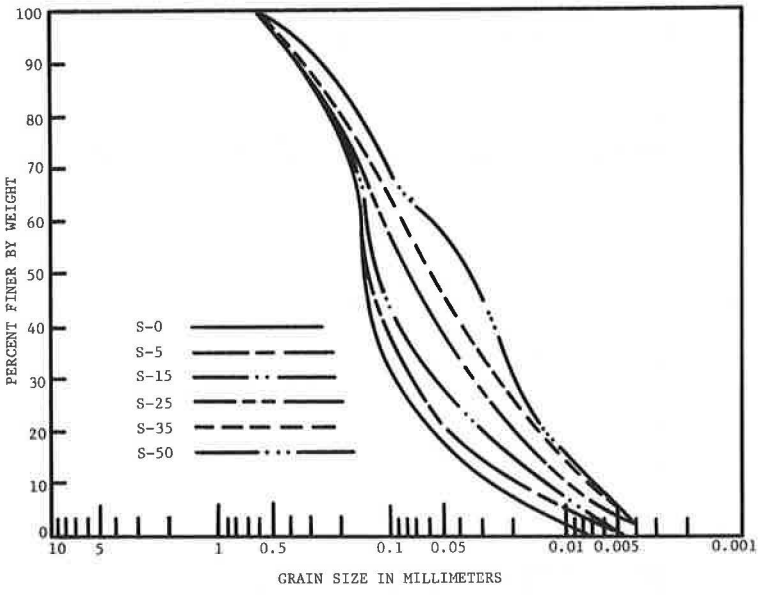

Figure 1. Grain size distribution curves for S-series soils.

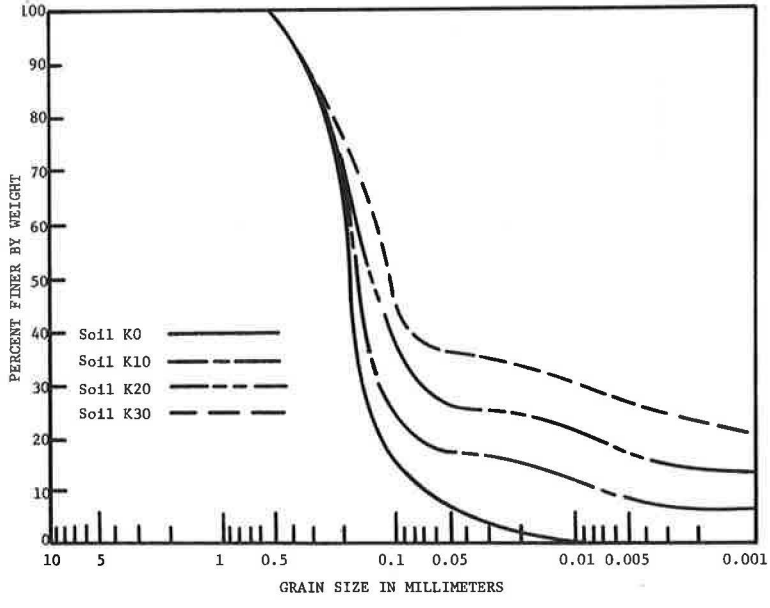

Figure 2. Grain size distribution curves for K-series soils.

Figure 3. Grain size distribution curves for M-series soils.

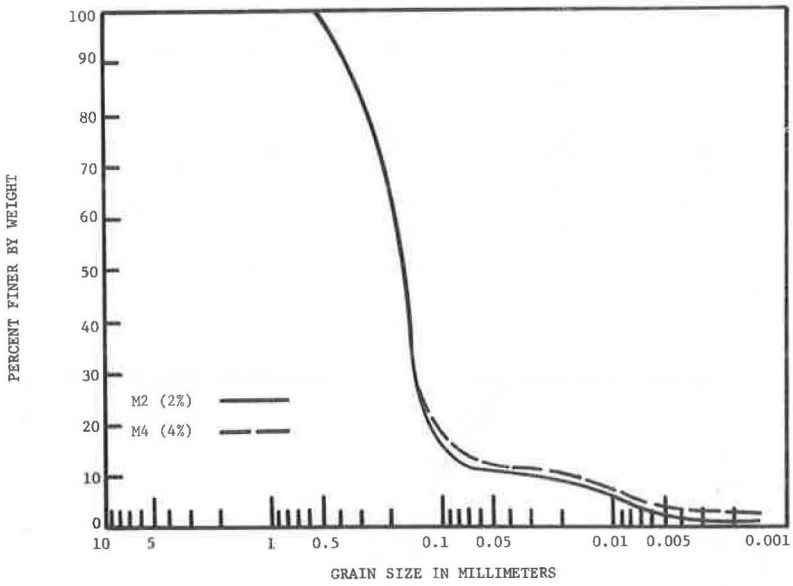

Figure 4. Permeability versus log-time curve for S-25 soil.

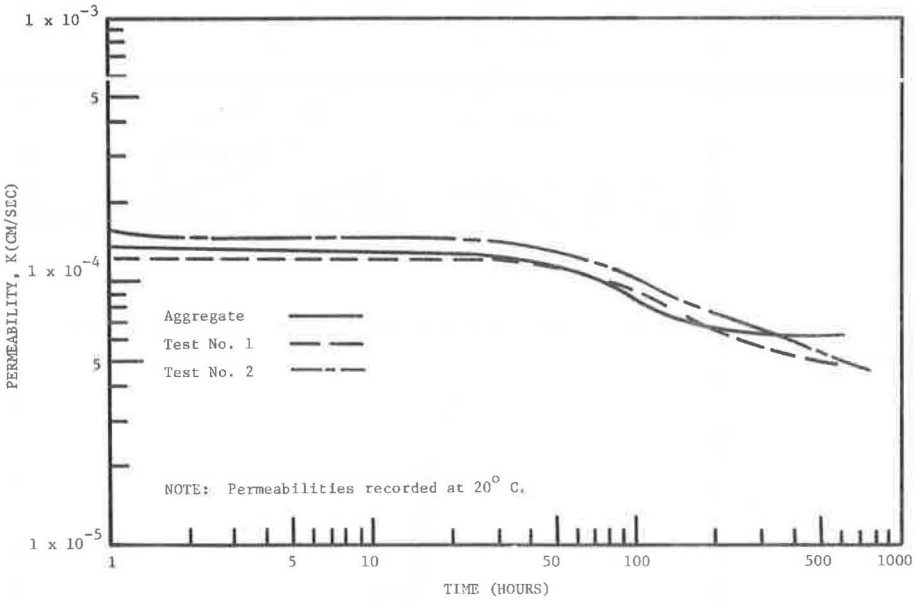

pylene, whereas the heterofilament fiber has a polypropylene core coated with nylon. Direct fusion at points of contact between the monofilaments and heterofilaments provides the nondirectional strength of the fabric structure. The average fiber diameter is 40 microns (40 μm) and has a fiber weight of 15 denure per fiber (DPF). One DPF is the weight in grams per 9000 m of fiber. The average mass/m^2 of the fabric was 140 g, and the fabric was approximately 20 mils (508 μm) thick.

DISCUSSION OF RESULTS

All soils tested with fabric filters exhibited a characteristic s-shaped permeability versus log-time curve. These curves indicated that, within the first few days of flow, the permeability of the system remained relatively constant; however, the log-time curves did not portray slight reductions in permeability during the first few minutes of flow, which were attributed to induced filtration and clogging of the fabric by particles immediately adjacent to the filter. These changes in permeability were insignificant relative to the overall behavior of the system.

After the initial period of flow, during which time the permeability of the system remained relatively constant, the permeability began to decrease to a minimum value after 2 to 3 weeks. This decrease in permeability was attributed to the formation of an internal filter cake within the soil immediately adjacent to the fabric. A typical permeability versus log-time curve is shown in Figure 4.

Analysis of the ratio of the hydraulic gradient across the fabric plus 2 in. (5.1 cm) of soil immediately above the fabric to the hydraulic gradient across the entire system substantiated the hypothesis of the formation of an internal filter cake immediately adjacent to the fabric. During the initial periods of flow, the ratio, which has been defined as the clogging ratio by other researchers (6), increased as a result of particles being piped through the fabric or clogging the fabric during induced filtration. The amount of increase in the clogging ratio varied with the percent fines contained in the soil. After the clogging ratio initially increased, the permeability and the ratio remained relatively constant for 2 to 3 days at which time the ratio again began to increase slightly as the permeability decreased. Analysis of data revealed that the relative decrease in permeability was closely related to relative increases in the hydraulic gradient ratio for various soil types. After this alteration in the hydraulic performance of the system, the permeability and clogging ratio again became constant. The clogging ratio versus log-time curve for various soils is an inverted image of the permeability versus log-time curve (Fig. 4).

So that the hypothesis about the formation of an internal filter cake could be substantiated, samples of the soil above the fabric filter were impregnated with an epoxy resin, EPO-TEK 301, to facilitate microscopic or pedographic analysis. Figure 5 shows a simplified model of the internal filter cake observed above the fabric. Those particles below the fabric are piped through the fabric during initial periods of induced filtration. The particles trapped in the fabric produce some clogging during the induced filtration period. The first stratum above the fabric contains particles remaining after induced filtration has removed the soil particles immediately adjacent to the fabric. The second stratum contains grain sizes that are trapped in the fabric in the event they are carried through the voids of the lower soil particle layer. The third soil stratum in the filter cake contains those particles that are piped through the fabric in the event they are carried through the voids of lower soil particle layers. Obviously, the schematic is somewhat idealized; however, visual examination of the cross section of impregnated samples has revealed that the individual strata of the internal filter cake can indeed be clearly distinguished.

As a result of this mechanism, most soil particles that are physically available to be trapped in the fabric and that produce clogging are those contained in a soil layer immediately adjacent to the fabric. This is because subsequent movement would be restricted by the soil voids remaining after these particles were removed. Similarly, the soil particles that are available for piping through the fabric are those contained in the first two soil strata previously described. Continued piping is restricted by the

Figure 5. Idealized internal filter gradation.

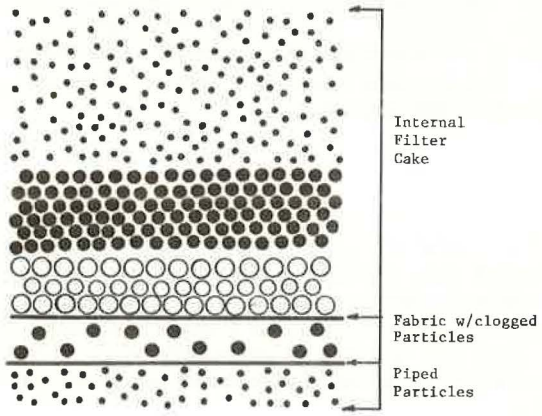

Table 2. Soil loss data.

Soil Type	Effective Grain Size, D_{10} (mm)	Uniformity Coefficient	Porosity (percent)	Piping (percent)	Clogging (percent)
S-0	0.025	6.8	54.2	3.0	0.05
S-5	0.020	8.0	53.1	2.0	0.04
S-15	0.014	10.7	53.0	1.6	0.05
S-25	0.010	11.0	53.0	2.0	0.04
S-35	0.007	12.2	53.2	1.8	0.04
S-50	0.007	8.6	53.0	1.4	0.05
K-0	0.059	4.2	52.7	1.2	0.03
K-10	0.007	27.1	54.1	1.1	0.04
K-20	0.0006	303.3	53.9	1.0	0.05
K-30	0.0006	214.3	53.9	1.5	0.04
M-2	0.046	4.4	54.3	1.3	0.03
M-4	0.0175	11.1	54.1	1.3	0.03

Figure 6. Range of grain size distribution for which fabric performed satisfactorily.

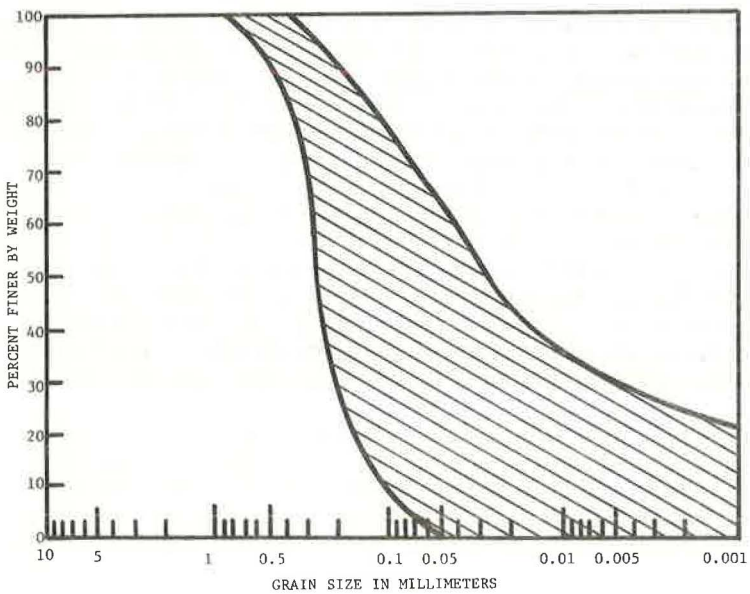

void spaces generated by the internal filter cake.

Obviously, the soil characteristics and fabric structure will be controlling parameters in the development of the internal filter cake formation. Inasmuch as only one fabric was used in this study, only the effect of soil characteristics could be analyzed. Table 2 gives clogging and piping data as a percentage of the total dry weight of the soil layer. As would be expected, the percentage of soil actually trapped in the fabric is quite small and does not vary significantly with soil type. The percentage of soil piped cannot be directly related to the grain size distribution of the soil type alone; however, the general trend indicates that less piping occurred with the more well graded soils, which possessed greater plasticity and cohesion.

SUMMARY AND CONCLUSIONS

The design criteria for fabric filter systems must be the same as those established for conventional aggregate filters: (a) to provide sufficient permeability so that seepage can be removed without the buildup of excessive hydrostatic pressures, and (b) to ensure that piping of soil particles does not occur during the drainage process.

Permeability and hydraulic gradient data collected during relatively long-term filtration tests were shown to be directly related to the formation of an internal soil-fabric filtration system. These data have been substantiated by visual examination of the soil-fabric filtration system that is produced under steady flow conditions.

As a result of this study, the nonwoven fabric used can be considered as effective in subdrainage applications for a relatively wide range of soil conditions. When consideration is given to grain size distribution alone, the range of soils for which the fabric is effective is shown in Figure 6.

ACKNOWLEDGMENT

The authors wish to extend their appreciation to the Celanese Fibers Marketing Company, producers of Mirafi 140, who made this study possible through its financial support.

REFERENCES

1. H. Darcy. Les Fontaines Publiques de la Ville de Dijon. Paris, 1957.
2. G. E. Bertram. An Experimental Investigation of Protective Filters. Harvard Univ., Soil Mechanics Series, No. 7, 1940.
3. Investigation of Filter Requirements for Underdrains. U.S. Army Engineer Waterways Experiment Station, Technical Memorandum 183-1, 1941.
4. K. P. Karpoff. The Use of Laboratory Tests to Develop Design Criteria for Protective Filters. Proc., American Society for Testing Materials, Vol. 55, 1955.
5. K. A. Healy and R. P. Long. Prefabricated Subsurface Drains. Highway Research Record 360, 1971, pp. 57-65.
6. C. C. Calhoun, Jr. Development of Design Criteria and Acceptance Specifications for Plastic Filter Cloths. U.S. Army Engineer Waterways Experiment Station, Technical Rept. S-72-7, 1972.
7. R. J. Barrett. Use of Plastic Filters in Coastal Structures. Proc., 10th Annual Conference on Coastal Structures.

DISCUSSION

G. W. Ring, Federal Highway Administration

Inasmuch as the conclusions of this study differ markedly from those of extensive earlier tests conducted by others, the authors were invited to publish this revised version of their paper in the interests of publicizing their research results. In that the amounts of fine-grained additives are not consistent from test series to test series, there may be some question about the applicability of the recommended filter system to the wide range of soils as suggested by the authors in Figure 6.

In the paper, it is emphasized that the design criteria for fabric filter systems must be the same as those established for conventional aggregate filters. Accordingly, the following two questions appear warranted:

1. What is the effective pore size of the fabric filter material?
2. What is the relationship between the reported clogging (Table 2) and the drop in hydraulic gradient across the clogged filter?

Finally, inasmuch as the fabric filter must withstand considerable abuse during some installations, it would be helpful for the designer to know the tensile strength of the material.

DETERMINATION OF DISPERSIVE CLAY SOIL ERODIBILITY BY USING A PHYSICAL TEST

Thomas M. Petry, University of Texas at Arlington; and
T. Allan Haliburton, Oklahoma State University

This paper introduces a new, physical, test method for identification of dispersive clay soil behavior. The significance of this form of internal erosion and the need for such a test are discussed. An analysis of dispersive clay soil behavior is included as a base for understanding the physical erosion test. The theoretical background, apparatus, and process of the proposed physical erosion test are presented. Data for average percentage of erosion were determined during 142 tests on 18 samples of varied properties. Physical erosion test results are correlated with those determined by a chemical property method and the method of plotting soil chemical data on a graph that has empirically derived zones of dispersive clay soil behavior (6). Correlations achieved are significant. We concluded that dispersive clay soil behavior depends on the particular combination of chemical, physical, and mineralogical properties of the soil. The physical erosion test and the erosion device used are shown to provide the measure of dispersive clay soil erodibility needed by soils engineers to predict accurate field behavior.

•DISPERSIVE clay soil phenomena were first noted by agronomists over 100 years ago. They encountered problems of piping (channelization) in clay soils normally thought to be immune to internal erosion. More recently, soil scientists were able to identify the causes of this internal erosion as the self-dispersion of clay particles into water available in soil voids and subsequent removal of these suspended clay particles from the soil by normal groundwater movement.

Soils engineers in North Dakota, Illinois, Mississippi, the southwestern United States, Australia, Israel (i.e., the Negev), and Venezuela have become acquainted with serious damage occurring in earth structures of dispersive clay soil within the last two decades. The destructive effects of this phenomenon of internal erosion on transportation structures in the western United States were described by Parker and Jenne (4) in 1967. In 1968, Bell (1) reported on the extensive dispersive clay soil erosion in the Badlands of North Dakota and its importance as a factor influencing construction of transportation structures. The investigators have found that serious piping erosion occurs in both cut and fill embankments.

Because of the desire to design and construct both safe and stable structures of earth, including dispersive clay soils, soils engineers and soil scientists have studied the dispersive clay phenomenon. Their research has been directed to finding a method for identifying dispersive clay soil erodibility so that they are able to predict the field behavior of these problem soils. These procedures range from qualitative tests of the self-dispersion of clay soils to the more quantitative tests that use soil chemistry properties to identify dispersive clay soil erodibility.

The difficulties associated with use of these previously proposed methods are twofold. First, and most important, the results obtained from the use of these methods are effectively qualitative so that accurate prediction of field behavior is not possible. Second, those methods that offer the more quantitative results are based on soil

Publication of this paper sponsored by Committee on Environmental Factors Except Frost.

chemistry properties not understood by most soils engineers. A physical test to determine internal erodibility of these problem soils was needed so that the measure of dispersive clay erodibility needed by soils engineers using an easily understood and accepted test method could be provided.

ANALYSIS OF DISPERSIVE CLAY SOIL BEHAVIOR

The behavior of dispersive clay soil, like that of all clay soils, is a result of the particular physicochemical environment within and surrounding it. There are several factors in this environment that must be present for a clay soil to exhibit the dispersive clay soil phenomenon of internal erosion.

First, there must be a disequilibrium of clay particles and water in the soil mass. This occurs when the chemical environment surrounding certain clay particles is such that they will disperse out of the soil mass and into available pore water if their physical surroundings permit. Many researchers of dispersive clay behavior have noted that either or both illite and smectite minerals must be present in the soil-clay ratio for clay particle dispersion to take place. Moreover, an inordinate quantity of sodium cations, as compared to the total quantity of other cations surrounding the clay particles, causes dispersion of the particles. Methods for determination of dispersive clay behavior based on soil chemical properties use some measure of the percentage of the sodium cation concentration to predict dispersion. These methods ignore all other factors affecting dispersive clay soil erosion.

Second, there must be soil mass porosity of sufficient size to allow continuing dispersion of clay particles into pure water and to allow removal of these dispersed clay particles by seepage. This may occur when the soil mass is desiccated and a system of interconnected cracks is present; when the soil consists of aggregates of material that is compacted dry of optimum, rather than discrete particles; or when either of these situations is combined with the presence of constructed or natural fissures in the soil. These systems of pores will promote dispersion and removal of clay particles as long as their size is not markedly reduced by swelling of the soil before significant loss of soil occurs.

Third, water that is relatively pure and in a large enough quantity to provide for clay particle dispersion and that supplies the required hydraulic gradient to cause removal of these particles by seepage must exist. This factor is complicated because the type and quantities of water moving through the soil vary greatly.

Finally, the soil must also have a propensity to exhibit surface erosion. When a surface is available within a soil pipe, loss of material occurs not only by dispersive clay soil action but also by surface sloughing and removal.

The severity of erosion caused by the phenomenon of the dispersive clay soil depends on the combined effects of these environmental factors. The variance of this severity is directly related to the combined physical, mineralogical, and chemical properties of the soil. Because of this fact, those methods for identifying dispersive clay soil erodibility based on less than an analysis that considers all the environmental factors can be only qualitative.

ENGINEERING CONSIDERATIONS

The need for a physical erosion test to determine the amount of dispersive clay soil or internal erodibility of a soil is based on the desire of soils engineers to predict and correct for detrimental field behavior. The measures taken to use problem soils in earth embankments depend highly on accurate appraisal of soil properties including internal erodibility. It is not sufficient that the general behavior of the soil be known but that a quantitative measure of behavior be available.

In 1972, Sherard, Decker, and Ryker (6) reported on a method they developed for identification of dispersive clay soil erodibility. Of the methods previously proposed for this purpose, this one is most adequate for use by soils engineers. By using test

data from 99 samples of varying physical and chemical properties with known field behavior, they developed a graph of selected soil chemistry data containing zones of soil behavior (Fig. 1). Inasmuch as the zones of behavior associated with this method were developed by observation of field behavior, results obtained may be directly used to predict field behavior, if the field situations under consideration are similar. This method (6), like others previously proposed, is limited in application because it does not consider all factors influencing dispersive clay soil field behavior. However, inasmuch as it represents the most acceptable method for use by soils engineers, it was chosen as a reference method for correlation of test results during development of the physical erosion test, which considers all the environmental factors present in and around the soil.

PHYSICAL EROSION TEST

During research recently completed at Oklahoma State University, we developed a physical test for identification of dispersive clay soil erodibility. It was believed that a physical test would provide a most acceptable method for directly studying the reactions of the proposed soil during dispersive clay soil erosion. Thought was directed at making the test accurately assess the one variable of internal erodibility practically and economically. The simplest and most direct approach of field simulation was decided on to accomplish these objectives and to provide results readily transformed into meaningful field behavior. The outcome of the development process was a laboratory test procedure that uses miniaturized equipment to supply a pseudofield environment that promotes dispersive clay soil erosion.

Five elements were needed to complete the field simulation desired, to provide consideration of all the environmental factors, and to accelerate the testing process to make it feasible:

1. A soil mass that would best represent the most internally erodible mass,
2. A water-flow system that would promote possible dispersive clay soil erosion,
3. A chamber that would provide the soil with a controlled environment,
4. A method that accelerated erosion so that laboratory testing of a few hours could simulate months of field behavior, and
5. A system that would provide measurement of loss due to dispersive clay soil erosion.

Each of these elements will be discussed in the following.

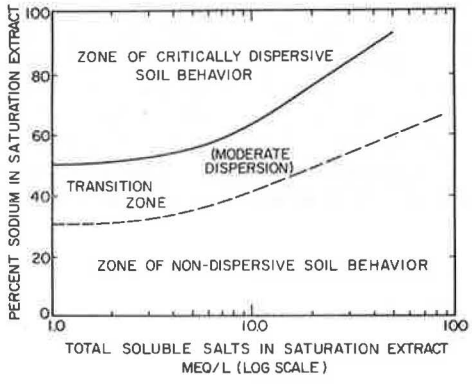

Figure 1. Determination of dispersive clay soil behavior (6).

Soil

The soil chosen for this laboratory simulation was a Harvard-miniature-sized cylinder [diameter = 1.3 in. (3.33 cm), length = 2.80 in. (7.11 cm)] compacted to specifications normally used for field density control by soils engineers. It was believed that with proper control of both density and compaction water these cylinders of soil would well represent the physical soil in the field. Tests were conducted on samples compacted at both standard and modified Proctor specifications by a mechanical device developed at Oklahoma State University. Demineralized distilled water was used to eliminate influences on test results by the chemical properties of compaction water. Finally, to ensure that there would be no variations in test results due to curing before or after compaction, water was added just before compaction, and the specimens were tested immediately following compaction. The product of these efforts was a soil of specified density and water content.

Artificial cracks or holes were drilled longitudinally through the cylinder so that a most internally erodible soil mass could be simulated. Much consideration was given to the development of a system of holes that would provide sufficient space for clay particle dispersion and removal but that would allow natural swelling and sloughing to stop internal erosion loss, as it may in the field. The final configuration (Fig. 2) contains three 0.0125-in. (0.0318-cm) holes evenly spaced throughout the cross section of the cylinder.

Water-Flow System

The erosion water used for physical erosion testing was distilled water, because of its close resemblance to relatively pure rainwater and because of its availability. A system to control water flow was necessary to minimize the quantities needed and to simulate field conditions. An intermittent flow sequence was adopted to approximate the holding of water in soil voids, the following seepage, and the recharging of the voids. In addition, the internal erosion occurring during constant, slow seepage and during this scheme of intermittent flow was essentially the same. The cycle that best promoted clay particle dispersion into nonmoving water and material removal with fresh-water replenishment had 7 sec of water flow each 6 min. This intermittent flow action was accomplished with timing units that controlled solenoid valves.

Environmental Chamber

The environmental chamber provided the desired pseudofield environment in which the soil mass could be tested. This most important part of the erosion device is a cell constructed of Lucite, into which the Harvard-miniature-sized cylinder is placed after compaction, slightly compressed to ensure a good soil-cell seal, and then perforated with the longitudinal holes. The completed cell with soil mass is shown in Figure 3. Water enters the top of this enclosure through a 0.25-in. (0.635-cm) tube (outside diameter) and is distributed over the top of the soil. Below the soil cylinder, there is a space for collection of suspension exiting the holes, and below this is a disk of U.S. No. 40 sieve wire, supported by a porous circular plate and a spacer ring. Suspension that passes through the sieve wire collects under this porous disk and exits the cell through a 0.25-in. (0.635-cm) tube. The combination of this environmental chamber, soil mass, and intermittent water-flow system was thought to be capable of best representing the field situation of critical dispersive clay soil erosion.

Figure 2. Longitudinal hole locations.

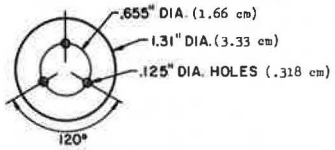

Figure 3. Cross section of assembled erosion device cell with soil cylinder.

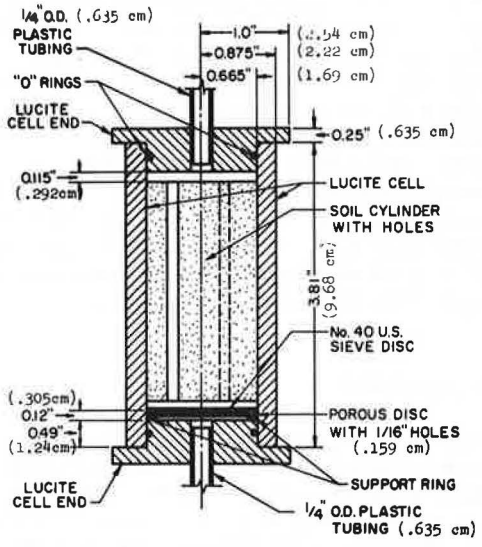

Figure 4. Water-flow system of erosion device.

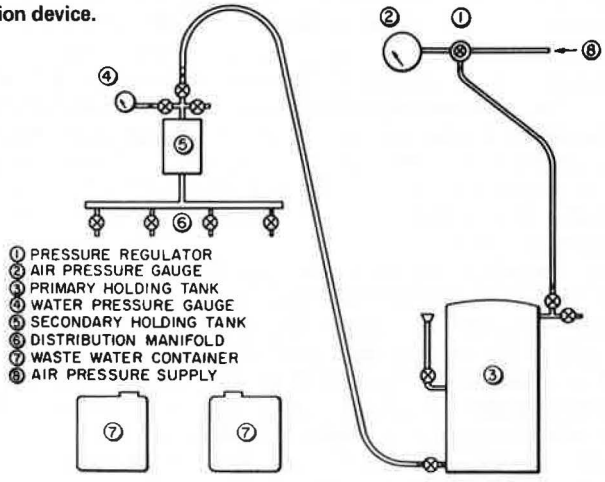

Figure 5. Timing and control system of erosion device.

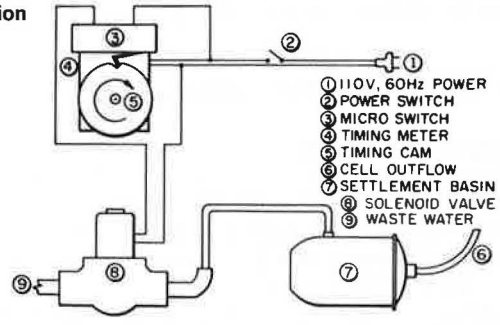

Erosion Acceleration

The method chosen to accelerate erosion to simulate months of erosion in hours was pressurization of the water-flow system. This hastened the movement of water into the soil and promoted the dispersion of the clay particles and a breakup of the soil mass. During the development process, several combinations of ways to introduce water into the soil and to pressurize the system were investigated so that the desired results could be achieved. So that maximum water absorption, soil mass breakup, and pseudorealistic soil action could be provided, water had to be introduced under atmospheric pressure and then pressurized to 15 psi (103.4 kPa). This meant that, initially, water entered the soil by normal physical and osmotic movement and that finally it was forced into the total soil to accelerate soil mass breakup and erosion. In addition, the pressurization used was beneficial to the movement of fresh water and soil suspension and to the operation of the solenoid valves.

Erosion Measurement

The final element for proper operation of the erosion device was some method to ensure that the erosion measured would be mainly that of the dispersive clay soil and only that of the surface, which occurs normally. Inasmuch as the accelerated erosion process used affected both types of erosion in approximately the same way, some device was needed in the test cell to permit, insofar as possible, loss of material by only dispersive clay soil erosion. Aggregates of soil containing flocculated clay particles were structurally coherent even under the flow conditions imposed in the test cells, but aggregates of soil containing dispersive clay particles melted. As a reference for defining coherence or melting of soil aggregates, a sieve was placed below the soil cylinder in the cell. Because of its standard use by soils engineers and relative availability, U.S. No. 40 sieve wire was used. This method of differentiating between aggregate coherence or disintegration proved to be effective and acceptable.

Determination of the length of test needed to observe long-term internal erodibility by using the procedure and apparatus explained was carried out while these elements were studied. It was found that, for soils that had critical internal erodibility, 4 hours was the optimum time.

The final decision concerned the quantity to be measured. This quantity had to be readily applicable for determining field behavior and precise enough to be considered quantitative. Because it was possible to easily determine the initial and final dry weight of soil in the cell, a relationship based on these values was selected. The percentage of erosion was thus defined as the ratio (× 100) of the weight of dry soil lost during the test to the initial dry weight of soil in the cell. This result was found to be directly related to potential internal field erosion.

Other than the erosion device cell shown in Figure 3, two other systems were necessary to complete the erosion device: (a) the water-flow system (Fig. 4) and (b) a system that provided control and timing for the desired intermittent flow (Fig. 5). The complete erosion device used for the physical erosion test is shown in Figure 6.

TEST RESULTS AND CORRELATIONS

During this research, testing was carried out on 18 different soils of various physical, mineralogical, chemical, and internal erodibility properties, which were native to Oklahoma, Arkansas, Mississippi, and Georgia. Fifteen of these were picked for this study because of their tendencies to exhibit dispersive clay soil erosion in the field. The remaining soils were added to provide a measure of control to this study, because they did not show this tendency.

The engineering properties determined for these soils were not indicative of their internal erodibility. According to plasticity, 15 were CL, 2 were CH, and the Georgia kaolinite was MH. Their textures ranged from almost pure clay, to silty clays, and to sandy clays.

Figure 6. Erosion device used in physical erosion test.

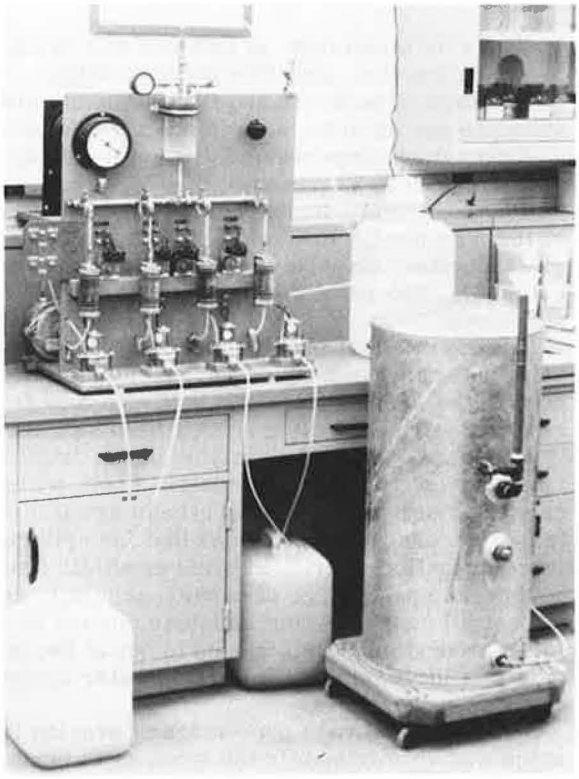

Table 1. Average physical erosion test results.

	Sample Number																	
Erosion (percent)	101	103	103	104	105	106	107	108	109	110	111	112	113	114	115	116	117	118
In standard Proctor compaction specimens	3.3	1.4	1.5	47.7	18.9	78.7	61.0	49.7	19.3	64.4	86.0	38.3	18.8	14.0	51.8	28.5	55.4	79.9
In modified Proctor compaction specimens	5.0	6.7	2.1	43.5	30.9	33.5	70.1	32.5	30.1	60.5	75.3	32.5	14.6	15.3	35.9	33.8	61.1	71.7

Figure 7. Correlation between physical erosion test results and exchangeable sodium percentage (clay).

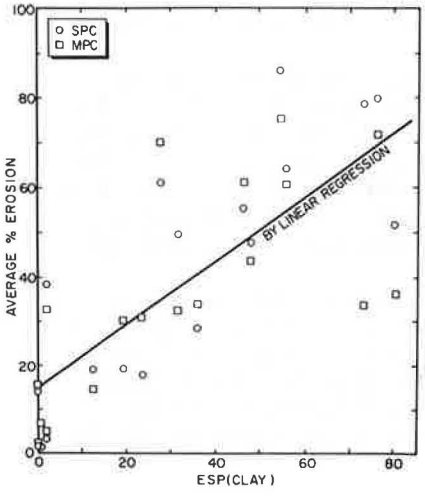

Figure 8. Correlation between physical erosion test results and field behavior determined by chemical properties of saturation extract.

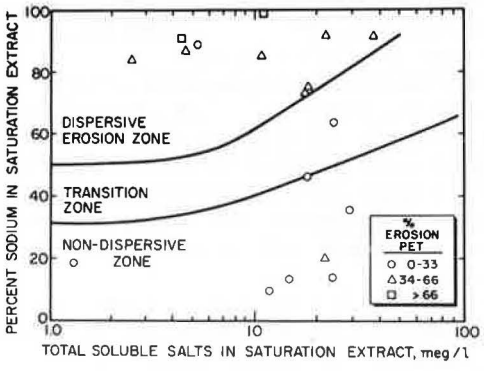

The clay mineralogy of samples was developed by differential thermal analysis, X-ray diffraction, and illite determination. Their clay fractions were found to consist of mixtures of smectite and illite, chlorite and smectite and illite, chlorite and illite, smectite and chlorite, and, in one case, kaolinite.

Laboratory dispersion test results indicated that none of these samples were nondispersive (0 to 33 percent), that 11 were moderately dispersive (34 to 66 percent), and that 7 were highly dispersive (67 to 100 percent). Soil chemistry testing described 10 of them as nondispersive [exchangeable sodium percentage (ESP) of 0 to 9], 6 of them as moderately dispersive (ESP of 10 to 15) and 2 of them as highly dispersive (ESP of over 16). The results of these qualitative indicators of internal erodibility are not in agreement.

During physical erosion testing, 142 specimens were prepared, 8 from each of the samples except in 2 cases for which material was in short supply. Half of these were compacted with standard and half with modified Proctor efforts. Compaction water contents were controlled so that field soil masses could best be simulated.

Close inspection and analysis of the detailed results obtained during erosion testing revealed several pertinent facts. First, within the limits of water contents tested for each compactive effort, a relatively small difference was found in dry density of the tested cylinders. This means that for cylinders of a sample prepared at each of the two compaction efforts, internal erodibility generally did not depend on dry density. Second, the percentage of erosion generally depended on compaction water content. In almost all cases, as this moisture content increased, the amount of erosion decreased. Internal erodibility is believed to occur because of changes in soil structure as they relate to increases in compaction water content. This agrees directly with the findings of other researchers.

Third, the average percentage of erosion in the standard Proctor compacted specimens was approximately the same as in those specimens compacted by using modified Proctor effort (Table 1). The explanation for this is based on the combination of two factors that influence internal erodibility. Generally, a substantial increase in dry density (e.g., from increased compactive effort) leads to a decreased susceptibility to internal erosion. On the other hand, the lower water contents associated with optimum compaction under increased compaction effort tend to increase erodibility. When both of these influences on behavior of a soil occurred simultaneously, the result was no general change in the average percentage of erosion. Because of the variations of results, it was considered reasonable to average the results found for each type of compaction effort (Table 1).

During analysis of these results, the influence of the physical, mineralogical, and chemical properties on the dispersive clay soil erodibility of each sample was considered. Although the chemical properties of samples largely dominated the action of the soil, both physical and mineralogical properties were determined to be important factors influencing the internal erosion process and, therefore, the behavior of the soil. The erosion device and its use in the physical erosion test were proved acceptable for providing the measure of dispersive clay soil erodibility needed by soils engineers to predict accurate field behavior.

Among the previously proposed methods for identification of dispersive clay soil erodibility, those believed most practical and useful by soils engineers were included in this research. Of these, two are of significant interest: (a) an indicator (i.e., ESP) of the surrounding chemical environment and of the exchange of clay particles and (b) the method developed by Sherard, Decker, and Ryker (6), which was previously discussed. Indications of dispersive clay soil erodibility as determined by the physical erosion test were correlated with those found by using these previously proposed methods of identification.

The modified ESP method is, in actuality, a previously proposed method of identification modified to better indicate the chemical environment of the clay particle. ESP is the percentage of the exchange complex of a clay soil that is taken up by sodium cations. Although we believed this was a fair indicator of clay particle dispersibility, it was decided that it could be significantly improved if it were related to the clay fraction rather than the whole soil. The method chosen was to amplify the ESP to the

ESP (clay) by dividing it by the decimal equivalent of the percentage of clay in the soil. The result is an indicator of the chemical environment of the clay particle, the constituent part of the soil mass that disperses.

The correlation between the average percentage of erosion achieved by using the physical erosion test and the respective sample ESP (clay) results is shown in Figure 7. There are two points plotted for each sample, one representing the average of results for cylinders compacted at each standard and modified Proctor effort. Linear regression was used to determine what relationship existed. The line shown intercepts the percentage-of-erosion axis at 14.7, which indicates that internal erosion depends on surface erosion potential. This line is inclined from the horizontal axis at about 35.5 deg, which shows that the internal erosion measured depends on the chemical environment surrounding the clay particle. The coefficient R^2 is 0.58, indicating that the majority of changes in measured erodibility may be due to changes in ESP (clay). Figure 7 shows the influence of all factors that affect internal erodibility, including physical and mineralogical properties. The correlation (Fig. 7) is significant and clearly indicates the validity of the physical erosion test.

$$\text{ESP(clay)} = \frac{\text{ESP}}{\% \text{ clay}/100}$$

Correlation of the identified erodibility by the physical erosion test and by the method proposed by Sherard, Decker, and Ryker (6) was also successful. Physical erosion test results were arbitrarily divided into groups of 0 to 33 percent, 34 to 66 percent, and 67 to 100 percent so that the percentage of erosion could be related to the zones of behavior. The appropriate chemical properties of the samples tested were plotted on the reference graph by using symbols for these groups. The resulting correlations are shown in Figure 8.

The correlation in Figure 8 is significant. Six of the eight samples with erosion from 0 to 33 percent had chemical data that were plotted in or below the transition zone. The sample from this group in the dispersive erosion zone had an average percentage of erosion of 31 percent and was a soil that evidently had physical properties that significantly reduced its erodibility. The group of eight samples that had 34 to 66 percent average erosion were all in the dispersive erosion zone except one. This nondispersive sample had an average erosion of 35 percent and was a soil known for its critical surface erosion potential. Finally, the chemical data of the two samples that had greater than 66 percent average erosion were plotted highest in the dispersive erosion zone. The results of the analysis of this correlation indicate the validity and acceptability of the physical erosion test.

CONCLUSIONS

The internal erosion phenomenon of dispersive clay soil has become a factor that must be considered during design and construction of earth embankments in many places in the world. So that the internal erodibility of a soil mass may be adequately assessed, all physical, mineralogical, and chemical properties must be considered. The simplest and most logical way to do this is with a physical test such as the physical erosion test. The findings of the analyses of correlations indicate that the physical erosion test is a significant addition to previously proposed methods. If it is applied by using a well thought-out program of sampling, it supplies a quantitative result that may be used to assess the combined effects of physical, mineralogical, and chemical properties on dispersive clay soil erosion potential and to predict field behavior.

REFERENCES

1. G. L. Bell. Piping in the Badlands of North Dakota. Proc., Sixth Annual Engineering Geology and Soils Engineering Symposium, 1968, pp. 242-257.

2. W. W. Emerson. The Slaking of Soil Crumbs as Influenced by Clay Mineral Composition. Australian Journal of Soil Research, Vol. 2, 1964, pp. 211-217.
3. O. G. Ingles and G. D. Aitchison. Soil-Water Disequilibrium as a Cause of Subsidence in Natural Soils and Earth Embankments. Proc., Tokyo Symposium on Land Subsidence, Vol. 2, 1969, pp. 342-353.
4. G. G. Parker and E. A. Jenne. Structural Failure of Western Highways Caused by Piping. Highway Research Record 203, 1967, pp. 57-77.
5. T. M. Petry. Identification of Dispersive Clay Soils by a Physical Test. Oklahoma State Univ., unpublished PhD dissertation, 1974.
6. J. L. Sherard, R. S. Decker, and N. L. Ryker. Piping in Earth Dams of Dispersive Clay. Proc., Specialty Conference on the Performance of Earth and Earth-Supported Structures, Vol. 1, Part 1, 1972, pp. 589-626.

SPONSORSHIP OF THIS RECORD

GROUP 2—DESIGN AND CONSTRUCTION OF TRANSPORTATION FACILITIES
W. B. Drake, Kentucky Department of Transportation, chairman

GENERAL DESIGN SECTION
F. W. Thorstenson, Minnesota Department of Highways, chairman

Committee on Subsurface Soil-Structure Interaction
Ernest T. Selig, State University of New York at Buffalo, chairman
Jay R. Allgood, Mike Bealey, Bernard E. Butler, T. Y. Chu, Robert M. Clementson, Hameed A. Elnaggar, Lester H. Gabriel, Delon Hampton, John G. Hendrickson, Jr., James Neil Kay, Raymond J. Krizek, Don A. Linger, Steven Majtenyi, Harry H. Ulery, Jr.

Committee on Subsurface Drainage
George W. Ring III, Federal Highway Administration, chairman
Charles C. Calhoun, Jr., Harry R. Cedergren, Barry J. Dempsey, Ernest L. Dodson, Edward N. Eiland, Jr., David S. Gedney, Alfred W. Maner, Glen L. Martin, K. H. McGhee, Lyndon H. Moore, William B. Nern, Travis W. Smith, W. T. Spencer, William D. Trolinger, Walter C. Waidelich, Thomas F. Zimmie

Committee on Frost Action
Arthur L. Straub, Clarkson College of Technology, chairman
Barry J. Dempsey, Wilbur J. Dunphy, Jr., L. F. Erickson, Wilbur M. Haas, Glenn E. Johns, Alfreds R. Jumikis, Miles S. Kersten, Clyde N. Laughter, George W. McAlpin, Richard W. McGaw, Stephen F. Obermeier, Marvin D. Oosterbaan, R. G. Packard, Edward Penner, Harold R. Peyton, A. Rutka

Committee on Environmental Factors Except Frost
William G. Weber, Jr., Pennsylvania Department of Transportation, chairman
Richard G. Ahlvin, K. A. Allemeier, Lindo J. Bartelli, Barry J. Dempsey, A. A. Fungaroli, Wilbur M. Haas, T. Allan Haliburton, Robert D. Krebs, Robert L. Lytton, Harry E. Marshall, Franklin Newhall, Leonard T. Norling, J. Frank Redus, Arthur L. Straub, Edgar Pierron Ulbricht, Larry M. Younkin

John W. Guinnee, Transportation Research Board staff

Sponsorship is indicated by a footnote on the first page of each report. The organizational units and the chairmen and members are as of December 31, 1974.